



HAL
open science

Contributions to modulation recognition for cooperative MIMO systems

Wassim Ben Chikha

► **To cite this version:**

Wassim Ben Chikha. Contributions to modulation recognition for cooperative MIMO systems. Networking and Internet Architecture [cs.NI]. Ecole Polytechnique de Tunisie, 2017. English. NNT : . tel-03880105

HAL Id: tel-03880105

<https://theses.hal.science/tel-03880105>

Submitted on 30 Nov 2022

HAL is a multi-disciplinary open access archive for the deposit and dissemination of scientific research documents, whether they are published or not. The documents may come from teaching and research institutions in France or abroad, or from public or private research centers.

L'archive ouverte pluridisciplinaire **HAL**, est destinée au dépôt et à la diffusion de documents scientifiques de niveau recherche, publiés ou non, émanant des établissements d'enseignement et de recherche français ou étrangers, des laboratoires publics ou privés.



République Tunisienne
Ministère de l'enseignement Supérieur et de la Recherche Scientifique
Université de Carthage



Thèse de doctorat

présentée à

l'École Polytechnique de Tunisie

dans la discipline

Électronique et Technologie de l'Information et de la Communication

par

Wassim BEN CHIKHA

Contributions to modulation recognition for cooperative MIMO systems

Soutenue le 19/04/2017 devant le jury composé de:

Président

Mr. Mohamed SIALA Professeur à l'École Supérieure des Communications de Tunis

Rapporteurs

Mr. Iyad DAYOUB Professeur à l'Université de Valenciennes et du Hainaut-Cambrésis

Mr. Hichem BESBES Professeur à l'École Supérieure des Communications de Tunis

Examineur

Mr. Ridha BOUALLEGUE Professeur à l'École Supérieure des Communications de Tunis

Directeur de thèse

Mr. Rabah ATTIA Professeur à l'École Polytechnique de Tunisie

Acknowledgments

Firstly and foremost, I would like to express my deepest gratitude to my supervisor Prof. Rabah Attia for giving me the opportunity to pursue a Ph.D. under his valuable guidance. I am grateful for his insightful discussions, encouragement, enthusiasm, and dedication.

Secondly, I would like to take this opportunity to thank Prof. Iyad Dayoub, Dr. Slim Chaoui and Prof. Walaa Hamouda for their valuable comments and suggestions on my manuscripts. Without their help, the work would have never achieved the quality presented here.

My sincere thanks go to my dear brother Haithem for his constant encouragement and help through the most difficult times.

I also express my special thanks to my beloved parents : Mohamed and Fatma, brothers : Haithem, Wissem and Sami, sisters : Ines and Randa, friends and colleagues for their unconditional support in the hardest times.

Finally, I would like to convey my warmest gratitude to my reviewing committee members for accepting to evaluate my thesis.

Title

Contributions to modulation recognition for cooperative MIMO systems

Abstract

With the increasing development of wireless communication systems, algorithms and techniques for multiple-input multiple-output (MIMO) signal interception have recently received significant attention. Modulation recognition represents an essential step in the signal interception process. It has attracted considerable interest on the part of the military in many applications, such as, communication intelligence, electronic support measures and spectrum surveillance. Within the context of cognitive radio, recent and rapid developments in software defined radio have given modulation recognition greater importance in civil applications. Furthermore, cooperative communication based on relay nodes has gained much attention since it can ensure better controlled transmission quality and improved access coverage. Thus, the concept of relaying has been put into the standard specifications of mobile broadband communication systems, such as worldwide interoperability for microwave access (WiMAX) and long-term evolution-advanced (LTE-A).

The aim of this thesis is to design modulation recognition algorithms for cooperative MIMO systems based on a pattern recognition approach. First, we propose a modulation recognition algorithm for cooperative MIMO systems over uncorrelated channels with perfect channel state information (CSI). Then, we study the utility of MIMO multi-relay networks for modulation recognition over spatially-correlated channels with imperfect CSI. In this work, the expression of the ergodic capacity for the proposed transmission system has also been derived in order to evaluate its performance in the presence of spatial correlation and imperfect CSI. Finally, we design an algorithm of superposed modulations recognition dedicated to two-way relaying channel. Simulations are provided to assess the efficiency of the proposed algorithms using the average probability of correct recognition.

Keywords : Cognitive radio, cooperative MIMO systems, modulation recognition, pattern recognition approach, relaying channels.

Titre

Contributions à la reconnaissance de modulation pour les systèmes MIMO coopératifs

Suite au développement progressif des systèmes de communication sans fil, les algorithmes et techniques d'interception des communications MIMO ont récemment reçu une attention particulière. La reconnaissance de la modulation constitue une étape essentielle dans le processus d'interception du signal. Elle a donc suscité un intérêt important pour les systèmes militaires dans de nombreuses applications telles que la communication des renseignements, les mesures de soutien électronique et la surveillance du spectre. Dans le contexte de la radio cognitive, les développements récents et rapides dans la radio logicielle ont donné une plus grande importance à la reconnaissance de modulation pour les applications civiles. En outre, la communication coopérative basée sur des nœuds relais a gagné une grande attention puisqu'elle peut assurer une qualité de transmission mieux contrôlée et une couverture d'accès améliorée. Ainsi, le concept de relayage a été pris en considération dans les spécifications du standard des systèmes de communication mobile à large bande, tels que WiMAX et LTE-A.

L'objectif de cette thèse est de concevoir des algorithmes de reconnaissance de modulation pour les systèmes MIMO coopératifs basés sur l'approche de reconnaissance de forme. D'abord, nous proposons un algorithme de reconnaissance de modulation pour les systèmes MIMO coopératifs dans le cas où les canaux sont non corrélés avec CSI parfait. Ensuite, nous étudions l'utilité de l'utilisation de plusieurs relais dans la reconnaissance de la modulation pour le cas où les canaux sont spatialement corrélés avec CSI imparfait. Dans ce travail, nous dérivons également l'expression de la capacité ergodique du système de transmission proposé afin d'évaluer sa performance à la présence de la corrélation spatiale et du CSI imparfait. Enfin, nous concevons un algorithme de reconnaissance des modulations superposées dédié pour un canal bidirectionnel à relais. Les simulations sont fournies pour évaluer l'efficacité des algorithmes proposés en utilisant la probabilité moyenne pour une reconnaissance correcte.

Mots-clés : Radio cognitive, systèmes MIMO coopératifs, reconnaissance de modulation, approche de reconnaissance de forme, canaux de relayage.

Contents

Mathematical notations, operations and abbreviations	xi
1 General Introduction	1
1.1 Context and Motivations	1
1.2 Key contributions	3
1.3 Thesis organisation	4
1.4 Publications List	5
2 Literature Review	6
2.1 Introduction	6
2.2 MIMO systems	7
2.2.1 Source entity	7
2.2.1.1 Modulator	7
2.2.1.2 Space-time encoder	10
2.2.1.3 Radio-frequency (RF) device	14
2.2.1.4 MIMO Precoding	15
2.2.2 Propagation Environment	16
2.2.2.1 Fading Channels	17
2.2.2.2 Additive Noise	21
2.2.3 Destination entity	22
2.3 Modulation Recognition for SISO and MIMO Systems	23
2.3.1 Modulation Recognition for SISO Systems	23
2.3.2 Modulation Recognition for MIMO Systems	24
2.4 Cooperative MIMO Systems	25

2.5	Conclusion	28
3	Modulation recognition for cooperative MIMO systems over uncorrelated channels with perfect CSI	29
3.1	Introduction	30
3.2	System Model and Preliminaries	30
3.2.1	Source Node Precoding Design based on RZF	31
3.2.2	Relay Node Beamforming Design Based on ZF-RZF	32
3.2.3	Destination Node Combining	33
3.3	Modulation Recognition Algorithm	33
3.3.1	Features Extraction	33
3.3.2	Classifiers	36
3.3.2.1	J48 classifier	37
3.3.2.2	MLP classifier	38
3.3.2.3	Bayesian Networks	38
3.3.2.4	Time complexities of J48, MLP, NBD and TAN classifiers	39
3.3.3	Metric for evaluating the effectiveness of classifiers	39
3.4	Results and Discussion	41
3.4.1	Performance comparison of J48 and MLP classifiers	42
3.4.2	Performance comparison of J48, NBD and TAN classifiers	44
3.5	Conclusion	47
4	Modulation recognition for cooperative MIMO systems over spatially-correlated channels with imperfect CSI	49
4.1	Introduction	50
4.2	System model and ergodic capacity	50
4.2.1	Model description	50
4.2.1.1	Considered cooperative MIMO system	50
4.2.1.2	Spatial correlation model	53
4.2.1.3	Imperfect channel estimation model	53
4.2.2	Ergodic capacity	54
4.2.2.1	Instantaneous SNR of RZF Beamforming	54
4.2.2.2	Instantaneous SNR of ZF-RZF Beamforming	56
4.3	Proposed modulation recognition algorithm	58

4.3.1	Extraction of discriminating features	58
4.3.2	Bagging classifier	59
4.4	Simulation Results	60
4.4.1	Ergodic capacity as a function of relays number	61
4.4.2	Performance comparison of Bagging and J48 classifiers	64
4.4.3	Performance comparison of Bagging, TAN, NBD and MLP classifiers	66
4.4.4	Probability of modulation recognition as a function of relays number	67
4.5	Conclusion	68
5	Recognition of superposed modulations for two way relay MIMO systems with PLNC	70
5.1	Introduction	71
5.2	Proposed modulation recognition algorithm	71
5.2.1	Motivation	71
5.2.2	Considered two-way MIMO relay channels	73
5.2.3	Extraction of discriminating features	75
5.2.4	Random forests classifier	76
5.3	Simulation results	77
5.3.1	Simulation setup	77
5.3.2	Effect of the relay position	78
5.3.3	Effect of the modulation types	79
5.3.4	Effect of the antennas number	81
5.3.5	Effect of the symbols number	81
5.3.6	Effect of the path loss exponent	82
5.4	Conclusion	83
6	General conclusion and Future Works	84
6.1	Summary of results	84
6.2	Future works	86
	References	87

List of Figures

2.1	Architecture of a MIMO source	7
2.2	Examples of constellations ASK with unit average symbol power ($\mathbb{E}\{ s ^2\} = 1$)	8
2.3	Examples of PSK constellations with unit average symbol power ($\mathbb{E}\{ s ^2\} = 1$)	9
2.4	Examples of QAM constellations with $\mathbb{E}\{ s ^2\} = 1$	10
2.5	Architecture of RF device	14
2.6	Schematic diagram of MIMO system with a linear precoder	15
2.7	Effects of radio wave propagation	16
2.8	Diagram of a MIMO system with N_{AS} transmit antennas and N_{AD} receive antennas	17
2.9	Propagation of a signal in a wireless environment, with and without LOS . .	18
2.10	Architecture of a MIMO destination	22
2.11	Estimation of the transmitted bitstream	22
2.12	Cooperative MIMO system using L -relay nodes	26
2.13	Two-way MIMO relay channels	27
3.1	MIMO relaying broadcast network with source, relay and destination nodes using two-time-slot protocol	31
3.2	Modulation recognition of an unknown received signal	37
3.3	Interpretation of the ROC curve for \mathcal{M}_s modulation	41
3.4	ROC curves of J48 and MLP classifiers for each type of modulation scheme when using cooperative MIMO system employing V-BLAST technique with $N_A = 4$, $\text{SNR}_{SR} = 30$ dB and $\text{SNR} = 5$ dB over Rayleigh fading channels	43

3.5	Performance comparison of J48 and MLP classifiers (Probability of correct recognition as a function of SNR for Θ_1 when using V-BLAST technique with $N_A = 4$ over Rayleigh fading channels)	44
3.6	ROC curves of J48 and NBD classifiers for each modulation scheme when using cooperative MIMO system employing V-BLAST technique with $N_A = 4$, $\text{SNR}_{SR} = 30$ dB and $\text{SNR} = 5$ dB over Rayleigh fading channels	45
3.7	ROC curves of J48 and TAN classifiers for each modulation scheme when using cooperative MIMO system employing V-BLAST technique with $N_A = 4$, $\text{SNR}_{SR} = 30$ dB and $\text{SNR} = 5$ dB over Rayleigh fading channels	45
3.8	Performance comparison of J48, NBD and TAN classifiers (Probability of correct recognition as a function of SNR for Θ_1 when using V-BLAST technique with $N_A = 4$ over Rayleigh fading channels)	46
3.9	Time model building in the case of cooperative MIMO system for Θ_1 employing V-BLAST technique with $N_A = 4$, $\text{SNR}_{SR} = 30$ dB and $\text{SNR} = 5$ dB over Rayleigh fading channels	47
4.1	MIMO relaying broadcast network with source, L -relay and destination nodes using two-time-slot protocol	51
4.2	Bagging process employing J48 classifier	60
4.3	Ergodic capacity as a function of L (number of relays) for different e^2 (variances of channel estimation error) with $N_A = 4$, $ \rho = 0$, $P_s = P_r = 12$ dB, $\text{SNR}_{SR} = 15$ dB and $\text{SNR} = 0$ dB	62
4.4	Ergodic capacity as a function of L (number of relays) for different $ \rho $ (Kronecker correlation coefficients) with $N_A = 4$, $e^2 = 0.1$, $P_s = P_r = 12$ dB, $\text{SNR}_{SR} = 15$ dB and $\text{SNR} = 0$ dB	63
4.5	ROC curves of Bagging and J48 methods for each type of modulation in the case of MIMO scheme using V-BLAST, $N_A = 4$, $L = 1$, $\text{SNR}_{SR} = 20$ dB, $\text{SNR} = -5$ dB, $e^2 = 0.1$ and $ \rho = 0.5$	64
4.6	Probability of recognition as a function of SNR for Θ_2 in MIMO schemes using V-BLAST with $N_A = 4$ and $\text{SNR}_{SR} = 20$ dB for Bagging and J48 classifiers	66
4.7	Probability of recognition as a function of SNR for Θ_2 in MIMO schemes using V-BLAST with $N_A = 4$, $e^2 = 0.1$, $ \rho = 0.5$ and $\text{SNR}_{SR} = 20$ dB for Bagging, TAN, NBD and MLP classifiers	67

4.8	Probability of recognition as a function of SNR for the proposed algorithm with different L (number of relay nodes) compared to the ZF-DMI algorithm [26] in MIMO schemes employing V-BLAST with $N_A = 4$, $\text{SNR}_{SR} = 20$ dB, $e^2 = 0.1$ and $ \rho = 0.5$ using the Bagging classifier	68
5.1	Constellations : BPSK signal, 16-QAM signal and superposed BPSK and 16-QAM signal	72
5.2	Two-way MIMO relay channels	73
5.3	Processes diagram of sources modulations recognition algorithm for an unknown received signal	75
5.4	The effect of the distance between S_1 and R , d_{S_1R} , on the average probability of correct recognition, P_{ra} , for Θ_3 , $N_{AS} = N_{AR} = 4$, $N = 10000$, $\delta = 2$ and $d_{S_1S_2} = d_{S_1R} + d_{S_2R} = 1$	79
5.5	The effect of the modulation schemes, Θ_d , $d = 3, 4, 5$, on the average probability of correct recognition, P_{ra} , for RFC and Bagging classifiers using $N_{AS} = N_{AR} = 4$, $N = 10000$, $\delta = 2$ and $d_{S_1R} = d_{S_2R} = 0.5$	80
5.6	The effect of the number of antennas, N_{AS} and N_{AR} , on the average probability of correct recognition, P_{ra} , for Θ_3 , $N = 10000$, $\delta = 2$ and $d_{S_1R} = d_{S_2R} = 0.5$	81
5.7	The effect of the number of symbols, N , on the average probability of correct recognition, P_{ra} , for Θ_3 , $N_{AS} = N_{AR} = 4$, $\delta = 2$ and $d_{S_1R} = d_{S_2R} = 0.5$	82
5.8	The effect of the path loss exponent, δ , on the average probability of correct recognition, P_{ra} , for Θ_3 , $N_{AS} = N_{AR} = 4$, $N = 10000$, and $d_{S_1R} = d_{S_2R} = 0.5$	83

List of Tables

3.1	Some theoretical moments and cumulants values for several modulation schemes (unit-variance signal constellations with equiprobable symbols) [18]	34
3.2	Time complexities of J48, MLP, NBD and TAN classifiers	39
3.3	Two-class confusion matrix	40
3.4	Accuracy measures derived from the two-class confusion matrix	40
3.5	AUC of each classifier in the case of cooperative MIMO system employing V-BLAST technique with $N_A = 4$, $\text{SNR}_{SR} = 30$ dB and $\text{SNR} = 5$ dB over Rayleigh fading channels	46
4.1	AUC of each recognition method (in the case of V-BLAST MIMO scheme with $N_A = 4$, $L = 1$, $\text{SNR}_{SR} = 20$ dB, $\text{SNR} = -5$ dB, $e^2 = 0.1$ and $ \rho = 0.5$)	65
4.2	Time model building (in the case of MIMO scheme using V-BLAST with $N_A = 4$, $L = 1$, $\text{SNR}_{SR} = 20$ dB, $\text{SNR} = -5$ dB, $e^2 = 0.1$ and $ \rho = 0.5$)	65
5.1	Superposition of two 4-ASK signals at the relay node and the corresponding mapped bits using XOR operation	72
5.2	AUC of each classifier for Θ_4 with $N_{AS} = N_{AR} = 4$, $N = 10000$, $\delta = 2$, $d_{S_1R} = d_{S_2R} = 0.5$ and $\bar{\gamma} = 3$ dB	80
5.3	Time model building for Θ_4 with $N_{AS} = N_{AR} = 4$, $N = 10000$, $\delta = 2$, $d_{S_1R} = d_{S_2R} = 0.5$ and $\bar{\gamma} = 3$ dB	81

Mathematical notations, operations and abbreviations

List of mathematical notations and operations

Here, we introduce the notations adopted in this thesis.

$\mathbb{E}\{\cdot\}$	Expectation operator.
$\bar{(\cdot)}$	Conjugate operation of matrix or vector.
$(\cdot)^T$	Transpose operation of matrix or vector.
$(\cdot)^H$	Hermitian conjugate transpose of matrix or vector.
$(\cdot)^{-1}$	Inverse operation.
$(\cdot)^\dagger$	Pseudoinverse operation of the matrix argument.
$\text{tr}(\cdot)$	Trace of a square matrix.
\mathbf{I}_N	Identity matrix of order N .
$\mathbb{C}^{M \times N}$	Set of $M \times N$ matrices over the field of complex numbers.
$\mathcal{CN}(x, y)$	Circularly symmetric complex Gaussian distribution with mean x and covariance y .
$(\cdot)_{pq}$	The (p, q) th entry in the p th row and the q th column of the matrix argument.
$(\cdot)_p$	The p th row of the matrix argument.
$(\cdot)_{:,q}$	The q th column of the matrix argument.
$\text{Var}(\cdot)$	Variance.
$\ \cdot\ $	Euclidean norm of the vector argument.
$ \cdot $	Absolute value of the scalar argument.
$\lceil \cdot \rceil$	Ceiling function.
$\Re(\cdot)$	Real part of complex number.

$\Im(\cdot)$	Imaginary part of complex number.
$a \ll b$	a is much smaller than b .
$a \simeq b$	a is approximately equal to b .
$a \rightarrow b$	a tends to b .
\otimes	Kronecker product.
$I_0(\cdot)$	Zero-order modified Bessel function of the first kind.
$\Gamma(\cdot)$	Gamma function.
$\log_a(\cdot)$	Logarithm of the scalar argument using the base $a \in \mathbb{R}^+$.
$\Pr(\cdot)$	The probability.
$\Pr(\cdot \cdot)$	The conditional probability.
$\text{card}(\cdot)$	The cardinality of a set.
$\exp(\cdot)$	Exponential function.
$\lfloor \cdot \rfloor$	Integer part of the scalar argument.
$\arg \max_x f(x)$	Maximising argument of the function $f(x)$.
$\mathcal{O}(\cdot)$	The complexity order of an algorithm.

List of notations

C_{op}	o^{th} -order cumulant.
$d_{S_u R}$	Distance between the source S_u , $u = 1, 2$ and R .
$d_{S_1 R}$	Distance between the sources S_1 and S_2 .
H_n	Number of hidden neurons in the multilayer perceptron classifier.
K	Rician fading parameter.
L	Number of relay nodes.
L_C	Code length.
m	Nakagami fading parameter.
M_{op}	o^{th} -order moment.
N_{AS}	Number of antennas at the source node.
N_{AR}	Number of antennas at the relay node.
N_{AD}	Number of antennas at the destination node.
N_s	Number of symbols.
N	Number of symbols at each antenna.
N_D	Number of samples in the training data set.
N_F	Number of selected features.
N_{epochs}	Number of epochs to train the training data in the multilayer perceptron classifier.
N_{trees}	Number of trees to grow in the random forests classifier.
N_{RF}	Number of random features to be considered in the random forests classifier at each node.
P_{ra}	Average probability of correct recognition.
P_{re}	Probability of correct recognition for a modulation \mathcal{M}_i .
P_s	Total transmit power at the source node.
P_r	Total transmit power at the relay node.
R_c	Coding rate.
T	Number of the generated training subsets in the Bagging classifier.
T_s	Symbol duration.
δ	Path-loss exponent.
γ_n	Postprocessing SNR per symbol of the n th stream.
$\bar{\gamma}$	Postprocessing SNR per symbol of the n th stream.
ρ_s	Source power control factor.
ρ_r	Relay power control factor.

- $\rho_{H_i, RX}$ Receive correlation coefficient, $c = \{SR, SD, RD\}$.
- $\rho_{H_i, TX}$ Transmit correlation coefficient, $c = \{SR, SD, RD\}$.
- σ_c^2 Gaussian noise variance, $c = \{SR, SD, RD\}$.
- Θ_d Considered set of modulation schemes, $d = 1, \dots, 5$.
- \mathbf{F}_l Beamforming matrix at the l^{th} relay node, $l = 1 \dots L$.
- \mathbf{H}_c Matrix of the c MIMO channel, $c = \{SR, SD, RD\}$.
- \mathbf{n}_c Noise vector, $c = \{SR, SD, RD\}$.
- \mathbf{P} Precoding matrix at the source node.
- $\mathbf{R}_{H_c, RX}$ Receiver correlation matrix, $c = \{SR, SD, RD\}$.
- $\mathbf{R}_{H_c, TX}$ Transmitter correlation matrix, $c = \{SR, SD, RD\}$.

List of abbreviations

AF	Amplify-and-forward.
ANN	Artificial neural network.
ASK	Amplitude shift keying.
AUC	Area under the curve ROC.
AWGN	Additive white Gaussian noise.
BM	Beamforming matrix.
CEG-noise power	Channel-error-generated noise power.
CR	Cognitive radio.
CSI	Channel state information.
DAC	Digital analog converter.
DNF	Denoise-and-forward.
ESM	Electronic support measures.
GA&IT	Genetic algorithm and information theory.
HOC	Higher order cumulants.
HOM	Higher order moments.
HOS	Higher order statistics.
i.i.d.	Independent and identically distributed.
LOS	Line of Sight.
LTE-A	Long term evolution-advanced.
MIMO	Multiple-input multiple-output.
MMSE	Minimum mean square error.
MLP	Multilayer perceptron.
NBD	Naive Bayes using discretization.
NLOS	Non Line of Sight.
OFDM	Orthogonal frequency division multiplexing.
OSTBC	Orthogonal space-time block codes.
PCA	Principal component analysis.
PDF	Probability distribution function.
PLNC	Physical-layer network coding.
PSK	Phase shift keying.

PM	Precoding matrix.
QAM	Quadrature amplitude modulation.
Q-OSTBC	Quasi-Orthogonal space-time block codes.
TWRC	Two-way relay channel.
RFC	Random forests classifier.
ROC	Receiver operating characteristic.
RPROP	Resilient backpropagation.
RZF	Regularized zero forcing.
SISO	Single-input single-output.
SNR	Signal-to-noise ratio.
SM	Spatial multiplexing.
STBC	Space-time block codes.
STC	Space-time coding.
TAN	Tree augmented naive Bayes.
V-BLAST	Vertical Bell Laboratories Layered Space-Time.
WiMAX	Worldwide interoperability for microwave access.
ZF	Zero forcing.
ZF-RZF	Zero forcing-Regularized zero forcing.

General Introduction

Contents

1.1 Context and Motivations	1
1.2 Key contributions	3
1.3 Thesis organisation	4
1.4 Publications List	5

1.1 Context and Motivations

Recently, wireless technology has received considerable attention since it can offer higher transmission rates with less error. Multiple-input multiple-output (MIMO) wireless technology is one of the most promising technologies that can be implemented to significantly enhance the throughput and robustness of wireless networks through the use of multiple antennas. In fact, this technology has been introduced as a means of enhancing the reliability of the received signal through the spatial diversity technique [1–3]. That is why it has been adopted by various wireless standards, including IEEE 802.11n, IEEE 802.16e, and 3GPP LTE [4] after being pioneered by Foschini [5]. However, due to the need of complex transceiver circuitry and the large power consumption at the circuit level caused by signal processing, MIMO communication has not received much attention as a viable technology for energy-limited wireless sensor networks. In addition, the implementation of multiple antennas at a small node may not be feasible due to physical limitations [6]. To overcome this problem, a cooperative communication concept has been proposed to achieve MIMO capability in single-input single-output (SISO) networks

[7–11]. Note that the cooperative MIMO system has attracted a great interest in recent technologies because an essential rate gain and an improvement of the diversity order are achieved [12, 13]. Also, the concept of relaying is supported by the standard specifications of the mobile broadband communication systems, such as worldwide interoperability for microwave access (WiMAX) and long-term evolution-advanced (LTE-A) [14]. For practical cooperative MIMO systems, the effect of spatial correlation has to be considered since the diversity, the multiplexing, and the capacity gains can be directly influenced by spatial correlation effects due to insufficient spacing between antenna elements and/or the existence of scatterers in the propagation environment [15]. In addition, it is usually difficult to obtain perfect channel state information (CSI) available at all nodes (source, relays and destination) in practical applications. In fact, an imperfect CSI may occur because of errors introduced by channel estimation, reciprocity mismatch, quantization, and delay [16].

Moreover, recognition of communication parameters has gained a great deal of attention. It presents an intermediate step between signal identification and signal decoding/demodulation. Modulation recognition of an identified signal represents an essential task for an intelligent receiver and plays an important role in demodulating the intercepted signals for many communication systems. In fact, a misrecognition of the modulation scheme results in significant performance degradation since the modulation recognition is performed prior to data demodulation. For this reason, it has found applications in various military and civilian communication systems, including communication intelligence, electronic support measures, spectrum surveillance, software-defined radio and cognitive radios [17–19]. In the literature, several modulation recognition techniques have been first proposed for SISO systems [18]. These techniques typically fall into two categories. The first is based on a decision-theoretic approach. It is a probabilistic solution based on certain hypotheses and requires prior knowledge of probability functions [18, 20]. The second category is based on a pattern recognition approach. It involves extracting key features from the received signal [21–23]. Furthermore, various modulation recognition algorithms have been proposed for MIMO systems [17, 24–26]. To the best of our knowledge, no previous work has addressed the problem of modulation recognition in the context of cooperative MIMO systems. Therefore, addressing the problem of modulation recognition for cooperative MIMO systems is essential and of critical importance.

In addition, network coding (NC) has been regarded in wireless networks such as ad hoc and wireless sensor networks to enhance the available throughput [27], energy efficiency [28], and robustness [29]. NC can decrease the bandwidth assigned to the relay transmission and hence increase the spectral efficiency of cooperative communications. Recently, the physical-layer network coding (PLNC) has attracted a great interest in the cooperative networks community since the transmission times at the multiple access phase are reduced to one single time [30]. In fact, PLNC enables the source nodes to send signals simultaneously to the relay node. The relay node maps the superposed signals and thereafter forwards the resulting signal to the destinations. In this context, a two-way relay channel (TWRC) can be considered where two source nodes communicate with each other with the help of a single relay node. For each transmission, the sources can vary the modulation scheme and the modulation order depending on the applications and their requirements. Hence, each source requires knowing the modulation type and order used by the other source to demodulate the received signal. A necessary requirement for ensuring correct data reception at the destinations is the perfect recognition of the sources modulations schemes and orders.

The aim of this thesis is to propose algorithms to recognize modulations used in broadband technologies such as LTE-A and WiMAX under cooperative MIMO systems, taking into account previous discussed constraints.

1.2 Key contributions

Based on the previously discussed problems and motivations, the main contributions of this dissertation are summarized as follows :

- ❖ A low-complexity modulation recognition algorithm is introduced for MIMO relaying broadcast channels with a direct link. In this work, we assume that the channels are uncorrelated with perfect CSI. Simulation results show that the proposed algorithm with the aid of a relay node can offer SNR gain compared to the non-cooperative one. We also show that J48 and Bayesian network classifiers allow for better monitoring of the intercepted signals in broadband technologies with reduced complexity.
- ❖ An algorithm for modulation recognition is designed for spatially-correlated MIMO

relaying broadcast channels using multi-relay nodes with a direct link under imperfect CSI. Here, the ergodic capacity of the proposed transmission system is derived to quantify the effect of imperfect CSI and spatial correlation. Simulation results show that the recognition performance degradation caused by both spatially correlated channels and channel estimation errors can be removed by means of a relaying scheme.

- ❖ An algorithm for modulation recognition dedicated to two-way relaying MIMO systems with PLNC is proposed. In contrast to the existing approaches in the literature, where a single M-ary modulation is identified, the proposed recognition algorithm has to recognize a pair of unknown sources modulations from the superposed symbols in the presence of PLNC. Simulations are provided to assess the accuracy of the proposed algorithm through the average probability of correct recognition for different modulation scheme pairs. It is shown that the algorithm achieves high modulation recognition in an acceptable signal-to-noise ratio (SNR) range at different relay positions.

1.3 Thesis organisation

The outline of the contents of this thesis is as follows :

Chapter 2 provides an overview of the theory relevant to this thesis. It covers the principles of the promising MIMO technology and subsequently reviews previous works in the literature dealing with modulation recognition algorithms for SISO and MIMO systems. Furthermore, the main characteristics of cooperative communications are highlighted.

Chapter 3 introduces a novel modulation recognition algorithm for cooperative MIMO systems over uncorrelated channels with perfect CSI. The performance of the proposed algorithm is assessed through Monte-Carlo simulations in terms of the probability of correct recognition and the time complexity. The superiority of the proposed algorithm compared to earlier relevant works is clearly demonstrated through intensive simulations.

Chapter 4 proposes a new modulation recognition algorithm dedicated for cooperative MIMO systems over spatially-correlated channels with imperfect SD and RD CSI. First, the ergodic capacity of the proposed transmission system is derived and verified through simulations. Second, the sensitivity of the proposed modulation recognition al-

gorithm is investigated under spatially-correlated channels in the presence of imperfect CSI. Finally, the increasing effect of the relay nodes on modulation recognition is evaluated through Monte-Carlo simulations.

Chapter 5 focuses on the recognition of superposed modulations in two-way relay MIMO systems with PLNC. The effectiveness of the proposed algorithm is evaluated through the probability of correct recognition at different relay positions. As a result, high recognition performance is achieved at an acceptable SNR range.

Chapter 6 presents a summary of the most important conclusions drawn from this thesis, and suggests several research paths in which further research could be carried out.

1.4 Publications List

International Journal Papers

[J1] **W. Ben Chikha**, S. Chaoui and R. Attia, "Identification of superposed modulations for two-way relaying MIMO systems with physical-layer network coding, " *IET Communications*, vol. 11, no. 2, pp. 225–231, 2017.

[J2] **W. Ben Chikha** and R. Attia, "On the utility of MIMO multi-relay networks for modulation identification over spatially-correlated channels," *Springer Telecommunication Systems*, vol. 64, no. 4, pp. 735–747, 2017.

[J3] **W. Ben Chikha**, I. Dayoub, W. Hamouda and R. Attia, "Modulation recognition for MIMO relaying broadcast channels with direct link," *IEEE Wireless Communications Letters*, vol. 3, no. 1, pp. 50-53, 2014.

International Conference Papers

[C1] **W. Ben Chikha** and R. Attia, "On the Performance evaluation of Bayesian network classifiers in modulation identification for cooperative MIMO systems, In " *23rd International Conference on Software, Telecommunications and Computer Networks (SoftCOM)*, Split-Croatia, IEEE, pp. 138-142, 2015.

[C2] **W. Ben Chikha**, I. Dayoub and R. Attia, "Modulation detection in intelligent transportation systems based on cooperative MIMO networks over Nakagami- m fading, In " *International Conference on Electrical Sciences and Technologies in Maghreb (CISTEM)*,

IEEE, pp. 1-6, 2014.

Literature Review

Contents

2.1 Introduction	6
2.2 MIMO systems	7
2.2.1 Source entity	7
2.2.2 Propagation Environment	16
2.2.3 Destination entity	22
2.3 Modulation Recognition for SISO and MIMO Systems	23
2.3.1 Modulation Recognition for SISO Systems	23
2.3.2 Modulation Recognition for MIMO Systems	24
2.4 Cooperative MIMO Systems	25
2.5 Conclusion	28

2.1 Introduction

This chapter presents an introduction to the fields of research in wireless communication systems, and the techniques on which the contents of this thesis are based on. First, we detail the entities of MIMO systems. Second, modulation recognition for SISO and MIMO systems is reviewed. In fact, some of the recently published algorithms are briefly described. Finally, cooperative MIMO systems are presented, which cover the topics of the MIMO relaying broadcast network and the TWRC.

2.2 MIMO systems

Recently, MIMO systems have received a lot of attention since a rate gain can be achieved over wireless links. In general, a MIMO wireless communication system consists of three entities : the source (i.e., multiple antennas transmitter), the propagation environment, and the destination (i.e., multiple antennas receiver). The characteristics of these entities are described respectively in subsections 2.2.1, 2.2.2 and 2.2.3.

2.2.1 Source entity

The source is the entity that converts the information message to be transmitted into electromagnetic waves. A MIMO source is divided into three main blocks : the modulator, the space-time encoder or the spatial multiplexer and the radio frequency (RF) device. These blocks are presented in Figure 2.1.

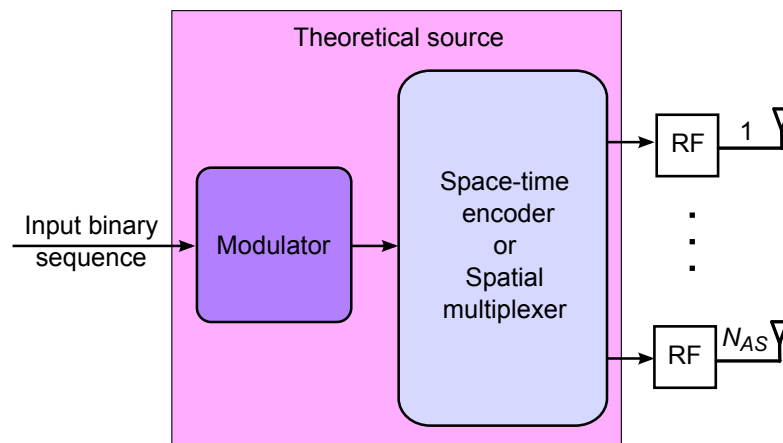


FIGURE 2.1 – Architecture of a MIMO source

Initially, the message to be transmitted is represented by a binary stream. This stream is first modulated into symbols using the modulator. Thereafter, a space-time encoder is used to divide the symbol stream into N_{AS} sample streams. Finally, an RF device performs the conversion of each sample into electromagnetic waves.

2.2.1.1 Modulator

The modulator is the element of the communication system that adapts the bitstream to the propagation channel, the required error rate and the available bandwidth. It maps

the digital information to appropriate signal waveforms. Modulation schemes are classified in several categories : with or without memory, linear or not. In our study, we consider linear modulation schemes without memory.

Mathematically, a linear modulation schemes without memory converts a block of $Bkc = \log_2(M)$ bits into a symbol s belonging to a constellation \mathcal{M} with $M = 2^{Bkc}$ complex elements. The throughput of the bandwidth is directly related to the number of bits per block. Indeed, increasing Bkc will improve the throughput, but it will also increase the probability of error in the demodulation phase.

In the present work, we focus on modulation schemes used by broadband technologies, which include M -ary amplitude shift keying (M -ASK), M -ary phase shift keying (M -PSK) and M -ary quadratic amplitude modulated (M -QAM) [31].

M -ASK modulation: This digital amplitude modulation encodes a block of Bkc bits into a real symbol s , in which the phase $\varphi(s)$ belongs to the set $\{0, \pi\}$ and the modulus $|s|$ belongs to a set composed by 2^{Bkc-1} elements. A M -ASK symbol is expressed mathematically as [31]

$$s = d \times (2v - 1 - M), \quad (2.1)$$

where $v \in [1, \dots, M]$ and $2 \times d$ is the distance between two adjacent amplitudes. Generally, the assignment of a block with Bkc bits into a ASK symbol is performed by a Gray code technique. Using this technique, the bit representation changes by only one bit between adjacent constellation points. This ensures the minimization of errors in the demodulation phase since only one bit will be erroneous when the constellation point is decoded by the adjacent one.

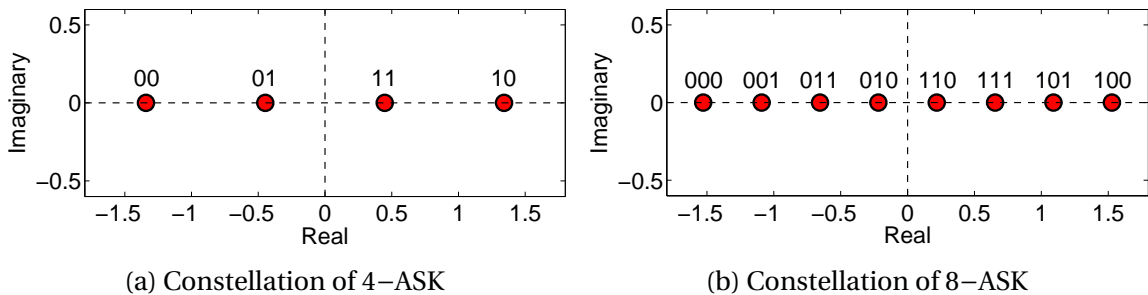


FIGURE 2.2 – Examples of constellations ASK with unit average symbol power ($E\{|s|^2\} = 1$)

As seen in Figure 2.2, 4-ASK encodes a block of $Bkc = 2$ bits into symbol belonging to a constellation $\mathcal{M} = \{-3d, -d, d, 3d\}$, while 8-ASK encodes a block of $Bkc = 3$ bits into

symbol belonging to a constellation $\mathcal{M} = \{-7d, -5d, -3d, -d, d, 3d, 5d, 7d\}$.

M -PSK modulation : This modulation scheme works by assigning a unique phase with a unitary module to each symbol s presented in the baseband waveform. An M -PSK symbol can be represented mathematically by [31]

$$s = \exp\left(\frac{2j\pi(v-1)}{M}\right) \quad (2.2)$$

where $v \in [0, \dots, M-1]$. For instance, a 2-PSK, which is also called a binary phase shift keying (BPSK), uses two opposite phases (see Figure 2.3a). As in ASK modulation, the assignment of a block with Bkc bits into a PSK symbol is generally performed by a Gray code technique.

Figure 2.3b presents the constellation of 4-PSK (also called quadrature phase shift keying (QPSK)). Here, QPSK encodes a block of $Bkc = 2$ bits into symbol belonging to a constellation $\mathcal{M} = \{1, \exp(j\frac{\pi}{2}), \exp(j\pi), \exp(-j\frac{\pi}{2})\}$.

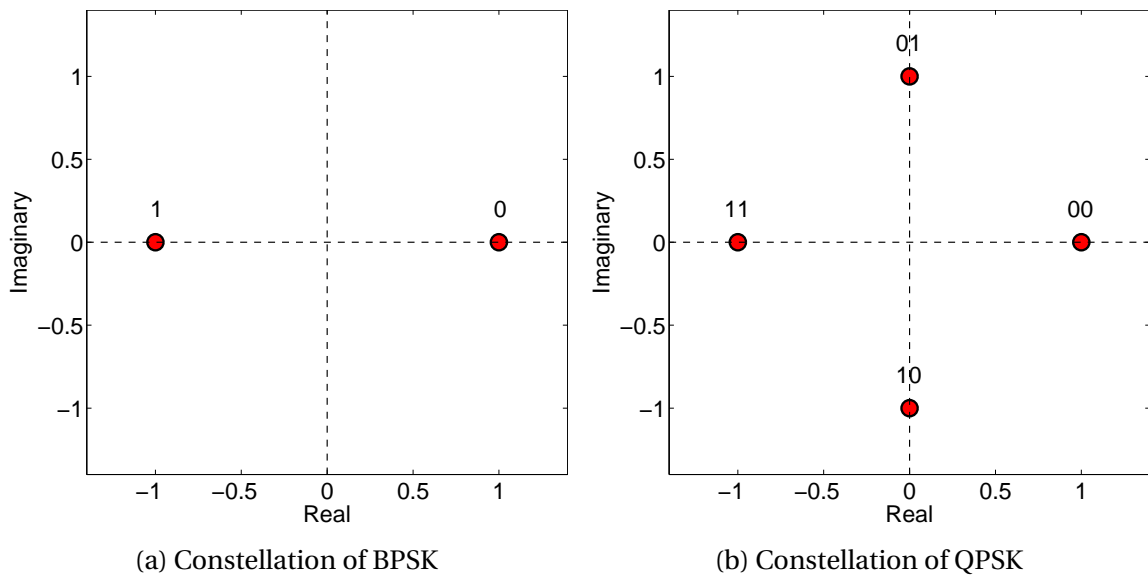


FIGURE 2.3 – Examples of PSK constellations with unit average symbol power ($E\{|s|^2\} = 1$)

Noting that there are variants of the M -PSK modulation introducing a constant phase shift to facilitate synchronization at the reception.

M -QAM modulation : Whereas PSK (ASK) only exploits the space of phases (amplitudes) to distinguish between symbols, QAM uses both the space of phases and the amplitudes jointly to optimize the bandwidth. A modulation M -QAM encodes a block of

Bkc bits into a complex symbol belonging to a constellation \mathcal{M} . For even values of Bkc , the constellations are square, while for odd values of Bkc the constellations have a cross shape and are hence called cross constellations. Figure 2.4a shows the constellation of 16-QAM which encodes a block of $Bkc = 4$ bits into complex symbol. The modulation scheme 32-QAM encodes a block of $Bkc = 5$ bits into complex symbol belonging to a cross constellation as seen in Figure 2.4b.

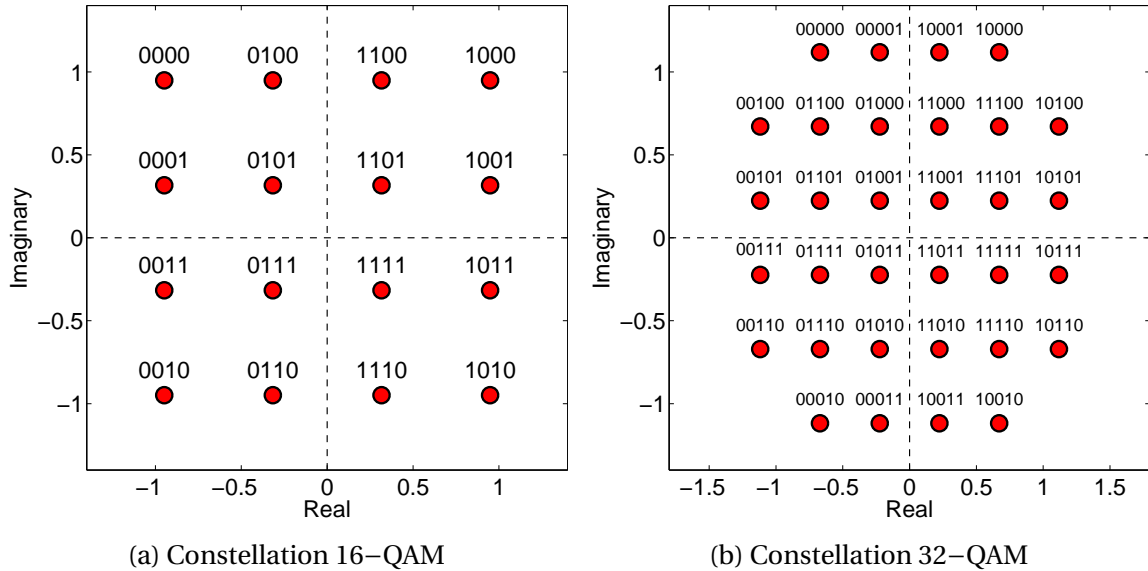


FIGURE 2.4 – Examples of QAM constellations with $E\{|s|^2\} = 1$

2.2.1.2 Space-time encoder

Space-time encoder is the entity that converts the symbols into N_{AS} sample stream, where N_{AS} is the number of the source antennas. Its purpose is to distribute information in the time-space domain in order to improve the throughput and/or robustness of a wireless transmission. Thus, they are useful for MIMO wireless systems to combat multipath fading and decrease the error probability. Since the pioneering work of Alamouti [2], this research area has received a lot of attention. Many space-time coding (STC) are designed for MIMO systems and implemented in several standards. An overview is provided in [32]. These codes fall into two main categories : space-time trellis codes (STTC) [33] and space-time block codes (STBC) [32]. In the current research, we focus on STBC codes because they are simpler to implement than STTC codes and thus are most commonly used. Indeed, MIMO-STBC wireless communication systems have been recently standardized in IEEE 802.16e and IEEE 802.11n and appear as a good technology for the next generation of wireless applications [34].

The main idea of STBC is to exploit the channel diversity through an appropriate encoding of the data streams into structured blocks. It has a coding rate $R_c = N_s/L_C$ which indicates that a block of N_s symbols are transmitted over L_C time slots. Mathematically, a space-time coding, denoted \mathcal{C} , encodes a block of N_s symbols, denoted $\mathbf{s} = [s_1, \dots, s_{N_s}]^T$ in a space-time block $\mathbf{C}(\mathbf{s})$ of size $N_{AS} \times L_C$. The columns of this block correspond to the temporal dimension, while the lines correspond to the spatial dimension. For a linear code, each element of $\mathbf{C}(\mathbf{s})$ is a linear combination of real and imaginary parts of symbols s_n , $n = 1 \dots N_s$. Given the fact that $\tilde{\mathbf{s}} = [\Re(\mathbf{s}^T), \Im(\mathbf{s}^T)]^T$ a vector of size $2N_s \times 1$ obtained by vertically concatenating the real and imaginary parts of \mathbf{s} , the block $\mathbf{C}(\mathbf{s})$ can be generally expressed as

$$\mathbf{C}(\mathbf{s}) = \underbrace{[\mathbf{B}_1(\tilde{\mathbf{s}}) \dots \mathbf{B}_{L_C}(\tilde{\mathbf{s}})]}_{\text{time}} \text{space} \quad (2.3)$$

$$= \sum_{n=1}^{N_s} (\mathbf{E}_n \Re(s_n) + j\mathbf{J}_n \Im(s_n)), \quad (2.4)$$

where \mathbf{E}_n and \mathbf{J}_n , are two matrices of size $N_{AS} \times L_C$ and \mathbf{B}_{l_c} , $1 \leq l_c \leq L_C$, are matrices of size $N_{AS} \times 2N_s$ correspond to the coding matrices, which depend only on the STBC used at the source node, where the first equation (2.3) corresponds to a temporal description of the coding while the second equation (2.4) corresponds to a symbol oriented description.

The linear block codes are numerous and divided into several subcategories. Spatial multiplexing, orthogonal codes [2, 35] and quasi-orthogonal codes [36] are being discussed in more details in the following paragraphs.

Spatial Multiplexing: The spatial multiplexing (SM) is not a space-time coding since it does not exploits the redundancy in the time domain (i.e., does not achieve space-time diversity). Nevertheless, for practical considerations, it is often considered as STBC [32].

SM favors the increase of the throughput with a coding rate of $R_c = N_{AS}$. This spatial encoding simultaneously transmits N_s symbols via the $N_{AS} = N_s$ source antennas. The transmitted blocks, $\mathbf{C}(\mathbf{s})$, have a length of $N_{AS} \times 1$ and can be expressed in terms of signals to be transmitted as

$$\mathbf{C}(\mathbf{s}) = \mathbf{s} = \begin{pmatrix} s_1 \\ \vdots \\ s_{N_s} \end{pmatrix}. \quad (2.5)$$

The coding matrix \mathbf{B}_1 is written as

$$\mathbf{B}_1 = [\mathbf{I}_{N_{AS}} \ j\mathbf{I}_{N_{AS}}],$$

where $\mathbf{I}_{N_{AS}}$ denotes the identity matrix of size $N_{AS} \times N_{AS}$.

It is well known that the optimum decoding of SM is very computationally expensive when the order M of the modulation \mathcal{M} is high and/or the number of the source antennas N_{AS} is large. Several techniques have been proposed in the literature to reduce the complexity of decoding, such as zero forcing (ZF), minimizing the mean square error (MMSE), vertical Bell laboratories layered space-time (V-BLAST) and sphere decoding (SD) [32].

Orthogonal Codes : The orthogonal codes (OSTBC) offer a dual benefit : first, they help to increase the robustness of wireless transmission by exploiting the spatial and temporal spatio-temporal redundancy. Secondly, they facilitate the implementation of the optimal decoder. The block matrix of an OSTBC code fulfills the following criterion of orthogonality [35]

$$\mathbf{C}(\mathbf{s})\mathbf{C}(\mathbf{s})^H = \lambda \left(\sum_{n=1}^{N_s} |s_n|^2 \right) \mathbf{I}_{N_{AS}}, \quad (2.6)$$

where λ is a real coefficient and $\mathbf{I}_{N_{AS}}$ denotes the identity matrix with dimension $N_{AS} \times N_{AS}$. Note that the criterion of orthogonality contributes to decoupling the decoding with respect to the transmitted symbols N_s .

These codes were originally proposed by Alamouti [2] for systems consisting of two transmitting antennas. In fact, the Alamouti code encodes a block of two symbols $\mathbf{s} = [s_1, s_2]^T$ into a matrix $\mathbf{C}(\mathbf{s})$ defined by

$$\mathbf{C}(\mathbf{s}) = [\mathbf{B}_1(\tilde{\mathbf{s}}) \ \mathbf{B}_2(\tilde{\mathbf{s}})] = \begin{pmatrix} s_1 & -\bar{s}_2 \\ s_2 & \bar{s}_1 \end{pmatrix}, \quad (2.7)$$

where the two coding matrices \mathbf{B}_1 and \mathbf{B}_2 are given, respectively, by

$$\mathbf{B}_1 = \begin{pmatrix} 1 & 0 & j & 0 \\ 0 & 1 & 0 & j \end{pmatrix}, \quad \mathbf{B}_2 = \begin{pmatrix} 0 & -1 & 0 & j \\ 0 & 0 & -j & 0 \end{pmatrix}. \quad (2.8)$$

In Equation (2.7), one can see that two symbols are transmitted over two consecutive time intervals. Indeed, s_1 and s_2 will be transmitted in the first time slot, from antennas 1 and 2, respectively. $-\bar{s}_2$ and \bar{s}_1 will be sent in the second time slot from antennas 1 and 2 respectively. Therefore, the Alamouti is a full rate code. The orthogonal property of this code can be shown in Equation (2.9).

$$\mathbf{C}_{:,1}^H \mathbf{C}_{:,2} = \begin{pmatrix} \bar{s}_1 & \bar{s}_2 \end{pmatrix} \begin{pmatrix} -\bar{s}_2 \\ \bar{s}_1 \end{pmatrix} = -\bar{s}_1 \bar{s}_2 + \bar{s}_2 \bar{s}_1 = 0. \quad (2.9)$$

Thereafter, Tarokh *et al.* designed OSTBC codes for systems which used more than two transmit antennas (i.e., $N_{AS} \geq 2$) [35]. The major drawback of these codes resides in their coding rate. Indeed, they have a coding rate strictly less than the unity. In the following, R_c OSTBC N_{AS} notation has been used to represent different codes. An orthogonal code using a coding rate of 1/2 with three transmit antennas 1/2OSTBC3 can be described as [35]

$$\mathbf{C}(\mathbf{s}) = \begin{pmatrix} s_1 & -s_2 & -s_3 & -s_4 & \bar{s}_1 & -\bar{s}_2 & -\bar{s}_3 & -\bar{s}_4 \\ s_2 & s_1 & s_4 & -s_3 & \bar{s}_2 & \bar{s}_1 & \bar{s}_4 & -\bar{s}_3 \\ s_3 & -s_4 & s_1 & s_2 & \bar{s}_3 & -\bar{s}_4 & \bar{s}_1 & \bar{s}_2 \end{pmatrix}. \quad (2.10)$$

Quasi-orthogonal Codes: The Quasi-Orthogonal codes (Q-OSTBC) allow to achieve coding rates higher than the rate of OSTBC codes for systems which employed greater than two transmit antennas (i.e., $N_{AS} > 2$). Most Q-OSTBC codes, which are presented in the literature, encode four symbols (i.e., $N_s = 4$) in a matrix $\mathbf{C}(\mathbf{s})$ of size 4×4 [36–38]. These codes are obtained by concatenating several orthogonal codes, so that the coding matrix $\mathbf{C}(\mathbf{s})$ satisfies the following criterion

$$\mathbf{C}(\mathbf{s})\mathbf{C}(\mathbf{s})^H = \sum_{n=1}^{N_s} |s_n|^2 \begin{pmatrix} \mathbf{I}_2 & \lambda \mathbf{D}^{(1)} \mathbf{M} \\ \lambda \mathbf{D}^{(2)} \mathbf{M} & \mathbf{I}_2 \end{pmatrix}, \quad (2.11)$$

where λ is a coefficient less than one (i.e., $\lambda < 1$), \mathbf{M} represents a permutation matrix of size 2×2 , $\mathbf{D}^{(1)}$ and $\mathbf{D}^{(2)}$ are two diagonal matrices of size 2×2 containing elements belonging to $\{-1, 1\}$. Like OSTBC, Q-OSTBC can be used to reduce the complexity of decoding.

Jafarkhani proposes in [36] a Q-OSTBC code with a unitary coding rate for $N_{AS} = 4$ defined as

$$\mathbf{C}(\mathbf{s}) = \begin{pmatrix} s_1 & -\bar{s}_2 & -\bar{s}_3 & s_4 \\ s_2 & \bar{s}_1 & -\bar{s}_4 & -s_3 \\ s_3 & -\bar{s}_4 & \bar{s}_1 & -s_2 \\ s_4 & \bar{s}_3 & \bar{s}_2 & s_1 \end{pmatrix}. \quad (2.12)$$

Furthermore, Tirkkonen *et al.* introduced a Q-OSTBC with a unitary coding rate for $N_{AS} = 4$ described as [37]

$$\mathbf{C}(\mathbf{s}) = \begin{pmatrix} s_1 & \bar{s}_2 & s_3 & \bar{s}_4 \\ s_2 & -\bar{s}_1 & s_1 & -\bar{s}_3 \\ s_3 & \bar{s}_4 & s_2 & \bar{s}_2 \\ s_4 & -\bar{s}_3 & s_4 & -\bar{s}_1 \end{pmatrix}. \quad (2.13)$$

2.2.1.3 Radio-frequency (RF) device

At the output of the encoder, the symbol stream is partitioned into N_{AS} blocks. The RF device is the entity that converts each block to an electromagnetic wave. Figure 2.5 illustrates the general architecture of this device.

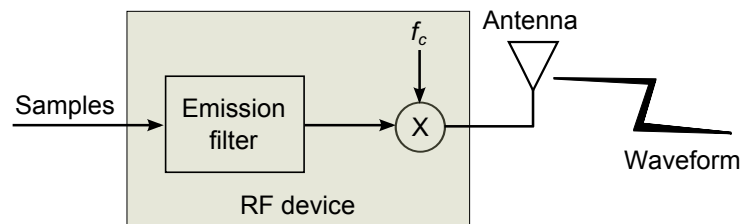


FIGURE 2.5 – Architecture of RF device

At the input of the RF device, the samples are clocked by a clock whose frequency is $f_s = \frac{1}{T_s}$, where T_s denotes the symbol duration. To limit the bandwidth of the signal, a low-pass filter, called an emission filter, is applied to the signal. At the output of this filter, the signal is transposed into the frequency domain to respect the allocation rules of the

propagation channel. This operation is performed by multiplying the signal by a carrier frequency f_c as shown in Figure 2.5. Finally, the signal is transmitted as an electromagnetic wave in the propagation environment.

2.2.1.4 MIMO Precoding

Precoding is a paradigm that exploits the CSI at the source node in order to match the transmission to the instantaneous channel conditions [39, 40]. Applying a precoding strategy at the source node before transmitting the signal can reduce the performance loss caused by channel fading and interference. In the literature, linear and non-linear precoding strategies have been proposed [41]. In practice, linear precoding methods are more feasible due to their lower complexity compared to non-linear methods. Figure 2.6 gives a simple illustration of a MIMO system with linear precoding. Note that linear precoding methods include ZF and RZF.

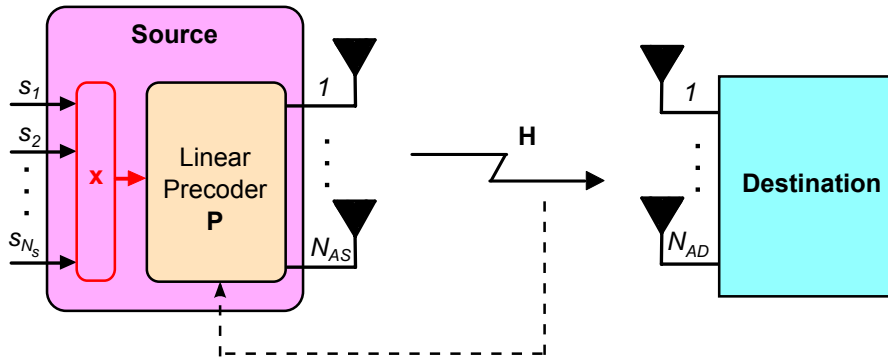


FIGURE 2.6 – Schematic diagram of a MIMO system with a linear precoder

Zero-Forcing Precoding : The ZF precoder is designed to completely force all interference terms to zero at the destination node, i.e., zero-force the interference. It is well studied in the literature through performance measures such as fairness and throughput under the assumptions of both total and per antenna power constraints [42]. This method is also referred to as "channel inversion" [43].

By using the MoorePenrose pseudoinverse [44] of the channel matrix \mathbf{H} , the ZF precoding matrix is given by

$$\mathbf{P}_{ZF} = \mathbf{H}^\dagger = \mathbf{H}^H (\mathbf{H}\mathbf{H}^H)^{-1}. \quad (2.14)$$

Note that the required computational time of matrix inversion in the ZF precoder is

high. On the other hand, ZF causes a noise increase when it is employed at the destination node. An additional term is added to equation (2.14) to give a regularized ZF, which can be expressed as [45]

$$\mathbf{P}_{\text{RZF}} = \mathbf{H}^H (\mathbf{H}\mathbf{H}^H + \alpha\mathbf{I})^{-1}. \quad (2.15)$$

where α is a regularization parameter.

2.2.2 Propagation Environment

The N_{AS} electromagnetic waves generated by the source node propagate in an environment before being received by multiple destination antennas. During the propagation, two phenomena are involved. First, the waves undergo various modifications related to their interaction with the environment. Depending on the geometry and material of the objects, these modifications are essentially of three types : reflection, diffraction and scattering [46] as displayed in Figure 2.7.

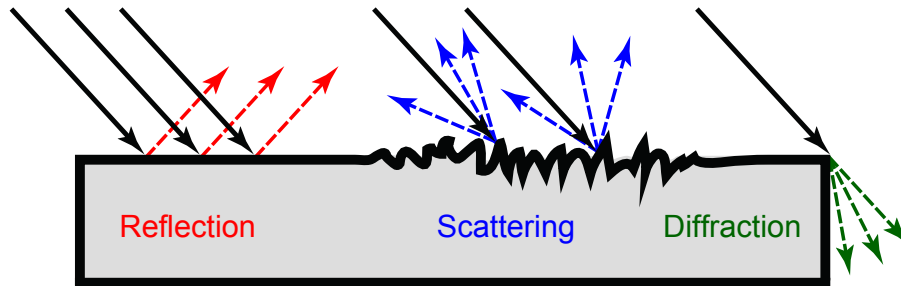


FIGURE 2.7 – Effects of radio wave propagation

Second, the received signals are degraded by the superposition of extraneous signals with the useful signal. These signals, called noise, are added to the received signal at each antenna.

Throughout this manuscript, we use the term "communication channel" to designate the set that is composed by the RF device of both the source and destination nodes and the propagation environment.

Assuming that the RF operations are performed perfectly, the received signals $\mathbf{y}(\tau) = [y_1(\tau), \dots, y_{N_{AD}}(\tau)]^T$ at the time instant τ are expressed in the baseband as

$$\mathbf{y}(\tau) = \mathbf{g}(\tau) + \mathbf{n}(\tau), \quad (2.16)$$

where $\mathbf{g}(\tau)$ depends on the propagation environment and the transmitted signals $\mathbf{x}(\tau)$, and $\mathbf{n}(\tau)$ models the additive noise (see Figure 2.8). In the following, we present these two terms, i.e., $\mathbf{g}(\tau)$ and $\mathbf{n}(\tau)$.

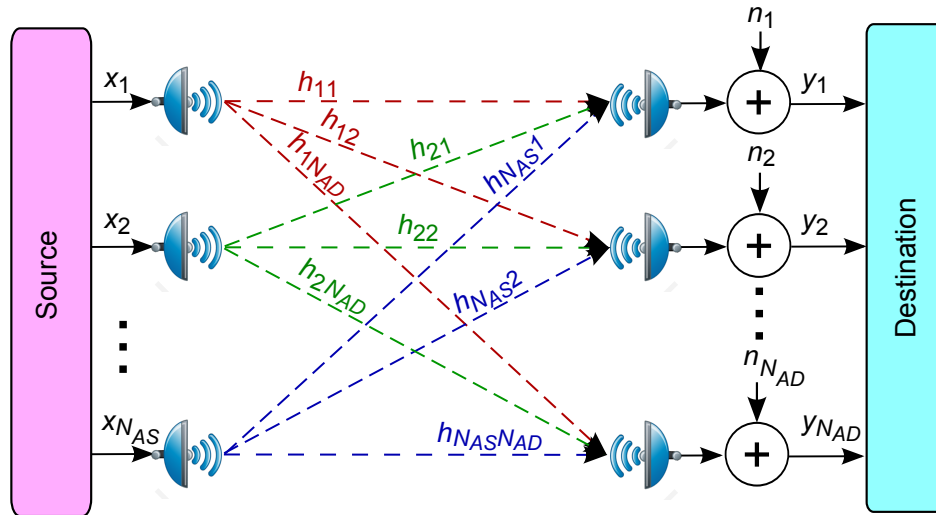


FIGURE 2.8 – Diagram of a MIMO system with N_{AS} transmit antennas and N_{AD} receive antennas

2.2.2.1 Fading Channels

In wireless communication systems, Surrounding objects like buildings, houses, mountains and trees cause reflection, diffraction, scattering and shadowing of the transmitted signals and provoke multipath propagation. The multipath phenomenon causes the arrival of transmitted signals to the destination node with different amplitudes, different phase angles and at different times. The signal fading, which represents the amplitude fluctuation of the received signal, is caused by the time variant or the frequency selective characteristics of the multipath channel. As shown in Figure 2.9, one can distinguish between two categories of components. The line of sight (LOS) components represent the strongest components. They are directly transmitted from the source to the destination without any reflection, while other components are reflected. They are referred to as scattering components or non-line of sight (NLOS). In a LOS environment (Figure 2.9a), the probability density function of the received signal follows a Rician distribution, while a Rayleigh distribution is followed in a NLOS environment (Figure 2.9b).

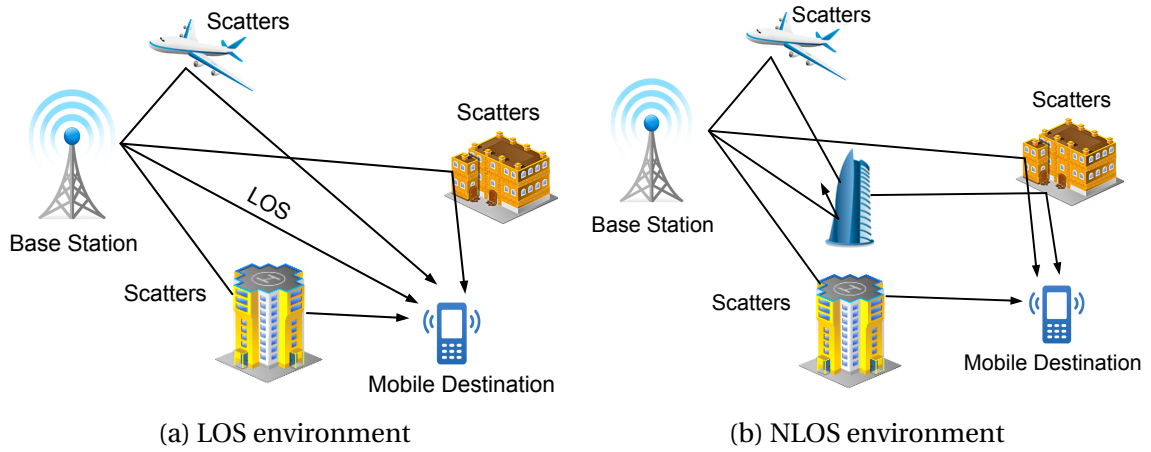


FIGURE 2.9 – Propagation of a signal in a wireless environment, with and without LOS

Assuming that the bandwidth of the transmitted signal is sufficiently smaller than the channel coherence band to neglect inter-symbol interference (ISI) and that the transmission time is lower than the channel coherence time, the characteristics of the communication channel do not depend on neither the frequency nor the time. Thus, the channel is known as a frequency-flat and time-invariant channel. Under this assumption, the samples $\mathbf{g}(\tau) = [g_1(\tau), \dots, g_{n_r}(\tau)]^T$ are expressed in terms of the transmitted samples $\mathbf{x}(\tau)$ as

$$\mathbf{g}(\tau) = \mathbf{H}\mathbf{x}(\tau) = \begin{pmatrix} h_{11} & \cdots & h_{1N_{AS}} \\ \vdots & \ddots & \vdots \\ h_{N_{AD}1} & \cdots & h_{N_{AD}N_{AS}} \end{pmatrix} \begin{pmatrix} x_1(\tau) \\ \vdots \\ x_{N_{AS}}(\tau) \end{pmatrix}, \quad (2.17)$$

where \mathbf{H} is an $N_{AD} \times N_{AS}$ matrix with h_{ds} the path gain between the destination antenna d and the source antenna s .

In the following, we give a mathematical description for different typical channel models which will be considered throughout the thesis.

Rayleigh Fading : The most widely employed fading model in the literature is Rayleigh fading. It is often used to model propagation paths consisting of NLOS component. Here, the channel fading amplitude distribution h_{ds} can be expressed as

$$p(h_{ds}) = \frac{2h_{ds}}{\Omega} \exp\left(-\frac{h_{ds}^2}{\Omega}\right), \quad h_{ds} \geq 0, \quad (2.18)$$

where $\Omega = \mathbb{E}\{h_{ds}^2\}$ is the average power.

Rician Fading : In contrast to Rayleigh fading, Rician fading provides a good fit for multipath fading channels with a LOS path and many random weaker components. The channel fading amplitude is distributed according to

$$p(h_{ds}) = \frac{2(1+n^2)\exp(-n^2)h_{ds}}{\Omega} \exp\left(-\frac{(1+n^2)h_{ds}^2}{\Omega}\right) I_0\left(2nh_{ds}\sqrt{\frac{1+n^2}{\Omega}}\right), h_{ds} \geq 0, \quad (2.19)$$

where n denotes the fading parameter, which ranges from 0 to ∞ , and is related to the Rician K factor by $K = n^2$ which corresponding to the ratio of the power of the LOS component to the average power of the scattered component. $I_0(\cdot)$ represents the zero-order modified Bessel function of the first kind.

Nakagami- m Fading : Nakagami- m fading model was shown to fit the experimental propagation data better than that of Rayleigh, Rician, and log-normal distributions [47]. In fact, this distribution is more flexible since it contains the one-sided Gaussian distribution ($m = 0.5$), the Rayleigh distribution ($m = 1$), and the uniform distribution on the unit circle ($m \rightarrow \infty$) as extreme cases. Thus, Nakagami distributions can model fading conditions that are more or less severe than those of Rayleigh [48]. It often gives the best fit to landmobile [47, 49] and indoor-mobile [50] multipath propagation, as well as scintillating ionospheric radio links [51].

The channel fading amplitude distribution is given by

$$p(h_{ds}) = \frac{2m^m h_{ds}^{2m-1}}{\Omega^m \Gamma(m)} \exp\left(-\frac{m h_{ds}^2}{\Omega}\right), h_{ds} \geq 0, \quad (2.20)$$

where $\Gamma(\cdot)$ expresses the Gamma function (i.e., $\Gamma(m) = \int_0^\infty t^{m-1} \exp(-t) dt$) and m represents the fading parameter, which ranges from $1/2$ to ∞ . In the case when $m = 1$, Nakagami- m distribution can be reduced to Rayleigh distribution. In addition, Nakagami- m distribution can closely approximate the Rician distribution using a one-to-one mapping between the m parameter and the K parameter [52]. This mapping is given by

$$K = \frac{\sqrt{m^2 - m}}{m - \sqrt{m^2 - m}}, m \geq 1, \quad (2.21)$$

or

$$m = \frac{(K+1)^2}{2K+1}, K \geq 0. \quad (2.22)$$

Spatially-Correlated MIMO Channel : Realistic MIMO channels present spatial correlation due to the clustering of scatterers in the propagation environment. Generally, this correlation has a negative effect on capacity and error rate performance [15, 53]. Therefore, the performance evaluation of practical MIMO systems requires considering realistically correlated channels. Various analytical models for simulating correlated MIMO channels can be found in the literature. In this thesis, we adopt the Kronecker model [15], which assumes that spatial transmitter and receiver correlations are separable into two correlation matrices as follows :

$$\mathbf{H} = \mathbf{R}_{Rx}^{1/2} \mathbf{H}_w \mathbf{R}_{Tx}^{1/2}, \quad (2.23)$$

where \mathbf{R}_{Tx} and \mathbf{R}_{Rx} represent the transmitter and the receiver correlation matrices, respectively. \mathbf{H}_w is a full rank gain matrix which the entries are independent, identically distributed (i.i.d.) and follow a circularly symmetric complex Gaussian distribution with zero-mean and unit variance. Under this model, the total correlation of the channel \mathbf{R}_H can be expressed as the Kronecker product (i.e., \otimes) of the correlation matrices \mathbf{R}_{Tx} and \mathbf{R}_{Rx} as follows :

$$\mathbf{R}_H = \mathbf{R}_{Tx} \otimes \mathbf{R}_{Rx}. \quad (2.24)$$

The fading correlation at the source and at the destination can be described by the exponential correlation model presented in [54]. In this case, the components of the correlation matrix \mathbf{R} are given by

$$(\mathbf{R})_{pq} = \begin{cases} \rho^{q-p}, & p \leq q \\ \overline{(\mathbf{R})_{qp}}, & p > q \end{cases}, |\rho| < 1, \quad (2.25)$$

where ρ represents the complex correlation coefficient of neighboring transmit branches and $(\mathbf{R})_{pq}$ denotes the $(p, q)^{\text{th}}$ entry in the p^{th} row and the q^{th} column of \mathbf{R} . The two matrices \mathbf{R}_{Rx} and \mathbf{R}_{Tx} are defined by the receive correlation coefficients ρ_{Rx} and the transmit correlation coefficients ρ_{Tx} , respectively. It is noteworthy that this correlation model is physically reasonable in the sense that the correlation between neighboring channels is

higher than that between distant channels.

Imperfect Channel Estimation Model : Assuming perfect CSI is untenable in practice to determine theoretically real performance. Note that this is a crucial assumption since poor CSI quality can greatly degrade the performance of all precoding techniques. Thus, the source has to know the CSI of the downlink channel by feedback signaling from the uplink. In practical systems, it is relatively difficult to obtain perfect CSI available at all nodes. For this reason, a great deal of research has been carried out to assess the impact of imperfect CSI on the system's behavior. An overview of this research area is provided in [55].

Imperfect CSI may arise due to errors caused by channel estimation, reciprocity mismatch, quantization, and delay [16, 56]. It can be modeled as a complex Gaussian distributed. Thus, the channel estimate can be expressed as [16]

$$\hat{\mathbf{H}} = \mathbf{H} + e\mathbf{\Omega}, \quad (2.26)$$

where $\mathbf{\Omega}$ is a matrix independent of \mathbf{H} , whose entries are i.i.d. zero-mean circularly symmetric complex Gaussian variables with unit variance and e is the estimation error variances of channel.

2.2.2.2 Additive Noise

In communication systems, noise is normally modeled as additive white Gaussian noise (AWGN). It is considered as a common noise model for numerical and analytical analysis since it can approximate many noise sources. It is additive, so it is added to the signal; it is white, meaning that the power for all frequencies is identical within the bandwidth of the system and it is Gaussian, meaning that their real and imaginary values follow a Gaussian distribution. One way to characterize the noise level is to calculate the SNR. Given the fact that the average power of the noise at each antenna is σ_n^2 , the SNR is defined as [57]

$$\text{SNR} = 10\log_{10} \left(N_{AS} \frac{\sigma_x^2}{\sigma_n^2} \right) \quad (2.27)$$

where σ_x^2 denotes the average power of samples at each source antenna.

2.2.3 Destination entity

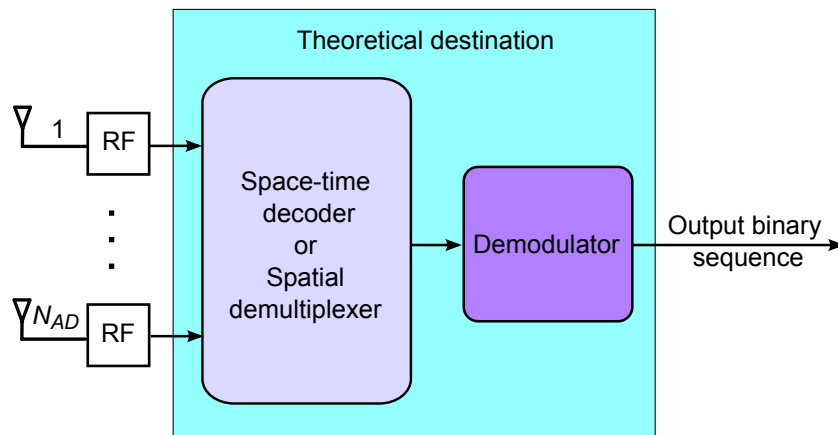


FIGURE 2.10 – Architecture of a MIMO destination

The destination is the entity that converts the N_{AS} received waves into a binary stream. Its architecture is shown in Figure 2.10. Here, the destination employs the decoder, or spatial demultiplexer and the demodulator to recover the transmitted binary information. Therefore, the estimation of the transmitted binary information requires a prior knowledge of the number of the source antennas (N_{AS}), the noise variance (σ_n^2), the coding (\mathcal{C}), the channel matrix (\mathbf{H}), and the modulation (\mathcal{M}) as depicted in Figure 2.11.

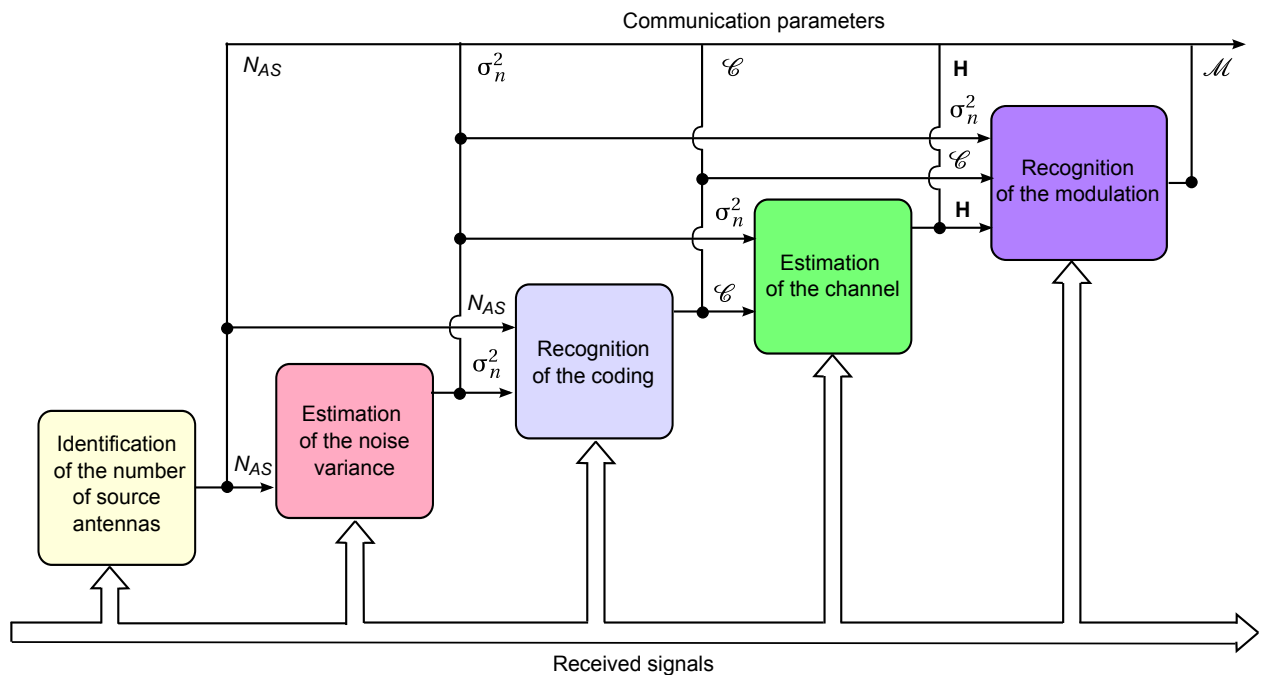


FIGURE 2.11 – Estimation of the transmitted bitstream

Many estimation algorithms of the number of the source antennas N_{AS} have been de-

veloped in literature [58–63]. Also, several approaches have been proposed for the recognition of the coding [64–66] and other algorithms for estimating the channel matrix are also available [67–69]. In the last few decades, there has been great interest in modulation recognition for SISO and MIMO communications systems [24, 26, 70, 71].

The current work is focusing on modulation recognition for cooperative MIMO communication systems. Therefore, in the following, we present a brief summary of the existing work on modulation recognition for SISO and MIMO systems.

2.3 Modulation Recognition for SISO and MIMO Systems

2.3.1 Modulation Recognition for SISO Systems

Most of the existing algorithms for modulation recognition assume that the source employs a single antenna. These algorithms can be divided into two categories. The first one is based on a decision-theoretic approach. It represents a probabilistic solution based on a priori knowledge of probability functions and certain hypotheses [18, 20]. This approach presents three weaknesses : high computational complexity, difficulties in forming the right hypothesis, and the need for careful analyses to set the correct threshold values. The second category is based on the pattern recognition approach. It is easier to implement and reaches a quasi-optimal performance if the proper features set is chosen. This approach is decomposed into two subsystems. The first subsystem is the features extraction. It involves extracting some basic characteristics of the received signal [21–23, 72]. Nevertheless, choosing an adequate feature set is an issue since there are many techniques used to extract the signal features necessary for digital modulation recognition. These techniques include cyclostationarity signatures [23], wavelets transforms [73], higher order statistics [22] and spectral based features set [21]. The second subsystem is the classifier subsystem, which is responsible of classifying the received signals based on the extracted features.

Nandi *et al.* proposed a modulation recognizer using several key features based on the instantaneous amplitude, the instantaneous phase and the instantaneous frequency of the intercepted signal [74]. The modulation schemes that can be classified by this recognizer are the 2–ASK, 4–ASK, 2–PSK, 4–PSK, 2–FSK, and 4–FSK digital modulation schemes. The classifier structure used in this work is a single hidden layer artificial neural

network (ANN) with 4-node input layer, 25 node hidden layer and 7 node output layer. It was shown that the ANN algorithm is more efficient than the decision theoretic algorithm where it achieves over 96% detection rate for an SNR of 15 dB.

Hong *et al.* investigated the use of wavelet transform to discriminate between QAM, PSK and FSK signals [75]. Their proposal consists of extracting the transient characteristics of a digital modulation signal using the wavelet transform and applying the distinct pattern in the wavelet transform domain for simple recognition. They claimed that the percentage of correct recognition is about 97% for SNR greater than 5 dB using 50 observation symbols.

A low complexity method based on elementary fourth-order cumulants is introduced by Swami *et al.* [76]. The purpose of this method is to recognize several digital modulation schemes in a hierarchical manner. By deriving the expressions for the variance of the estimates of the cumulants, classification thresholds were developed. Furthermore, the statistics employed by the classifier can be recursively updated. Their proposed approach is robust due to the resistance offered by the higher order statistics (HOS) to additive colored Gaussian noise and a natural robustness to constellation rotation and phase jitter.

Wong *et al.* [21] extended the work proposed by Nandi *et al.* [74], where a resilient backpropagation (RPROP) is used as a training algorithm for multi-layer ANN classifier, which enhances the performance and epoch times by a large margin. Moreover, additional modulation schemes were included (e.g., V29, V32, 16-QAM and 64-QAM), and an extra features set based on the HOS of the signal was investigated. To select the best feature subset from the combined statistical and spectral features sets, the authors employed a genetic algorithm (GA). RPROP ANN classifier achieves about 99% recognition performance on most SNR levels using only six features selected by GA.

2.3.2 Modulation Recognition for MIMO Systems

Various modulation identification algorithms have been proposed for MIMO systems [17, 24, 25, 58, 77] and references therein.

For uncorrelated MIMO systems, two likelihood based modulation classifiers have been proposed by Choqueuse *et. al* [78]. The first classifier is named the average likelihood ratio test (ALRT). This approach is optimal in the Bayesian sense but requires the knowledge of the CSI. The second classifier is named the hybrid likelihood ratio test

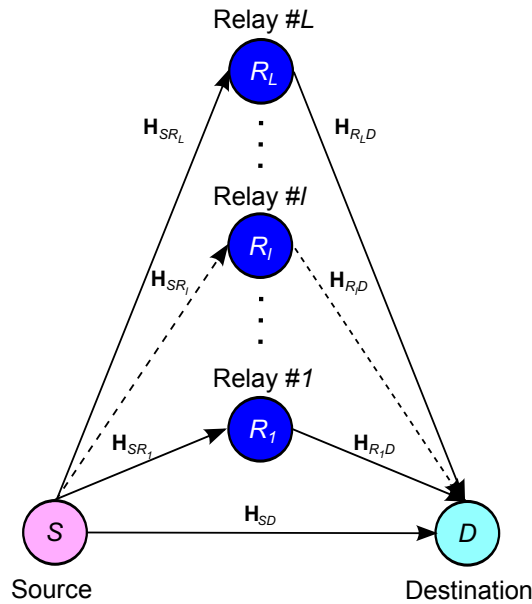
(HLRT). It approximates the ALRT by replacing the channel matrix with its estimate. Here, two steps are performed to estimate the channel by using an independent component analysis and a phase correction algorithm, respectively. At a SNR of 5 dB, the two classifiers perform well since they have the ability to perfectly recognize 2-PSK, 4-PSK, 16-PSK and 16-QAM modulations.

Hassan *et al.* [26] studied blind digital modulation recognition for spatially-correlated MIMO systems in the non-cooperative context, based on the use of an ANN classifier. However, this classifier has a complicated network structure, needs a long training time and has a low speed of convergence. Besides, the proposed zero forcing digital modulation recognition (ZF-DMI) algorithm is sensitive to channel estimation errors and suffers from rapid performance degradation when the variance of the channel estimation error becomes greater than or equal to 0.1.

Even many works have been carried out in the last years, the optimal modulation recognition algorithm never achieved. Indeed, some algorithms demand high SNR to perform well, or require some prior information, while others are too complex to be used in online applications such as modulation recognition for CR. Recently, there has been a great deal of research on cooperative MIMO systems and all previous works, however, did not consider modulation recognition in this context. Indeed, cooperative communications with the aid of relay nodes have garnered significant interest [9, 10, 79–81].

2.4 Cooperative MIMO Systems

A cooperative MIMO system is an extension of the MIMO system described in Section (2.2) [80, 82, 83]. As shown in Figure 2.12, the transmission of data signals from the source (S) node to the destination (D) node is aided by L -relay (R_l , $l = 1, 2, \dots, L$) nodes. Thus, R_l can offer a spatial multiplexing gain, even if S does not have multiple source antennas, as long as D has multiple antennas [84]. Here, \mathbf{H}_{SD} , \mathbf{H}_{SR_l} , and \mathbf{H}_{R_lD} , $l = 1, 2, \dots, L$, denote the channels.

FIGURE 2.12 – Cooperative MIMO system using L -relay nodes

To achieve cooperative diversity, various cooperation strategies with different relaying techniques have been proposed [79]. The most popular forwarding modes are the amplify-and-forward (AF, also known as “non-regenerative”) [79,85,86] and the decode-and-forward (DF) [87, 88]. The term “non-regenerative” implies that the relay does not regenerate (decode) the signal, but it does not necessarily mean a linear weighting (amplification) at the relay. Indeed, other strategies like quantize-and-forward can also fit into the category of non-regenerative relaying. In the AF mode, the relay nodes simply amplify the received signals prior to retransmitting them, while in the DF mode, the relay nodes decode the received signals and then transmit them to the destination node. AF mode is of a particular interest due to its low complexity compared to the DF [89,90]. In fact, this mode only requires the multiplication of the received signal with an amplification factor, whereas the DF mode requires decoding the received signal at the relay node before the retransmission to the destination node.

In recent years, MIMO relaying broadcast networks have attracted a great deal of attention from both academic and industrial communities. This communication strategy assumes that information source is transmitted via two independent channels : (i) relay channel consisting of backward channel (i.e., SR links) and forward channel (i.e., RD links) and (ii) direct channel (i.e., SD link). Ignoring the direct link is reasonable in some scenarios, such as; where the distance between the source and destination is very large, causing significant link loss and absorption of the source signal. Practically, this consideration is

not always true. Indeed, cooperative systems based on relaying with direct link [11, 91] can improve the transmission performance, where spatial diversity is improved and the coverage of wireless networks is extended. In MIMO relaying broadcast networks, linear transmission strategies have been well investigated [11, 92–94]. In [11], a linear transmission strategy is used to design the linear precoding matrix (PM) at S and the beamforming matrix (BM) at each R . Specifically, a regularized zero forcing (RZF) [95] and a zero forcing-RZF (ZF-RZF) [11] are respectively employed to the backward channel and forward channel to ensure a good performance.

Moreover, the use of the PLNC scheme can be used to improve the throughput performance of wireless relaying networks [30]. In the literature, two relaying strategies of PLNC are generally used, namely the denoise-and-forward (DNF) [96] strategy and the AF [97] strategy. When using the AF strategy, the relay node simply amplifies the received signals before forwarding them to the destinations. Despite the latter method is easy to implement, it suffers from noise amplification and signal attenuation [98]. In contrast, the DNF strategy can reduce the effect of noise amplification and hence achieve better performance compared to the AF method [99]. In chapter 5, we will consider a TWRC where two source nodes S_1 and S_2 communicate with each other using a relay node R (See Figure 2.13). For each transmission, S_1 and S_2 can diversify the modulation depending on the applications according to their requirement. Noting that S_1 (S_2) requires the recognition of the the modulation used by S_2 (S_1) to demodulate the received signal. Thus, a perfect recognition of the sources modulations schemes and orders is mandatory to guarantee a correct data reception at the destinations.

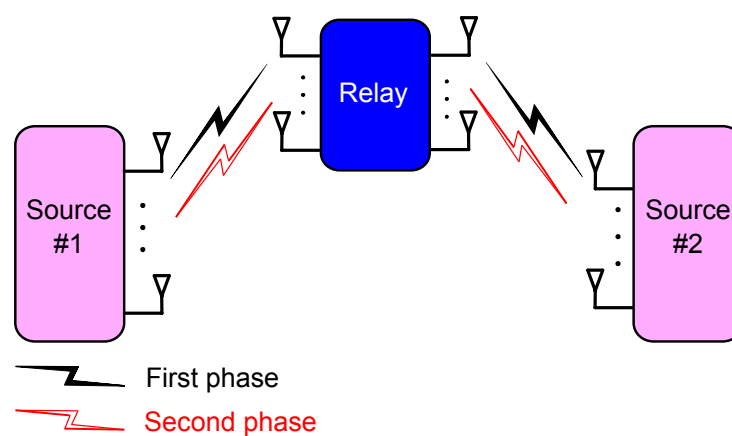


FIGURE 2.13 – Two-way MIMO relay channels

2.5 Conclusion

This chapter presented a historical overview of the most related work in the fields of MIMO systems, modulation recognition for SISO and MIMO systems and cooperative MIMO networks. Although this literature review showed that significant progress has been made in all these fields of research, none of them address the issue of modulation recognition in cooperative MIMO systems.

The purpose of this dissertation is to address the challenges in existing work and move forward the state of the art. To achieve this goal while considering the earlier discussed constraints, the next chapter is discussing the modulation recognition for cooperative MIMO system over uncorrelated channels with perfect CSI.

Modulation recognition for cooperative MIMO systems over uncorrelated channels with perfect CSI

Contents

3.1 Introduction	30
3.2 System Model and Preliminaries	30
3.2.1 Source Node Precoding Design based on RZF	31
3.2.2 Relay Node Beamforming Design Based on ZF-RZF	32
3.2.3 Destination Node Combining	33
3.3 Modulation Recognition Algorithm	33
3.3.1 Features Extraction	33
3.3.2 Classifiers	36
3.3.3 Metric for evaluating the effectiveness of classifiers	39
3.4 Results and Discussion	41
3.4.1 Performance comparison of J48 and MLP classifiers	42
3.4.2 Performance comparison of J48, NBD and TAN classifiers	44
3.5 Conclusion	47

3.1 Introduction

As already mentioned in Chapter 2, the bitstream of a digital communication is adapted to the transmission channel through the modulation process. The modulation must be adapted to the required performance, the available bandwidth, and the characteristics of the propagation channel. There are a variety of modulation schemes and knowledge of this parameter is essential for the reception to select the appropriate demodulator at the destination node and, hence, recover the transmitted bitstream. Currently, modulation recognition is an issue that has a significant literature in the context of SISO and MIMO communications. To the best of our knowledge, its extension to the cooperative context is a recent topic.

In this chapter, we introduce an algorithm for modulation recognition designed for cooperative MIMO systems over uncorrelated channels with perfect CSI. The goal is to recognize different modulation schemes supported by broadband technologies that include M -PSK and M -QAM signals.

The remainder of this chapter is organized as follows : Section 3.2 describes the system model. We present in Section 3.3 the proposed modulation recognition algorithm. Section 3.4 is dedicated to the performance analysis of the proposed algorithm. Finally, Section 3.5 concludes the chapter and summarizes the key findings.

3.2 System Model and Preliminaries

In this chapter, the considered transmission system is a MIMO relaying broadcast channel with one source (S), relay (R) and destination (D) nodes as depicted in Figure 3.1. Here, we assume that S , R and D are equipped with N_{AS} , N_{AR} and N_{AD} antennas, respectively. A two-time-slot protocol is used to transmit data from S to D via the direct link SD and the cooperative one SR - RD . When S implements SM, the requirements $\{N_{AD} \geq N_{AS}, N_{AR} \geq N_{AS}\}$ must be satisfied if D and R are to support all the N_{AS} independent substreams simultaneously. Here, we assume that $N_{AS} = N_{AR} = N_{AD} = N_A$ for the sake of simplicity. We also assume that a non-regenerative and half-duplex relaying scheme applied at R to process and forward the received signals [79].

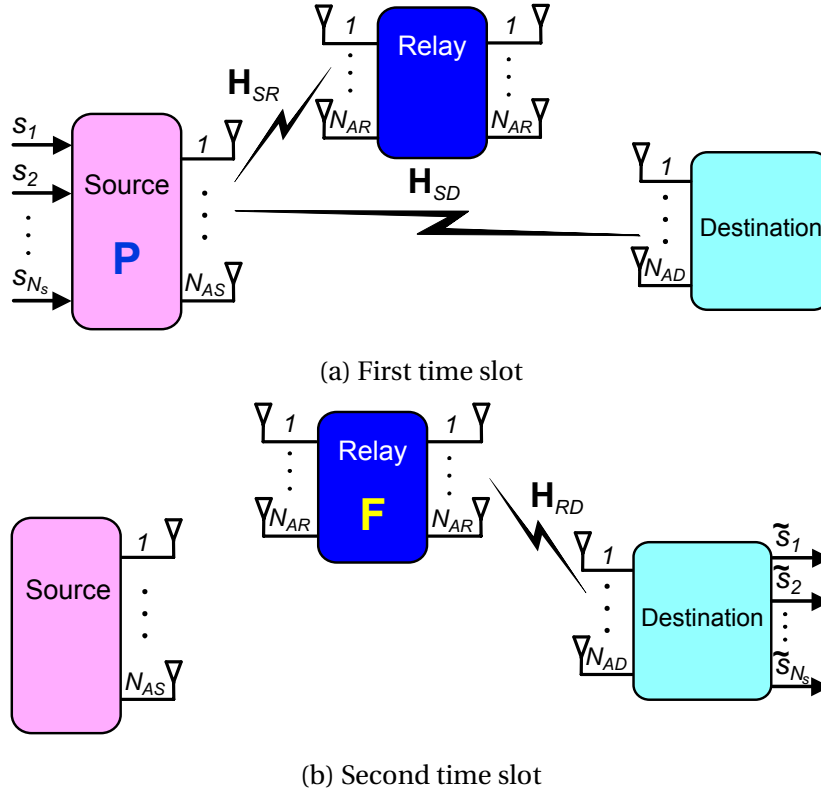


FIGURE 3.1 – MIMO relaying broadcast network with source, relay and destination nodes using two-time-slot protocol

3.2.1 Source Node Precoding Design based on RZF

During the first time slot (see Figure 3.1a), we use spatial multiplexing (SM) to transmit multiple data stream. Thus, the coding rate $R_c = N_{AS} = N_A$ because the code length $L_C = 1$ and $N_s = N_A$, i.e., $\mathbf{x} = [s_1, s_2, \dots, s_{N_A}]^T$.

Next, a RZF precoder [45] is applied to the data vector $\mathbf{x} = [x_1, x_2, \dots, x_{N_A}]^T$.

The RZF is defined by a linear precoding matrix \mathbf{P} as

$$\mathbf{P} = \mathbf{H}_{SD}^H (\mathbf{H}_{SD} \mathbf{H}_{SD}^H + \alpha_1 \mathbf{I}_{N_A})^{-1}, \quad (3.1)$$

where $\mathbf{H}_{SD} \in \mathbb{C}^{N_A \times N_A}$ is the full rank gain matrix of the SD MIMO channel and α_1 is equal to the ratio of total noise variance to the total transmit power (i.e., $\alpha_1 = N_A \sigma_{SD}^2 / P_s$) [45]. The entries of \mathbf{H}_{SD} follow a circularly symmetric complex Gaussian distribution with zero-mean and unit variance. Thereafter, S will broadcast the N_A precoded data streams to R and D simultaneously.

Here, the received signal vectors at D and R , respectively, can be expressed as

$$\begin{aligned}\mathbf{y}_{SD} &= [y_{SD1}, y_{SD2}, \dots, y_{SDN_A}]^T \\ &= \rho_s \mathbf{H}_{SD} \mathbf{P} \mathbf{x} + \mathbf{n}_{SD},\end{aligned}\quad (3.2)$$

$$\begin{aligned}\mathbf{y}_{SR} &= [y_{SR1}, y_{SR2}, \dots, y_{SRN_A}]^T \\ &= \rho_s \mathbf{H}_{SR} \mathbf{P} \mathbf{x} + \mathbf{n}_{SR},\end{aligned}\quad (3.3)$$

where $\rho_s = \sqrt{P_s / \text{tr}(\mathbf{P} \mathbf{P}^H)}$ is the source power control factor. $\mathbf{H}_{SR} \in \mathbb{C}^{N_A \times N_A}$ is the full rank gain matrix of the SR MIMO channel. The entries of \mathbf{H}_{SR} follow a circularly symmetric complex Gaussian distribution with zero-mean and unit variance. Each $\mathbf{n}_c = \{[n_{c1}, n_{c2}, \dots, n_{cN_A}]^T \sim \mathcal{CN}(0, \sigma_c^2 \mathbf{I}_{N_A})$, $c = SD, SR\}$, is a vector corresponds to the additive zero-mean spatially-white circularly complex Gaussian noise with variance σ_c^2 .

3.2.2 Relay Node Beamforming Design Based on ZF-RZF

During the second time slot (see Figure 3.1b), R forwards the received signal vector to D after applying a linear beamforming matrix \mathbf{F} , based on ZF-RZF filter [11], given by

$$\mathbf{F} = \mathbf{H}_{RD}^H (\mathbf{H}_{RD} \mathbf{H}_{RD}^H + \alpha_2 \mathbf{I}_{N_A})^{-1} (\mathbf{P}^H \mathbf{H}_{SR}^H \mathbf{H}_{SR} \mathbf{P})^{-1} \mathbf{P}^H \mathbf{H}_{SR}^H, \quad (3.4)$$

where $\mathbf{H}_{RD} \in \mathbb{C}^{N_A \times N_A}$ is the full rank gain matrix of the RD MIMO channel and α_2 is equal to the ratio of total noise variance to the total transmit power (i.e, $\alpha_2 = N_A \sigma_{RD}^2 / P_r$) [45]. The entries of \mathbf{H}_{RD} follow a circularly symmetric complex Gaussian distribution with zero-mean and unit variance. Therefore, the received signal vector at D can be expressed as

$$\begin{aligned}\mathbf{y}_{RD} &= [y_{RD1}, y_{RD2}, \dots, y_{RDN_A}]^T \\ &= \rho_r \rho_s \mathbf{H}_{RD} \mathbf{F} \mathbf{H}_{SR} \mathbf{P} \mathbf{x} + \rho_r \mathbf{H}_{RD} \mathbf{F} \mathbf{n}_{SR} + \mathbf{n}_{RD},\end{aligned}\quad (3.5)$$

where $\rho_r = \sqrt{P_r / \text{tr}(\rho_s^2 \mathbf{F} \mathbf{H}_{SR} \mathbf{P} \mathbf{P}^H \mathbf{H}_{SR}^H \mathbf{F}^H + \sigma_{RD}^2 \mathbf{F} \mathbf{F}^H)}$ is the relay power control factor and $\mathbf{n}_{RD} \sim \mathcal{CN}(0, \sigma_{RD}^2 \mathbf{I}_{N_A})$ is a vector corresponds to the additive zero-mean spatially-white circularly complex Gaussian noise with variances σ_{RD}^2 .

3.2.3 Destination Node Combining

The destination receives two representations of the data vector \mathbf{x} ; \mathbf{y}_{SD} (3.2) and \mathbf{y}_{RD} (3.5) through SD and $SR-RD$, respectively. In order to maximize the combined SNR at D , the received signal vector \mathbf{y}_D can be expressed as

$$\begin{aligned}\mathbf{y}_D &= [y_{D1}, y_{D2}, \dots, y_{DN_A}]^T \\ &= \mathbf{y}_{SD} + \mathbf{y}_{RD}.\end{aligned}\tag{3.6}$$

In the following, to implement the classifier, features must be extracted for each signal \mathbf{y}_D to provide a basis for discriminating between the modulation schemes.

3.3 Modulation Recognition Algorithm

Our proposal is based on pattern recognition to distinguish among different modulation schemes. This approach is generally divided into two subsystems : the features extraction subsystem and the classifier subsystem. In the following, we describe the details of the extraction of discriminating features and the classifiers.

3.3.1 Features Extraction

Extraction of discriminating features is of prime importance in modulation recognition algorithms. It is necessary to extract key features that enable the algorithm to correctly recognize the source modulation from the received signal \mathbf{y}_D . The HOS, which includes the higher order moments (HOM) and the higher order cumulants (HOC) of a received signal, are the most adopted features giving higher modulation recognition accuracies in SISO and MIMO systems [18, 26, 76, 100]. In this work, based on [18], we employ the features with a combination of HOM and HOC up to order eight since they can discriminate the different modulation schemes. We report in Table 3.1 some HOM and HOC up to order eight to see how they can distinguish between several modulation schemes.

TABLE 3.1 – Some theoretical moments and cumulants values for several modulation schemes (unit-variance signal constellations with equiprobable symbols) [18]

	2-PSK	4-PSK	8-PSK	16-QAM	64-QAM
M40	1	1	0	-0.68	-0.619
M42	1	1	1	1.32	1.38
C40	-2	1	0	-0.68	-0.619
C42	-2	-1	-1	-0.68	-0.619
M60	1	0	0	0	0
M61	1	1	0	-1.32	-1.298
M63	1	1	1	1.96	2.22
C60	16	0	0	0	0
C61	16	-4	0	2.08	1.7972
C63	16	4	4	2.08	1.7972
M80	1	1	1	2.20	1.91
M82	1	1	0	-2.48	-2.75
C80	-272	-34	1	-13.9808	-11.5022
C82	-272	34	0	-13.9808	-11.5022

Let $\mathbf{y}_D^{(a)} = (y_{D1}^{(a)}, \dots, y_{DN}^{(a)})$ be the received sequence at the a^{th} antenna with size of N symbols. The o^{th} -order HOM of $\mathbf{y}_D^{(a)}$ is defined as [101]

$$M_{op}(\mathbf{y}_D^{(a)}) = \mathbb{E} \left\{ \left(\mathbf{y}_D^{(a)} \right)^{o-p} \left(\overline{\mathbf{y}_D^{(a)}} \right)^p \right\}, \quad a = 1, \dots, N_A. \quad (3.7)$$

The HOMs can be estimated as follows :

$$M_{op}(\mathbf{y}_D^{(a)}) = \frac{1}{N} \sum_{n=1}^N \left(y_{Dn}^{(a)} \right)^{o-p} \left(\overline{y_{Dn}^{(a)}} \right)^p. \quad (3.8)$$

Accordingly, the second-order HOM can be expressed as

$$M_{20} = \mathbb{E} \left\{ \left(\mathbf{y}_D^{(a)} \right)^2 \right\} \quad \text{or} \quad M_{21} = \mathbb{E} \left\{ \left| \mathbf{y}_D^{(a)} \right|^2 \right\} \quad (3.9)$$

The o^{th} -order HOC of the zero-mean signal $\mathbf{y}_D^{(a)}$ is given by

$$C_{op} \left(\mathbf{y}_D^{(a)} \right) = \text{Cum} \left[\underbrace{\mathbf{y}_D^{(a)}, \dots, \mathbf{y}_D^{(a)}}_{(o-p) \text{ terms}}, \underbrace{\overline{y_D^{(a)}}, \dots, \overline{y_D^{(a)}}}_{(p) \text{ terms}} \right]. \quad (3.10)$$

Using the above equation (3.10), C_{20} and C_{21} are written as

$$C_{20} \left(\mathbf{y}_D^{(a)} \right) = \text{Cum} \left[\mathbf{y}_D^{(a)}, \mathbf{y}_D^{(a)} \right], \quad C_{21} \left(\mathbf{y}_D^{(a)} \right) = \text{Cum} \left[\mathbf{y}_D^{(a)}, \overline{y_D^{(a)}} \right]. \quad (3.11)$$

It is worth noting that the HOC can be derived in terms of HOMs. In fact, the o^{th} -order HOC is expressed as functions of equal and lower ordered HOMs as

$$\text{Cum} \left[\mathbf{y}_{D1}^{(a)}, \dots, \mathbf{y}_{Do}^{(a)} \right] = \sum_{\Psi} (-1)^{\beta-1} (\beta-1)! \prod_{z \in \Psi} \mathbb{E} \left\{ \prod_{i \in z} \mathbf{y}_{Di}^{(a)} \right\}, \quad (3.12)$$

where Ψ runs through the list of all partitions of $1, \dots, o$, z runs through the list of all blocks of the partition Ψ and β denotes the cardinality of the partition Ψ .

Assuming $o = 3$, the available set of indices is $(1, 2, 3)$ and four distinct types of partitioning can be obtained for that set : $\{(1), (2), (3)\}$ leading to $\beta = 3$, $\{(1), (2, 3)\}$ leading to $\beta = 2$, $\{(2), (1, 3)\}$ leading to $\beta = 2$, $\{(3), (1, 2)\}$ leading to $\beta = 2$, $\{(1, 2, 3)\}$ leading to $\beta = 1$. Hence,

$$\begin{aligned} \text{Cum} \left[\mathbf{y}_{D1}^{(a)}, \mathbf{y}_{D1}^{(a)}, \mathbf{y}_{D3}^{(a)} \right] &= (-1)^{1-1} (1-1)! \mathbb{E} \left\{ \mathbf{y}_{D1}^{(a)} \mathbf{y}_{D2}^{(a)} \mathbf{y}_{D3}^{(a)} \right\} \\ &\quad + (-1)^{2-1} (2-1)! \mathbb{E} \left\{ \mathbf{y}_{D1}^{(a)} \right\} \mathbb{E} \left\{ \mathbf{y}_{D2}^{(a)} \mathbf{y}_{D3}^{(a)} \right\} \\ &\quad + (-1)^{2-1} (2-1)! \mathbb{E} \left\{ \mathbf{y}_{D2}^{(a)} \right\} \mathbb{E} \left\{ \mathbf{y}_{D1}^{(a)} \mathbf{y}_{D3}^{(a)} \right\} \\ &\quad + (-1)^{2-1} (2-1)! \mathbb{E} \left\{ \mathbf{y}_{D3}^{(a)} \right\} \mathbb{E} \left\{ \mathbf{y}_{D1}^{(a)} \mathbf{y}_{D2}^{(a)} \right\} \\ &\quad + (-1)^{3-1} (3-1)! \mathbb{E} \left\{ \mathbf{y}_{D1}^{(a)} \right\} \mathbb{E} \left\{ \mathbf{y}_{D2}^{(a)} \right\} \mathbb{E} \left\{ \mathbf{y}_{D3}^{(a)} \right\} \\ &= \mathbb{E} \left\{ \mathbf{y}_{D1}^{(a)} \mathbf{y}_{D2}^{(a)} \mathbf{y}_{D3}^{(a)} \right\} - \mathbb{E} \left\{ \mathbf{y}_{D1}^{(a)} \right\} \mathbb{E} \left\{ \mathbf{y}_{D2}^{(a)} \mathbf{y}_{D3}^{(a)} \right\} \\ &\quad - \mathbb{E} \left\{ \mathbf{y}_{D2}^{(a)} \right\} \mathbb{E} \left\{ \mathbf{y}_{D1}^{(a)} \mathbf{y}_{D3}^{(a)} \right\} - \mathbb{E} \left\{ \mathbf{y}_{D3}^{(a)} \right\} \mathbb{E} \left\{ \mathbf{y}_{D1}^{(a)} \mathbf{y}_{D2}^{(a)} \right\} \\ &\quad + 2 \mathbb{E} \left\{ \mathbf{y}_{D1}^{(a)} \right\} \mathbb{E} \left\{ \mathbf{y}_{D2}^{(a)} \right\} \mathbb{E} \left\{ \mathbf{y}_{D3}^{(a)} \right\} \end{aligned} \quad (3.13)$$

By following the same manner, one can express the HOC up to eighth order in terms of HOMs.

For example, C_{40} , C_{60} and C_{80} are defined, respectively, as

$$C_{40} = M_{40} - 3(M_{20})^2, \quad (3.14)$$

$$C_{60} = M_{60} - 15M_{20}M_{40} + 30(M_{20})^3, \quad (3.15)$$

$$C_{80} = M_{80} - 35(M_{40})^2 - 630(M_{20})^4 + 420(M_{20})^2M_{40}. \quad (3.16)$$

In order to mitigate the effect of the increase in the cumulants' magnitude with their order, we raise each cumulant to the power of $2/o$ [102].

3.3.2 Classifiers

The modulation recognition problem can be seen as a pattern recognition problem, where modulation schemes can be recognized through features extraction. Here, we denote by $\Theta_1 = \{\mathcal{M}_i, i = 1, \dots, \mu_1\}$ the considered set of modulation schemes, where μ_1 is the cardinality of Θ_1 . Typically, classifiers include two processing steps : training and testing. Before triggering the training step, it is recommended to select the best subset from the combined HOM and HOC features set in order to obtain a good prediction for all sample sets. For this, we apply the principal component analysis (PCA) technique since it can reduce and equalize the original dimensionality of the features set [103]. In fact, the PCA technique builds a low-dimensional representation of data (extracted features) that describes as much of the variance in that data as possible. This technique is also known as a "linear transformation" in which the components of data are transformed into orthogonal components and then the resulting orthogonal components are ordered so that those with the largest variation come first. This moves as much of the variance as possible into the first few components. Thus, the remaining components are highly correlated and may be eliminated with minimal loss of information. Therefore, the selected subset contains the orthogonal components with the largest variance. In this study, only ten orthogonal components (i.e., $N_F = 10$) among twenty eight are selected for both training and testing. After that, the training process is launched. It involves building a classifier from a training database. After training, the test step is triggered to recognize the modulation scheme of each unknown signal based on the classifier already built. We illustrate the modulation

recognition of an unknown received signal in Figure 3.2.

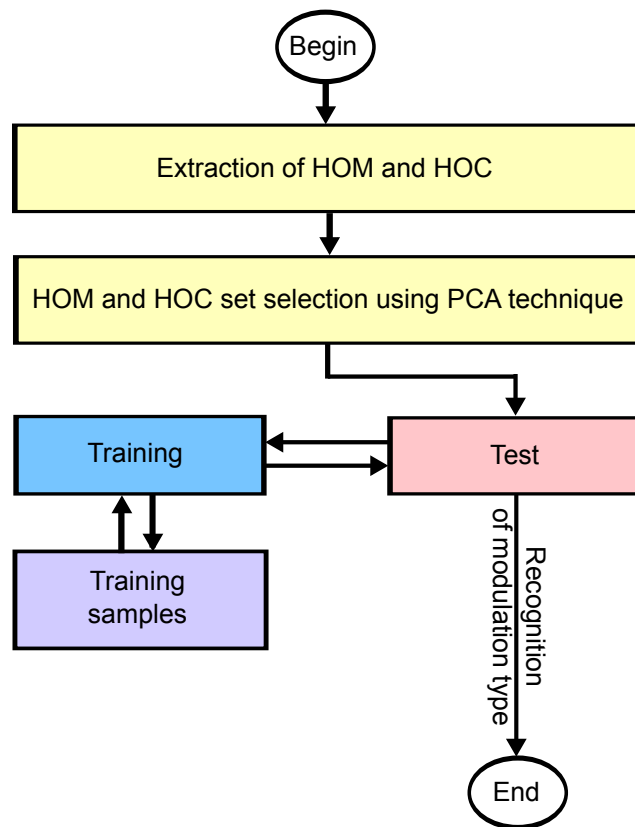


FIGURE 3.2 – Modulation recognition of an unknown received signal

In this work, we carry out a comparative study of the decision tree (J48) with the multilayer perceptron (MLP), the naive Bayes using discretization (NBD), the tree augmented naive Bayes (TAN) and the classifiers.

In the following, we briefly describe the J48, MLP, NBD and TAN classifiers.

3.3.2.1 J48 classifier

A decision tree is a decision support tool that uses a tree graph of decisions and their possible consequences. It is an excellent tool for helping to decide between several courses of action. In our work, we use C4.5 decision tree. In fact, C4.5 creates a model based on a tree structure [104]. In the tree, nodes and branches correspond to features and possible values connecting features, respectively. A leaf that symbolizes the class, terminates a set of nodes and branches. Thus, tracing the path of nodes and branches to the terminating leaf leads to determining the class of an instance. J48 algorithm is an implementation of the C4.5.

3.3.2.2 MLP classifier

Many researchers have focused on ANN to develop high performance modulation classifiers for various M -ary shift keying linear modulation schemes [21, 26]. Besides, many ANN models have been developed, of which the MLP network is the most widely used. Here, the proposed classifier is a MLP using the RPROP introduced in [105], known by its high performance on pattern recognition problems. MLP is composed of an input layer, one or more hidden layers and an output layer, where each neuron in a layer is connected to all the neurons in the next layer. The addition of this hidden layer allows the network to model the functions of complex nonlinear decision between any input and output space. However, ANN approaches suffer from complex network structure, long training times and low convergence speeds.

3.3.2.3 Bayesian Networks

Bayesian network is a graphical probabilistic model that includes a directed acyclic graph of nodes and links, and a set of conditional probability tables [106]. In fact, nodes correspond to classes or features, whereas links correspond to relationships between nodes. The weight of each link is defined in the conditional probability tables based on the Bayesian theorem [107]. Here, a learner attempts to construct a classifier based on a given set of training examples with class labels. Let $E = (f_1, f_2, \dots, f_{N_F})$ an example where f_i is the value of the feature F_i , $i = 1 \dots N_F$. Assuming that C represents the class variable (corresponding to the modulation scheme). We denote by c the value that C takes and $c(E)$ the class of E . The Bayesian classifier represented by a Bayesian network is given by

$$c(E) = \arg \max_{c \in C} \left(\Pr(c) \Pr(E|c) \right), \quad (3.17)$$

where $\Pr(c)$ is the probability of c , and $\Pr(E|c)$ denotes the conditional probability of E given c .

Naive Bayes using Discretization (NBD) : Naive Bayes is the simplest form of Bayesian networks, in which only the class node directly points to all features (conditional independence assumption).

Under this assumption, the resulting classifier is given by

$$c(E) = \arg \max_{c \in C} \left(\Pr(c) \prod_{i=1}^{N_F} \Pr(f_i | c) \right). \quad (3.18)$$

Because the continuous features have a large value range, the probability cannot be estimated from the frequency distribution. Thus, we apply the Fayyad and Irani discretization method [108] to transform continuous features into discrete features.

Tree Augmented Naive Bayes (TAN) : TAN is an extended tree-like naive Bayes [109]. In this case, the class node directly points to all features and a feature can have only one parent from another feature. Here, the tree is formed by calculating the maximum weight spanning tree using the Chow-Liu algorithm [110]. Over naive Bayes, this latter algorithm allows to efficiently find the best TAN, and hence leads to considerable improvement.

3.3.2.4 Time complexities of J48, MLP, NBD and TAN classifiers

The time complexities of J48, MLP, NBD and TAN classifiers are given in Table 3.2, where N_D is the size of the training data, N_F is the number of selected features, H_n is the number of hidden neurons and N_{epochs} is the number of epochs to train the training data.

TABLE 3.2 – Time complexities of J48, MLP, NBD and TAN classifiers

Classifiers	Time complexities
J48	$\mathcal{O}((N_D \cdot N_F^2))$
MLP	$\mathcal{O}(H_n \cdot N_{epochs} \cdot N_D \cdot N_F)$
TAN	$\mathcal{O}(N_D \cdot N_F^2)$
NBD	$\mathcal{O}(N_D \cdot N_F)$

3.3.3 Metric for evaluating the effectiveness of classifiers

The efficiency indicators used in the evaluation of classifiers applications are numerous. However, most of them are built based on the two-class confusion matrix as shown in Table 3.3.

TABLE 3.3 – Two-class confusion matrix

Predicted Class \ Actual Class	\mathcal{M}_s	$\mathcal{M}_{q \neq s}$
\mathcal{M}_s	True Positive (<i>TP</i>)	False Negative (<i>FN</i>)
$\mathcal{M}_{q \neq s}$	False Positive (<i>FP</i>)	True Negative (<i>TN</i>)

Note that $s, q = 1, \dots, \text{card}(\Theta_1)$ where Θ_1 is the considered set of modulation schemes and \mathcal{M}_i is the modulation of the index i .

TP : \mathcal{M}_s is correctly recognized,

FN : \mathcal{M}_s is recognized as $\mathcal{M}_{q \neq s}$,

FP : $\mathcal{M}_{q \neq s}$ is recognized as \mathcal{M}_s ,

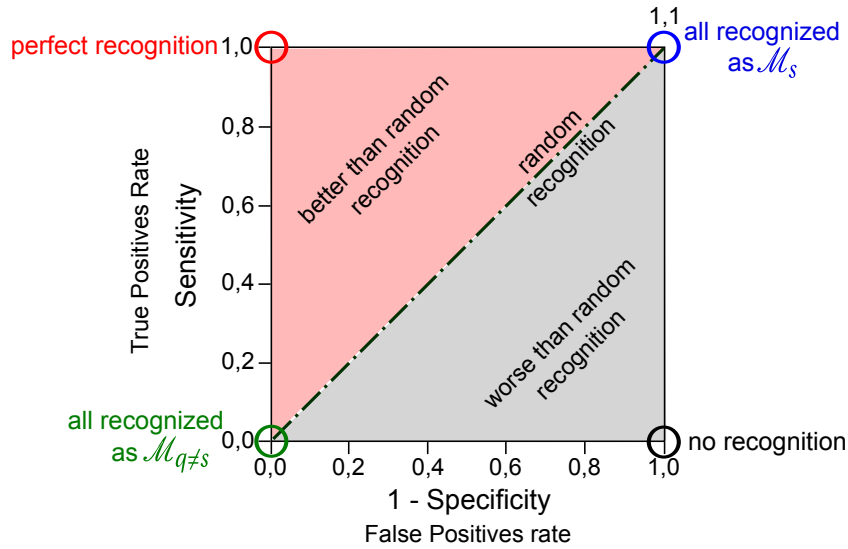
TN : $\mathcal{M}_{q \neq s}$ is correctly recognized.

Through Table 3.3, we can extract various accuracy measures. We summarize some of these metrics in Table 3.4.

TABLE 3.4 – Accuracy measures derived from the two-class confusion matrix

Indicators	Definition
Sensitivity	$\frac{TP}{TP+FN}$
Specificity	$\frac{TN}{TN+FP}$
False Positive Rate	$\frac{FP}{TN+FP}$
False Negative Rate	$\frac{FN}{TP+FN}$
Accuracy	$\frac{TP+TN}{TP+TN+FP+FN}$
Global Error Rate	$\frac{FP+FN}{TP+TN+FP+FN}$
Precision	$\frac{TP}{TP+FP}$

An effective method of evaluating the recognition performance is to plot the receiver operating characteristic (ROC) curve (sensitivity against 1-specificity) [111]. The interpretation of the ROC curve for \mathcal{M}_s modulation is shown in Figure 3.3.

FIGURE 3.3 – Interpretation of the ROC curve for \mathcal{M}_s modulation

By computing the area under the curve ROC (AUC) [112], we can compare multiple classifiers. In fact, the most efficient classifier is the one that has the largest AUC.

3.4 Results and Discussion

In this section, we evaluate the performance of the proposed modulation recognition algorithm for cooperative MIMO system with $N_A = 4$. The set of modulation schemes is $\Theta_1 = \{2 - \text{PSK}, 4 - \text{PSK}, 8 - \text{PSK}, 16 - \text{QAM}, 64 - \text{QAM} \text{ and } 256 - \text{QAM}\}$. Let the training set contains 200 realizations of test MIMO signals with $N \times N_A$ symbols for each modulation type, where N is the number of symbols at each antenna. Unless otherwise mentioned, N is set to 512 i.i.d. symbols, all channels are subject to Rayleigh fading and V-BLAST is used as a spatial multiplexing technique. The test set consists of 6000 Monte Carlo trials in total ($N_{total} = 6000$), i.e., 1000 Monte Carlo trials for each modulation scheme. For each trial, N_A test signals are considered where each signal consists of N i.i.d. symbols. For all the simulations, the source messages and the channels matrices are randomly generated. The features set is formed by calculating the combined HOM and HOC of the equalized signals (i.e., \mathbf{y}_D). Then, features subset selection was performed to implement the classifier. Here, we use the data mining tool Weka [113] to carry out a comparative study between J48, MLP, NBD and TAN. After training the classifier using the selected features set, the N_A destination antennas cooperate to make a better decision for each test trial i.e., each N_A test signals. In fact, the modulation that receives the majority of votes is considered

the estimated modulation. In the case where no modulation has the majority number of votes, the trial is considered to be misrecognized. Here, the average probability of correct recognition in percentage can be expressed as

$$P_{ra} = \frac{\sum_{\mathcal{M}_i \in \Theta_1} N_{\mathcal{M}_i}}{N_{total}} \times 100, \quad (3.19)$$

where $N_{\mathcal{M}_i}$ is equal to the number of trials for which the modulation $\mathcal{M}_i \in \Theta_1$ is correctly recognized. We assume that the SNRs for sub-channels SD and RD are equal (i.e., $\text{SNR} = \text{SNR}_{SD} = \text{SNR}_{RD}$). However, the SNR for sub-channel SR (i.e., SNR_{SR}) can be different. In this work, we evaluate the performance of the proposed algorithm in the case where all channels (i.e., SR , RD and SD) follow Rayleigh fading with perfect CSI.

3.4.1 Performance comparison of J48 and MLP classifiers

Through intensive simulations, we show that the optimal MLP structure to be used for the proposed algorithm is a two hidden layers network (excluding the input and output layers), where the first layer consists of 10 nodes and the second of 15 nodes. Thus, we compare the recognition performance of J48 classifier to this structure of the MLP classifier based on the ROC curves, the probability of identification and the training time.

Figure 3.4 depicts the ROC curves for both J48 and MLP classifiers when using cooperative MIMO systems employing the V-BLAST technique with $N_A = 4$, $\text{SNR}_{SR} = 30$ dB and $\text{SNR} = 5$ dB over Rayleigh fading channels. Here, it is clear that the AUC of the J48 classifier is larger than that of the MLP classifier. Indeed, J48 and MLP classifiers can recognize perfectly the 16, 64 and 256-QAM (i.e., $\text{AUC} = 1$). However, for {2, 4 and 8}-PSK, by comparing the ROC curves of these two classifiers, we can conclude that the J48 classifier is more efficient as it offers a better AUC.

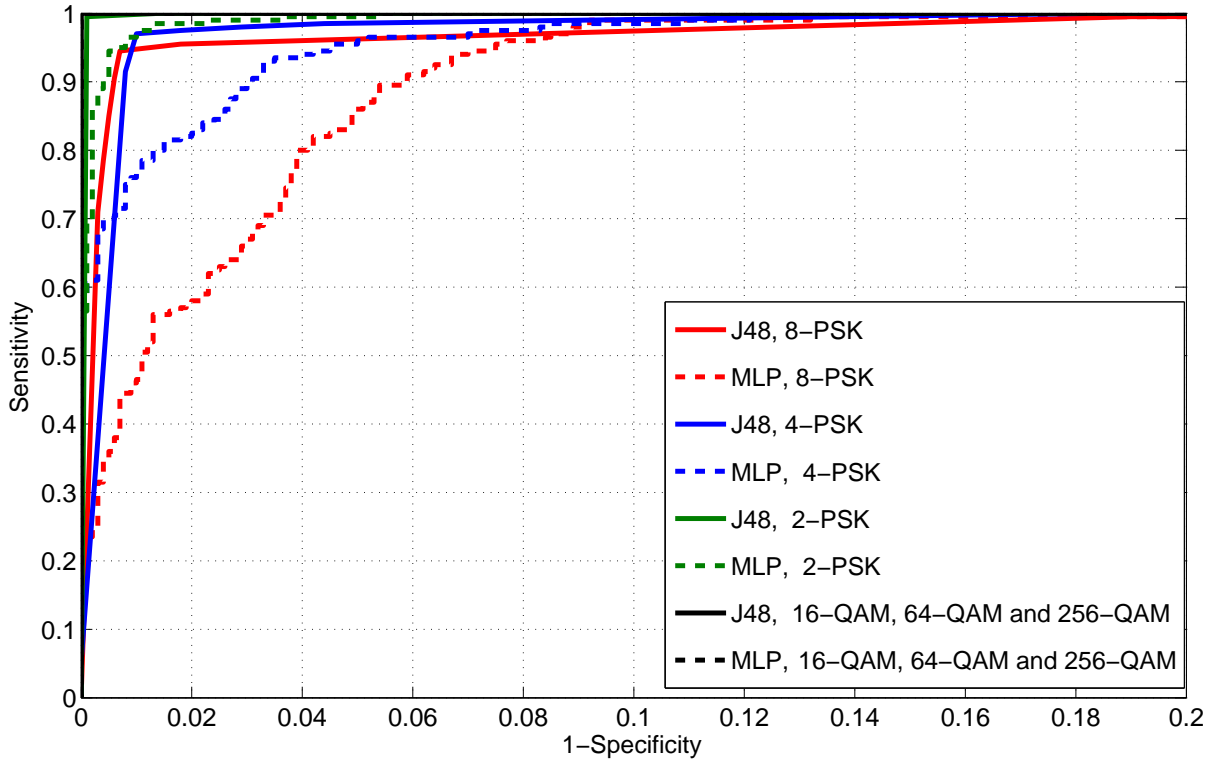


FIGURE 3.4 – ROC curves of J48 and MLP classifiers for each type of modulation scheme when using cooperative MIMO systems employing the V-BLAST technique with $N_A = 4$, $\text{SNR}_{SR} = 30$ dB and $\text{SNR} = 5$ dB over Rayleigh fading channels

To confirm these results, we show the average probability of recognition for J48 and MLP classifiers in the case of non-cooperative and cooperative MIMO systems using V-BLAST technique with $N_A = 4$ over Rayleigh fading channels in Figure 3.5. As can be seen from these results, at 95% of recognition, the J48 classifier offers an SNR gain of about 0.7 dB and 2.1 dB compared to the MLP classifier for the cooperative and non-cooperative cases, respectively.

It is noteworthy that the duration of the training phases for J48 and MLP in the case of a cooperative MIMO system for Θ_1 employing the V-BLAST technique with $N_A = 4$, $\text{SNR}_{SR} = 30$ dB and $\text{SNR} = 5$ dB over Rayleigh fading channels given by the data mining tool Weka are 0.19 and 8.59 seconds, respectively. Therefore, the J48 classifier is more adapted for the proposed algorithm in terms of both the performance of modulation recognition and the training time.

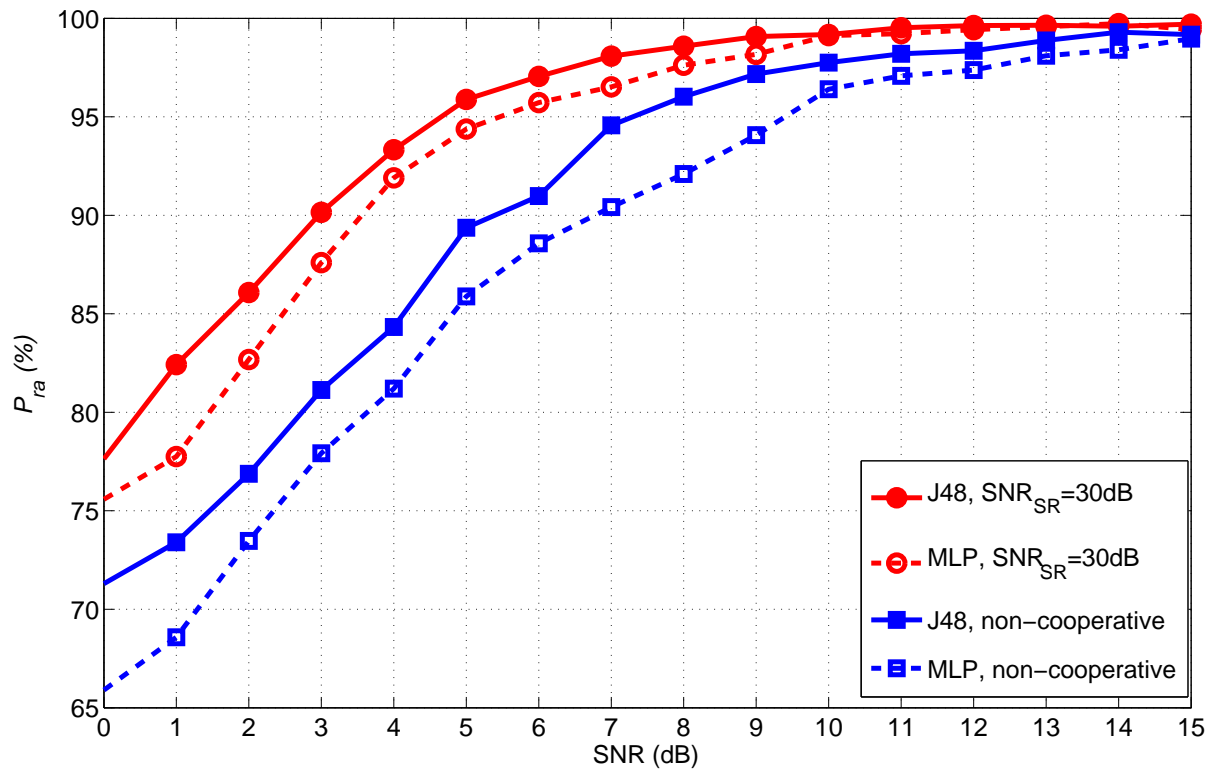


FIGURE 3.5 – Performance comparison of J48 and MLP classifiers (Probability of correct recognition as a function of SNR for Θ_1 when using V-BLAST technique with $N_A = 4$ over Rayleigh fading channels)

3.4.2 Performance comparison of J48, NBD and TAN classifiers

Figures 3.6 and 3.7 show the ROC curves for NBD and TAN classifiers compared to the J48 classifier for a cooperative MIMO system using the V-BLAST technique with $N_A = 4$, $\text{SNR}_{\text{SR}} = 30\text{ dB}$ and $\text{SNR} = 5\text{ dB}$ over Rayleigh fading channels. The AUC of each classifier given by the data mining tool Weka is summarized in Table 3.5. By comparing the weighted average of AUC, it is clear that these three classifiers (J48, NBD and TAN) are nearly similar in terms of modulation recognition.

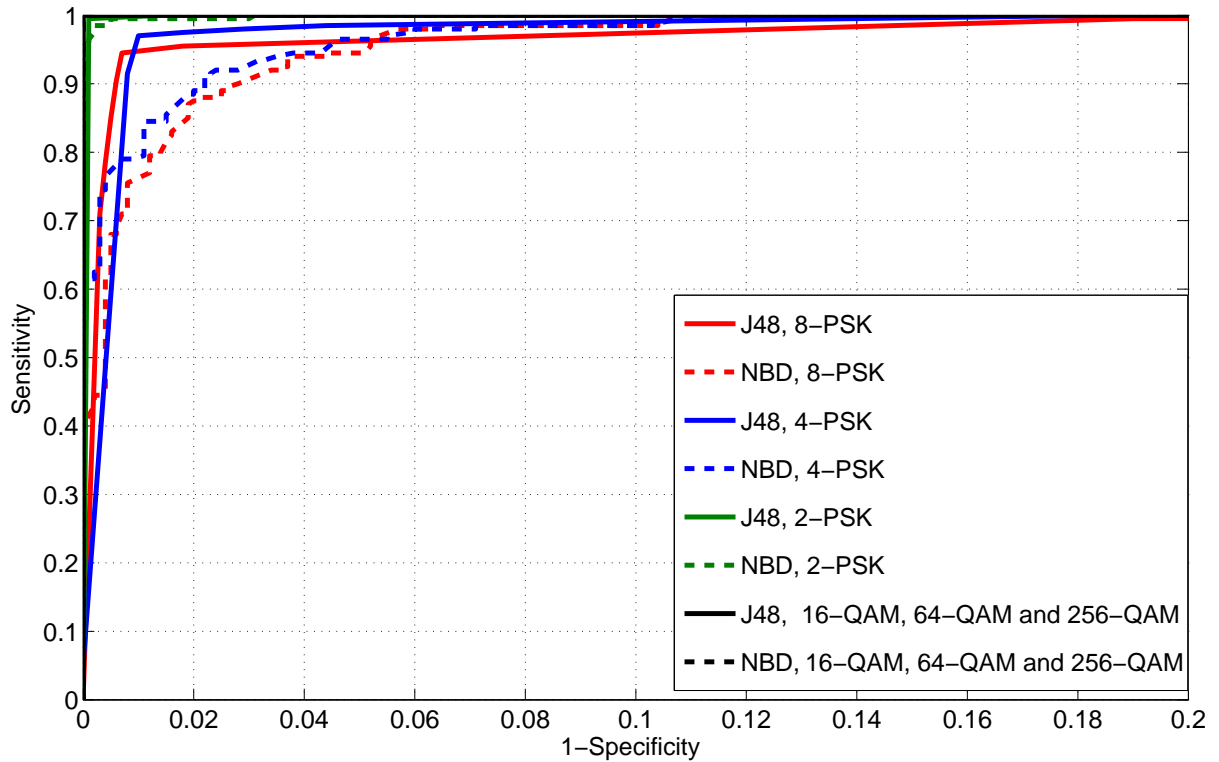


FIGURE 3.6 – ROC curves of J48 and NBD classifiers for each modulation scheme when using a cooperative MIMO system employing the V-BLAST technique with $N_A = 4$, $SNR_{SR} = 30$ dB and $SNR = 5$ dB over Rayleigh fading channels

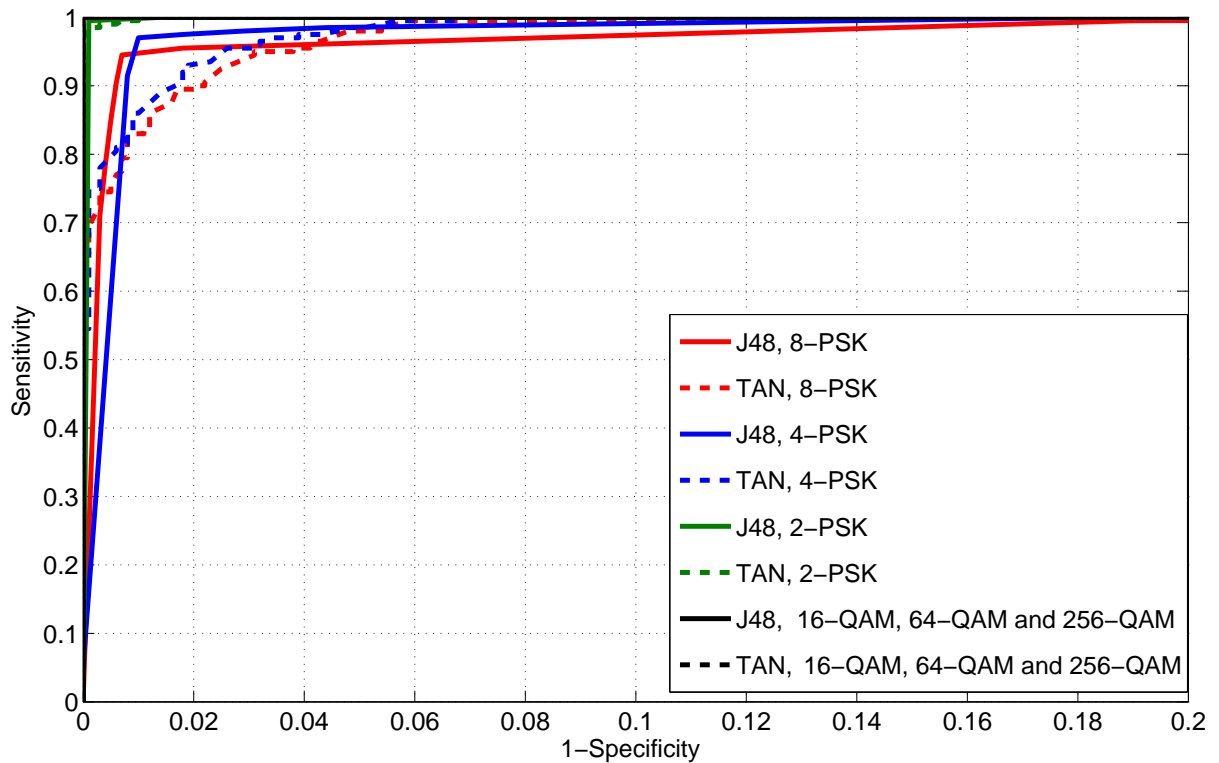


FIGURE 3.7 – ROC curves of J48 and TAN classifiers for each modulation scheme when using a cooperative MIMO system employing the V-BLAST technique with $N_A = 4$, $SNR_{SR} = 30$ dB and $SNR = 5$ dB over Rayleigh fading channels

TABLE 3.5 – AUC of each classifier in the case of a cooperative MIMO system employing the V-BLAST technique with $N_A = 4$, $\text{SNR}_{SR} = 30$ dB and $\text{SNR} = 5$ dB over Rayleigh fading channels

Classifier	NBD	TAN	J48
2-PSK	1	1	0.999
4-PSK	0.993	0.995	0.994
8-PSK	0.991	0.994	0.992
16-QAM	1	1	1
64-QAM	1	1	1
256-QAM	1	1	1
Weighted Avg. of AUC	0.997	0.998	0.998

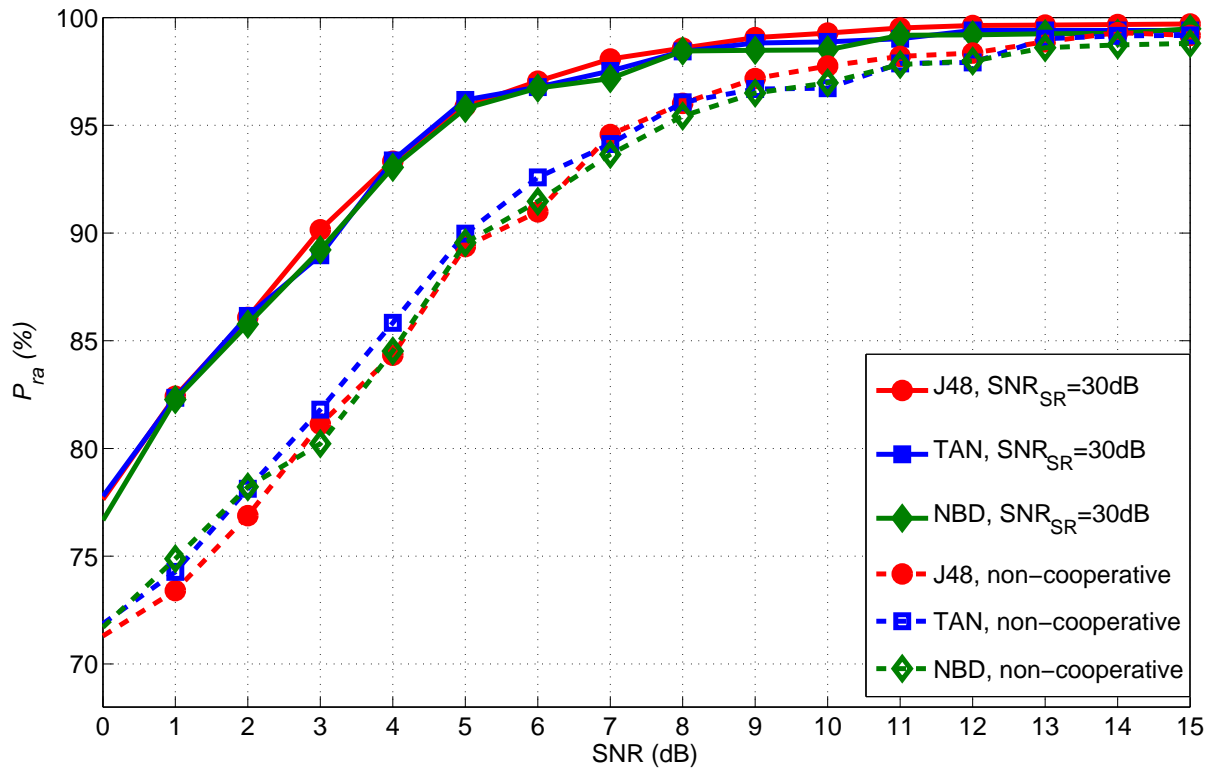


FIGURE 3.8 – Performance comparison of J48, NBD and TAN classifiers (Probability of correct recognition as a function of SNR for Θ_1 when using V-BLAST technique with $N_A = 4$ over Rayleigh fading channels)

To confirm these results, we depict in Figure 3.8 the average probability of recognition for NBD, TAN and J48 classifiers in the case of non-cooperative and cooperative MIMO

systems using V-BLAST technique with $N_A = 4$ over Rayleigh fading channels. As can be seen from these results, the NBD and TAN classifiers achieve nearly similar performance compared to the J48 classifier in cooperative and non-cooperative cases.

From Figure 3.9, it is clearly shown that the duration of the training phase for NBD, TAN are nearly equal that of the J48. Therefore, the NBD and TAN methods are also adapted for the proposed recognition algorithm in terms of both the performance of modulation recognition and the training time.

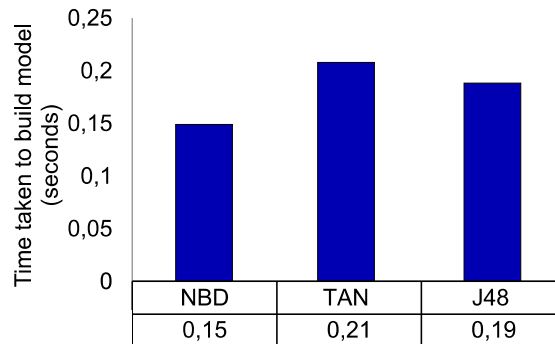


FIGURE 3.9 – Time model building in the case of cooperative MIMO system for Θ_1 employing V-BLAST technique with $N_A = 4$, $\text{SNR}_{SR} = 30$ dB and $\text{SNR} = 5$ dB over Rayleigh fading channels

3.5 Conclusion

We have presented an algorithm for modulation recognition dedicated to cooperative MIMO systems over uncorrelated channels with perfect CSI. Through the ROC curves, the probability of correct recognition and the training period time, we carried out a comparative study of the J48, MLP, NBD and TAN classifiers. Simulation results show the superiority of J48 and Bayesian network classifiers to discriminate among different linear modulation schemes with a reasonable training time. Consequently, J48 and Bayesian network classifiers allow for better monitoring of the intercepted signals in broadband technologies with reduced complexity. We have also shown that the effectiveness of modulation recognition based on cooperative schemes is remarkably better than the non-cooperative case.

Assuming uncorrelated channels is not a practical consideration. Indeed, spatial correlation effects caused by insufficient spacing between antenna elements and/or the existence of scatterers in the propagation environment can influence diversity, multiplexing, and capacity gains. Hence, the effect of spatial correlation has to be addressed for prac-

tical cooperative MIMO systems. Additionally, the assumption of perfect CSI at all nodes is often difficult to obtain in practical systems. In fact, errors, which are introduced by channel estimation, reciprocity mismatch, quantization, and delay produce imperfect CSI. Thus, modulation recognition for spatially-correlated MIMO channels with imperfect CSI in a cooperative context is desirable. To the best of our knowledge, no work has yet examined the effect of imperfect CSI on modulation recognition in cooperative MIMO systems with spatially correlated channels. So, in the next chapter, under correlated Rayleigh fading channels, we will address the problem of modulation recognition for cooperative MIMO systems in the presence of imperfect CSI.

Modulation recognition for cooperative MIMO systems over spatially-correlated channels with imperfect CSI

Contents

4.1 Introduction	50
4.2 System model and ergodic capacity	50
4.2.1 Model description	50
4.2.2 Ergodic capacity	54
4.3 Proposed modulation recognition algorithm	58
4.3.1 Extraction of discriminating features	58
4.3.2 Bagging classifier	59
4.4 Simulation Results	60
4.4.1 Ergodic capacity as a function of relays number	61
4.4.2 Performance comparison of Bagging and J48 classifiers	64
4.4.3 Performance comparison of Bagging, TAN, NBD and MLP classifiers	66
4.4.4 Probability of modulation recognition as a function of relays number	67
4.5 Conclusion	68

4.1 Introduction

In this Chapter, under correlated Rayleigh fading channels, we address the problem of modulation recognition for MIMO relaying broadcast channels with multi-relay nodes in the presence of perfect CSI of the backward (source–relay) links and imperfect CSI of both the direct (source–destination) link and the forward (relay–destination) links at the source and the relay nodes, respectively. We also derive the expression of the ergodic capacity to evaluate the proposed transmission system in the presence of imperfect CSI and spatial correlation.

The remainder of this chapter is organized as follows : In Section 4.2, the system model of a MIMO relaying broadcast channels with a direct link using a multi-relay network is introduced. Then, we derive the ergodic capacity of the proposed transmission model under imperfect CSI in the presence of spatial correlation. Section 4.3 provides a description of the proposed modulation recognition algorithm. Section 4.4 is devoted to simulation results, followed by a conclusion in Section 4.5.

4.2 System model and ergodic capacity

This section explains in detail the transmission system model and the derivation of the ergodic capacity.

4.2.1 Model description

In the following subsection, we present the considered cooperative MIMO system.

4.2.1.1 Considered cooperative MIMO system

In this chapter, we consider a cooperative MIMO system that consists of a single source (S) node and destination (D) node and L relay nodes (R_l , $l = 1, 2, \dots, L$) as shown in Figure 4.1. Let N_{AS} , N_{AR} and N_{AD} denote the number of antennas at S , each R_l and D . In this transmission scheme, a two-time-slot protocol is employed to transmit data from S to D via the

direct SD link and the cooperative $SR_l - R_lD$ links. For simplicity and practical consideration, we assume that a non-regenerative and half-duplex relaying strategy is utilized at R_l to process and forward the received signals [79]. When SM is applied at S , two necessary conditions $\{N_{AD} \geq N_{AS}, N_{AR} \geq N_{AS}\}$ must be satisfied if all R_l and D are to support all the N_{AS} independent substreams simultaneously. To simplify the analysis, we suppose that all nodes have the same number of antennas, i.e., $N_{AS} = N_{AR} = N_{AD} = N_A$.

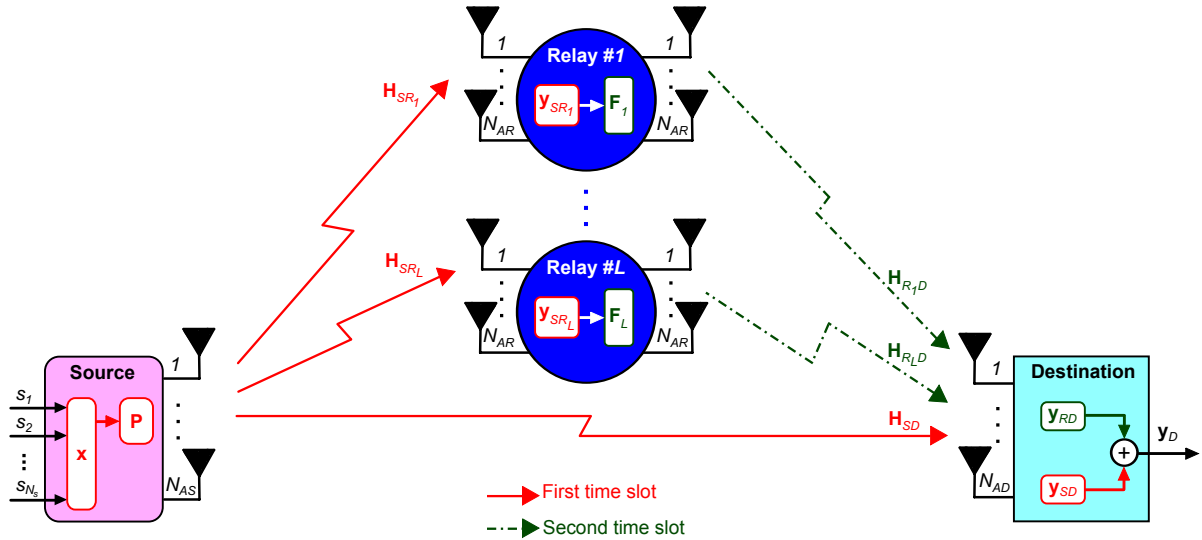


FIGURE 4.1 – MIMO relaying broadcast network with source, L -relay and destination nodes using two-time-slot protocol

At the first time slot, the source signals \mathbf{s} are encoded using SM. Therefore, the signals \mathbf{x} can be written as

$$\mathbf{x} = [s_1, s_2, \dots, s_{N_A}]^T, \quad (4.1)$$

where \mathbf{s} are assumed to be i.i.d., and mutually independent. Note that \mathbf{s} satisfies the power constraint $\mathbb{E}\{\mathbf{s}\mathbf{s}^H\} = \frac{P_s}{N_A} \mathbf{I}_{N_A}$, where P_s is defined as the transmit power at S .

Next, we employ a RZF filter at S as a linear PM since it can achieve near-capacity at sum-rate [45]. Thus, the linear PM can be expressed as

$$\mathbf{P} = \hat{\mathbf{H}}_{SD}^H (\hat{\mathbf{H}}_{SD} \hat{\mathbf{H}}_{SD}^H + \alpha_3 \mathbf{I}_{N_A})^{-1}, \quad (4.2)$$

where $\hat{\mathbf{H}}_{SD} \in \mathbb{C}^{N_A \times N_A}$ is the estimated channel matrix of SD with a Gaussian distributed error at the source node and α_3 is calculated by the ratio of the total noise variance to the total transmit power (i.e., $\alpha_3 = N_A \sigma_{SD}^2 / P_s$) [45]. Next, S broadcasts its N_A precoded data

streams simultaneously to all R_l and D . Then, the received signal vectors at D and each R_l , respectively, can be written as

$$\begin{aligned}\mathbf{y}_{SD} &= [y_{SD1}, y_{SD2}, \dots, y_{SDN_A}]^T \\ &= \rho_s \mathbf{H}_{SD} \mathbf{P} \mathbf{x} + \mathbf{n}_{SD},\end{aligned}\quad (4.3)$$

$$\begin{aligned}\mathbf{y}_{SR_l} &= [y_{SR_l1}, y_{SR_l2}, \dots, y_{SR_lN_A}]^T \\ &= \rho_s \mathbf{H}_{SR_l} \mathbf{P} \mathbf{x} + \mathbf{n}_{SR_l},\end{aligned}\quad (4.4)$$

where $\rho_s = \sqrt{P_s / \text{tr}(\mathbf{P}\mathbf{P}^H)}$ represents the source power control factor. $\mathbf{H}_{SD} \in \mathbb{C}^{N_A \times N_A}$ and $\mathbf{H}_{SR_l} \in \mathbb{C}^{N_A \times N_A}$ are the complex spatial correlation matrices of the SD and SR_l MIMO channels, respectively. Each $\mathbf{n}_c = \{[n_{c1}, n_{c2}, \dots, n_{cN_A}]^T \sim \mathcal{C}\mathcal{N}(0, \sigma_c^2 \mathbf{I}_{N_A})\}$, $c = SD, SR_l$, is a vector corresponding to an additive zero-mean spatially-white circularly complex Gaussian noise with variance σ_c^2 .

At the second time slot, all R_l simultaneously forward the received signal vector to D after applying a linear BM, denoted by \mathbf{F}_l . In fact, \mathbf{F}_l is divided into two parts, which are the receiving BM \mathbf{F}_{R_l} and the transmitting BM \mathbf{F}_{T_l} . Based on ZF-RZF [11], we model \mathbf{F}_{T_l} and \mathbf{F}_{R_l} , respectively, as

$$\mathbf{F}_{T_l} = \hat{\mathbf{H}}_{R_l D}^H \left(\hat{\mathbf{H}}_{R_l D} \hat{\mathbf{H}}_{R_l D}^H + \alpha_4 \mathbf{I}_{N_A} \right)^{-1}, \quad (4.5)$$

$$\mathbf{F}_{R_l} = \left((\mathbf{H}_{SR_l} \mathbf{P})^H \mathbf{H}_{SR_l} \mathbf{P} \right)^{-1} (\mathbf{H}_{SR_l} \mathbf{P})^H, \quad (4.6)$$

where $\hat{\mathbf{H}}_{R_l D} \in \mathbb{C}^{N_A \times N_A}$ is the estimated channel matrix of $R_l D$ with a Gaussian distributed error at the l th relay node and α_4 represents the ratio of the total noise variance to the total transmit power (i.e., $\alpha_4 = N_A \sigma_{RD}^2 / P_r$) [45]. Thus, \mathbf{F}_l is given by

$$\mathbf{F}_l = \mathbf{F}_{T_l} \mathbf{F}_{R_l}. \quad (4.7)$$

The received signal vector at D without any time oversampling and optimum symbol timing and with perfect carrier frequency and phase estimation can be expressed as

$$\begin{aligned}\mathbf{y}_{RD} &= [y_{RD1}, y_{RD2}, \dots, y_{RDN_A}]^T \\ &= \sum_{l=1}^L \rho_{r_l} \rho_s \mathbf{H}_{R_l D} \mathbf{F}_l \mathbf{H}_{SR_l} \mathbf{P} \mathbf{x} + \sum_{l=1}^L \rho_{r_l} \mathbf{H}_{R_l D} \mathbf{F}_l \mathbf{n}_{SR_l} + \mathbf{n}_{RD},\end{aligned}\quad (4.8)$$

where $\mathbf{H}_{R_l D} \in \mathbb{C}^{N_A \times N_A}$ is the complex spatial correlation matrix of the $R_l D$ MIMO channel,

$\rho_{r_l} = \sqrt{P_r / \text{tr} \left(\rho_s^2 \mathbf{F}_l \mathbf{H}_{SR_l} \mathbf{P} \mathbf{P}^H \mathbf{H}_{SR_l}^H \mathbf{F}_l^H + \sigma_{RD}^2 \mathbf{F}_l \mathbf{F}_l^H \right)}$ denotes the l th relay power control factor and $\mathbf{n}_{RD} \sim \mathcal{CN} \left(0, \sigma_{RD}^2 \mathbf{I}_{N_A} \right)$ is a vector corresponding to the additive zero-mean spatially-white circularly complex Gaussian noise with variance σ_{RD}^2 .

4.2.1.2 Spatial correlation model

The reasons for the spatial correlation that occurs at all nodes include insufficient antenna spacing, the presence of scatterers in the propagation environment, and the antenna geometry [15]. In this study, our focus is on the Kronecker model for MIMO correlated channels which was modeled in [15]. The channel correlation matrices \mathbf{H}_{SD} , \mathbf{H}_{SR_l} and \mathbf{H}_{R_lD} can be written as

$$\mathbf{H}_c = \mathbf{R}_{H_c, RX}^{1/2} \mathbf{H}_{w_c} \mathbf{R}_{H_c, TX}^{1/2}, \quad c = (SD, SR_l, R_lD), \quad (4.9)$$

where \mathbf{H}_{w_c} is a full rank gain matrix, of which the entries are i.i.d. and follow a circularly symmetric complex Gaussian distribution with zero-mean and unit variance. $\mathbf{R}_{H_c, RX}$ and $\mathbf{R}_{H_c, TX}$ represent the receiver and the transmitter correlation matrices, respectively. To model the spatial correlation matrices, we employ the exponential correlation model that was presented in [54, 114]. Thus, the entries of the correlation matrix \mathbf{R} are given by

$$(\mathbf{R})_{pq} = \begin{cases} \rho^{q-p}, & p \leq q \\ \overline{(\mathbf{R})_{qp}}, & p > q \end{cases}, \quad |\rho| < 1, \quad (4.10)$$

where ρ represents the complex correlation coefficient of neighboring transmit branches. The two matrices $\mathbf{R}_{H_c, RX}$ and $\mathbf{R}_{H_c, TX}$ are, respectively, defined by the receive correlation coefficients $\rho_{H_c, RX}$ and the transmit correlation coefficients $\rho_{H_c, TX}$.

4.2.1.3 Imperfect channel estimation model

Due to large delay and reciprocity mismatch, we assume the imperfect CSI of both SD and R_lD to be complex Gaussian distributed. Thus, the imperfect SD at S and the imperfect R_lD received at R_l can be modeled by [16]

$$\hat{\mathbf{H}}_c = \mathbf{H}_c + e_c \boldsymbol{\Omega}_c, \quad c = (SD, R_lD), \quad (4.11)$$

where $\mathbf{\Omega}_{SD}$ and $\mathbf{\Omega}_{R_lD}$ are matrices independent of \mathbf{H}_{SD} and \mathbf{H}_{R_lD} , respectively, whose entries are i.i.d. zero-mean circularly symmetric complex Gaussian variables with unit variance. We denote by e_{SD}^2 and $e_{R_lD}^2$ the estimation error variances of the *SD* and *R_lD* channels, respectively. It is worth noting that each relay node R_l has a perfect knowledge of \mathbf{H}_{SR_l} since the estimation of the backward channels can be performed based on pilot signaling [93].

In the following, we will derive the ergodic capacity under the condition of imperfect *SD* and *R_lD* CSI at S and R_l , respectively.

4.2.2 Ergodic capacity

4.2.2.1 Instantaneous SNR of RZF Beamforming

Assuming that the channel estimation error is small (i.e., $e_{SD} \ll 1$), the linear PM \mathbf{P} (equation 4.2) can be approximated by using the Taylor expansion as [115]

$$\tilde{\mathbf{P}} = \mathbf{H}_{SD}^\dagger \left(\mathbf{I}_{N_A} - e_{SD} \mathbf{\Omega}_{SD} \mathbf{H}_{SD}^\dagger \right) \left(\mathbf{I}_{N_A} - \alpha_3 \mathbf{H}_{SD}^{\alpha_3} + e_{SD} \alpha_3 \mathbf{H}_{SD}^{\alpha_3} \mathbf{H}_{SD}^e \mathbf{H}_{SD}^{\alpha_3} \right), \quad (4.12)$$

where $\mathbf{H}_{SD}^\dagger = \mathbf{H}_{SD}^H (\mathbf{H}_{SD} \mathbf{H}_{SD}^H)^{-1}$, $\mathbf{H}_{SD}^{\alpha_3} = (\mathbf{H}_{SD} \mathbf{H}_{SD}^H + \alpha_3 \mathbf{I}_{N_A})^{-1}$ and $\mathbf{H}_{SD}^e = \mathbf{H}_{SD} \mathbf{\Omega}_{SD}^H + \mathbf{\Omega}_{SD} \mathbf{H}_{SD}^H$. Therefore, the source power control factor becomes

$$\tilde{\rho}_s = \sqrt{P_s / \text{tr}(\tilde{\mathbf{P}} \tilde{\mathbf{P}}^H)}. \quad (4.13)$$

By replacing equation (4.12) in (4.3) and after neglecting some small terms, the received signal vectors \mathbf{y}_{SD} in the presence of imperfect CSI can be further expressed as

$$\mathbf{y}_{SD} \cong \tilde{\rho}_s (\mathbf{I}_{N_A} - \alpha_3 \mathbf{H}_{SD}^{\alpha_3}) \mathbf{x} + e_{SD} \tilde{\rho}_s \alpha_3 \mathbf{H}_{SD}^{\alpha_3} \mathbf{H}_{SD}^e \mathbf{H}_{SD}^{\alpha_3} \mathbf{x} + \mathbf{n}_{SD}. \quad (4.14)$$

From the above expression (4.14), we observe that the second term represents an additional noise caused by the channel estimation error of *SD*.

We denote the last two terms of equation (4.14) as

$$\hat{\mathbf{n}}_{SD} = e_{SD} \tilde{\rho}_s \alpha_3 \mathbf{H}_{SD}^{\alpha_3} \mathbf{H}_{SD}^e \mathbf{H}_{SD}^{\alpha_3} \mathbf{x} + \mathbf{n}_{SD}, \quad (4.15)$$

and we refer to it as the "effective post-processing noise". The effective transmitting ma-

trix is given by

$$\mathbf{H}_{SD,RZF} = \tilde{\rho}_s (\mathbf{I}_{N_A} - \alpha_3 \mathbf{H}_{SD}^{\alpha_3}). \quad (4.16)$$

Hence, we have

$$\mathbf{y}_{SD} \cong \mathbf{H}_{SD,RZF} \mathbf{x} + \hat{\mathbf{n}}_{SD}. \quad (4.17)$$

Then, the power of the n th transmitted signal stream becomes $\frac{P_s}{N_A} (\mathbf{H}_{SD,RZF})_{n,n}^2$. The covariance matrix of the effective post-processing noise $\hat{\mathbf{n}}_{SD}$ can then be computed as

$$\begin{aligned} \mathbb{E} \{ \hat{\mathbf{n}}_{SD} \hat{\mathbf{n}}_{SD}^H \} &= e_{SD}^2 \tilde{\rho}_s^2 \alpha_3^2 \frac{P_s}{N_A} \mathbf{H}_{SD}^{\alpha_3} \left[\text{tr} \left(\mathbf{H}_{SD}^{\alpha_3} (\mathbf{H}_{SD}^{\alpha_3})^H \right) \mathbf{H}_{SD} \mathbf{H}_{SD}^H + \text{tr} \left(\mathbf{H}_{SD}^H \mathbf{H}_{SD}^{\alpha_3} (\mathbf{H}_{SD}^{\alpha_3})^H \mathbf{H}_{SD} \right) \mathbf{I}_{N_A} \right] \\ &\quad \times (\mathbf{H}_{SD}^{\alpha_3})^H + \sigma_{SD}^2 \mathbf{I}_{N_A}, \end{aligned} \quad (4.18)$$

where we used the fact that $\mathbb{E} \{ \Omega \mathbf{H} \Omega^H \} = \text{tr}(\mathbf{H}) \mathbf{I}_{N_A}$ for any $\mathbf{H} \in \mathbb{C}^{N_A \times N_A}$ [115]. Thus, the effective noise power of the n th data stream is

$$\begin{aligned} \mathbb{E} \{ (\hat{\mathbf{n}}_{SD} \hat{\mathbf{n}}_{SD}^H)_{n,n} \} &= e_{SD}^2 \tilde{\rho}_s^2 \alpha_3^2 \frac{P_s}{N_A} \left[\text{tr} \left(\mathbf{H}_{SD}^{\alpha_3} (\mathbf{H}_{SD}^{\alpha_3})^H \right) \left\| (\mathbf{H}_{SD}^{\alpha_3} \mathbf{H}_{SD})_n \right\|^2 + \left\| (\mathbf{H}_{SD}^{\alpha_3})_n \right\|^2 \right. \\ &\quad \left. \times \text{tr} \left(\mathbf{H}_{SD}^H \mathbf{H}_{SD}^{\alpha_3} (\mathbf{H}_{SD}^{\alpha_3})^H \mathbf{H}_{SD} \right) \right] + \sigma_{SD}^2. \end{aligned} \quad (4.19)$$

Based on equation (4.19), the postprocessing SNR per symbol of the n th stream can be written as

$$\gamma_n^{SD} = \frac{\frac{P_s}{N_A} (\mathbf{H}_{SD,RZF})_{n,n}^2}{e_{SD}^2 \tilde{\rho}_s^2 \alpha_3^2 \frac{P_s}{N_A} \left(\text{tr} \left(\mathbf{H}_{SD}^{\alpha_3} (\mathbf{H}_{SD}^{\alpha_3})^H \right) \left\| (\mathbf{H}_{SD}^{\alpha_3} \mathbf{H}_{SD})_n \right\|^2 + \text{tr} \left(\mathbf{H}_{SD}^H \mathbf{H}_{SD}^{\alpha_3} (\mathbf{H}_{SD}^{\alpha_3})^H \mathbf{H}_{SD} \right) \left\| (\mathbf{H}_{SD}^{\alpha_3})_n \right\|^2 \right) + \sigma_{SD}^2} \quad (4.20)$$

Here, we see an additional term is added to the covariance of the effective postprocessing noise under the condition of imperfect SD CSI compared to the perfect CSI (i.e., $e_{SD} = 0$), which is related to the transmit power P_s and the channel estimation error variance of SD (i.e., e_{SD}^2). We define this term as the channel-error-generated noise power (CEG-noise power) of SD , which can be written as

$$\begin{aligned} (\text{CEG - noise power})_n^{SD} &= e_{SD}^2 \tilde{\rho}_s^2 \alpha_3^2 \frac{P_s}{N_A} \left(\text{tr} \left(\mathbf{H}_{SD}^{\alpha_3} (\mathbf{H}_{SD}^{\alpha_3})^H \right) \left\| (\mathbf{H}_{SD}^{\alpha_3} \mathbf{H}_{SD})_n \right\|^2 \right. \\ &\quad \left. + \text{tr} \left(\mathbf{H}_{SD}^H \mathbf{H}_{SD}^{\alpha_3} (\mathbf{H}_{SD}^{\alpha_3})^H \mathbf{H}_{SD} \right) \left\| (\mathbf{H}_{SD}^{\alpha_3})_n \right\|^2 \right). \end{aligned} \quad (4.21)$$

4.2.2.2 Instantaneous SNR of ZF-RZF Beamforming

Supposing $e_{RlD} \ll 1$, the transmitting BM \mathbf{F}_{Tl} (equation 4.5) can be approximated by using the Taylor expansion as

$$\tilde{\mathbf{F}}_{Tl} = \mathbf{H}_{RlD}^\dagger \left(\mathbf{I}_{N_A} - e_{RlD} \boldsymbol{\Omega}_{RlD} \mathbf{H}_{RlD}^\dagger \right) \left(\mathbf{I}_{N_A} - \alpha_4 \mathbf{H}_{RlD}^{\alpha_4} + e_{RlD} \alpha_4 \mathbf{H}_{RlD}^{\alpha_4} \mathbf{H}_{RlD}^e \mathbf{H}_{RlD}^{\alpha_4} \right), \quad (4.22)$$

where $\mathbf{H}_{RlD}^\dagger = \mathbf{H}_{RlD}^H \left(\mathbf{H}_{RlD} \mathbf{H}_{RlD}^H \right)^{-1}$, $\mathbf{H}_{RlD}^{\alpha_4} = \left(\mathbf{H}_{RlD} \times \mathbf{H}_{RlD}^H + \alpha_4 \mathbf{I}_{N_A} \right)^{-1}$ and $\mathbf{H}_{RlD}^e = \mathbf{H}_{RlD} \boldsymbol{\Omega}_{RlD}^H + \boldsymbol{\Omega}_{RlD} \mathbf{H}_{RlD}^H$. Since $e_{SD} \ll 1$, the transmitting BM \mathbf{F}_{Rl} (equation 4.6) can be approximated by using the Taylor expansion as

$$\tilde{\mathbf{F}}_{Rl} = \left(\left(\mathbf{H}_{SRl} \tilde{\mathbf{P}} \right)^H \mathbf{H}_{SRl} \tilde{\mathbf{P}} \right)^{-1} \left(\mathbf{H}_{SRl} \tilde{\mathbf{P}} \right)^H. \quad (4.23)$$

Thus, the l th relay power control factor can be re-expressed as

$$\tilde{\rho}_{r_l} = \sqrt{P_r / \text{tr} \left(\rho_s^2 \tilde{\mathbf{F}}_l \mathbf{H}_{SRl} \tilde{\mathbf{P}} \tilde{\mathbf{P}}^H \mathbf{H}_{SRl}^H \tilde{\mathbf{F}}_l^H + \sigma_{RD}^2 \tilde{\mathbf{F}}_l \tilde{\mathbf{F}}_l^H \right)}, \quad (4.24)$$

where $\tilde{\mathbf{F}}_l = \tilde{\mathbf{F}}_{Tl} \tilde{\mathbf{F}}_{Rl}$.

Substituting equations (4.22) and (4.23) into (4.8) and ignoring some small terms, the received signal vectors \mathbf{y}_{RD} under imperfect CSI may be written as

$$\begin{aligned} \mathbf{y}_{RD} \cong & \sum_{l=1}^L \tilde{\rho}_{r_l} \tilde{\rho}_s \left(\mathbf{I}_{N_A} - \alpha_4 \mathbf{H}_{RlD}^{\alpha_4} \right) \mathbf{x} + \sum_{l=1}^L \tilde{\rho}_{r_l} \left(\mathbf{I}_{N_A} - \alpha_4 \mathbf{H}_{RlD}^{\alpha_4} \right) \tilde{\mathbf{F}}_{Rl} \mathbf{n}_{SRl} \\ & + \sum_{l=1}^L e_{RlD} \tilde{\rho}_{r_l} \tilde{\rho}_s \alpha_4 \mathbf{H}_{RlD}^{\alpha_4} \mathbf{H}_{RlD}^e \mathbf{H}_{RlD}^{\alpha_4} \mathbf{x} + \mathbf{n}_{RD}. \end{aligned} \quad (4.25)$$

The third term in equation (4.25) represents the additional noises generated by the channel estimation error of RlD . We define the last three terms as

$$\hat{\mathbf{n}}_{RD} = \sum_{l=1}^L \tilde{\rho}_{r_l} \left(\mathbf{I}_{N_A} - \alpha_4 \mathbf{H}_{RlD}^{\alpha_4} \right) \tilde{\mathbf{F}}_{Rl} \mathbf{n}_{SRl} + \sum_{l=1}^L e_{RlD} \tilde{\rho}_{r_l} \tilde{\rho}_s \alpha_4 \mathbf{H}_{RlD}^{\alpha_4} \mathbf{H}_{RlD}^e \mathbf{H}_{RlD}^{\alpha_4} \mathbf{x} + \mathbf{n}_{RD}, \quad (4.26)$$

and we refer to it as the "effective post-processing noise". The effective transmitting matrix is calculated as

$$\mathbf{H}_{RD,ZF-RZF} = \sum_{l=1}^L \tilde{\rho}_{r_l} \tilde{\rho}_s \left(\mathbf{I}_{N_A} - \alpha_4 \mathbf{H}_{RlD}^{\alpha_4} \right). \quad (4.27)$$

Thus, we can rewrite (4.8) as

$$\mathbf{y}_{RD} \cong \mathbf{H}_{RD,RZF}\mathbf{x} + \hat{\mathbf{n}}_{RD}. \quad (4.28)$$

Consequently, the power of the n th transmitted signal stream can be written as $\frac{P_s}{N_A} (\mathbf{H}_{RD,ZF-RZF})_{n,n}^2$.

Then, we obtain the covariance matrix of the effective post-processing noise $\hat{\mathbf{n}}_{RD}$ as follows

$$\begin{aligned} \mathbb{E} \{ \hat{\mathbf{n}}_{RD} \hat{\mathbf{n}}_{RD}^H \} &= \sum_{l=1}^L \tilde{\rho}_{r_l}^2 (\mathbf{I}_{N_A} - \alpha_4 \mathbf{H}_{R_l D}^{\alpha_4}) \tilde{\mathbf{F}}_{R_l} \tilde{\mathbf{F}}_{R_l}^H (\mathbf{I}_{N_A} - \alpha_4 \mathbf{H}_{R_l D}^{\alpha_4})^H \sigma_{SR_l}^2 + \tilde{\rho}_s^2 \alpha_4^2 \frac{P_s}{N_A} \left[\sum_{l=1}^L e_{R_l D}^2 \mathbf{H}_{R_l D}^{\alpha_4} \mathbf{H}_{R_l D} \right. \\ &\quad \times \text{tr} \left(\mathbf{H}_{R_l D}^{\alpha_4} (\mathbf{H}_{R_l D}^{\alpha_4})^H \right) \mathbf{H}_{R_l D}^H (\mathbf{H}_{R_l D}^{\alpha_4})^H + \sum_{l=1}^L \tilde{\rho}_{r_l}^2 e_{R_l D}^2 \mathbf{H}_{R_l D}^{\alpha_4} \text{tr} \left(\mathbf{H}_{R_l D}^H \mathbf{H}_{R_l D}^{\alpha_4} (\mathbf{H}_{R_l D}^{\alpha_4})^H \right. \\ &\quad \left. \left. \times \mathbf{H}_{R_l D} \right) (\mathbf{H}_{R_l D}^{\alpha_4})^H \right] + \sigma_{RD}^2 \mathbf{I}_{N_A}. \end{aligned} \quad (4.29)$$

Hence, the effective noise power of the n th data stream is given by

$$\begin{aligned} \mathbb{E} \{ (\hat{\mathbf{n}}_{RD} \hat{\mathbf{n}}_{RD}^H)_{n,n} \} &= \sum_{l=1}^L \tilde{\rho}_{r_l}^2 \sigma_{SR_l}^2 \left\| \left((\mathbf{I}_{N_A} - \alpha_4 \mathbf{H}_{R_l D}^{\alpha_4}) \tilde{\mathbf{F}}_{R_l} \right)_n \right\|^2 + \tilde{\rho}_s^2 \alpha_4^2 \frac{P_s}{N_A} \left[\sum_{l=1}^L \tilde{\rho}_{r_l}^2 e_{R_l D}^2 \right. \\ &\quad \times \left\| \left(\mathbf{H}_{R_l D}^{\alpha_4} \mathbf{H}_{R_l D} \right)_n \right\|^2 \text{tr} \left(\mathbf{H}_{R_l D}^{\alpha_4} (\mathbf{H}_{R_l D}^{\alpha_4})^H \right) + \sum_{l=1}^L \tilde{\rho}_{r_l}^2 e_{R_l D}^2 \left\| \left(\mathbf{H}_{R_l D}^{\alpha_4} \right)_n \right\|^2 \\ &\quad \left. \times \text{tr} \left(\mathbf{H}_{R_l D}^H \mathbf{H}_{R_l D}^{\alpha_4} (\mathbf{H}_{R_l D}^{\alpha_4})^H \mathbf{H}_{R_l D} \right) \right] + \sigma_{RD}^2. \end{aligned} \quad (4.30)$$

Accordingly, we obtain the following expression for postprocessing SNR per symbol of the n th stream at D

$$\begin{aligned} \gamma_n^{SR-RD} &= \frac{P_s}{N_A} (\mathbf{H}_{RD,ZF-RZF})_{n,n}^2 \times \left[\sum_{l=1}^L \tilde{\rho}_{r_l}^2 \sigma_{SR_l}^2 \left\| \left((\mathbf{I}_{N_A} - \alpha_4 \times \mathbf{H}_{R_l D}^{\alpha_4}) \tilde{\mathbf{F}}_{R_l} \right)_n \right\|^2 + \tilde{\rho}_s^2 \alpha_4^2 \frac{P_s}{N_A} \right. \\ &\quad \times \left(\sum_{l=1}^L \tilde{\rho}_{r_l}^2 e_{R_l D}^2 \left[\left\| \left(\mathbf{H}_{R_l D}^{\alpha_4} \mathbf{H}_{R_l D} \right)_n \right\|^2 \text{tr} \left(\mathbf{H}_{R_l D}^{\alpha_4} (\mathbf{H}_{R_l D}^{\alpha_4})^H \right) + \left\| \left(\mathbf{H}_{R_l D}^{\alpha_4} \right)_n \right\|^2 \right. \right. \\ &\quad \left. \left. \times \text{tr} \left(\mathbf{H}_{R_l D}^H \mathbf{H}_{R_l D}^{\alpha_4} (\mathbf{H}_{R_l D}^{\alpha_4})^H \mathbf{H}_{R_l D} \right) \right] + \sigma_{RD}^2 \right]^{-1}. \end{aligned} \quad (4.31)$$

Thus, the CEG-noise power of SR – RD is

$$\begin{aligned} (\text{CEG – noise power})_n^{SR-RD} &= \tilde{\rho}_s^2 \alpha_4^2 \frac{P_s}{N_A} \left(\sum_{l=1}^L \tilde{\rho}_{r_l}^2 e_{R_l D}^2 \left[\left\| \left(\mathbf{H}_{R_l D}^{\alpha_4} \mathbf{H}_{R_l D} \right)_n \right\|^2 \text{tr} \left(\mathbf{H}_{R_l D}^{\alpha_4} (\mathbf{H}_{R_l D}^{\alpha_4})^H \right) \right. \right. \\ &\quad \left. \left. + \left\| \left(\mathbf{H}_{R_l D}^{\alpha_4} \right)_n \right\|^2 \text{tr} \left(\mathbf{H}_{R_l D}^H \mathbf{H}_{R_l D}^{\alpha_4} (\mathbf{H}_{R_l D}^{\alpha_4})^H \mathbf{H}_{R_l D} \right) \right] \right). \end{aligned} \quad (4.32)$$

By adding up all the data rates on each antenna path, we obtain the ergodic capacity expression of the SD link and $SR_l - R_lD$ links, respectively, as follows.

$$C_{SD} = \mathbb{E}_{\{\mathbf{H}_{SD}\}} \left\{ \sum_{n=1}^{N_A} \log_2 (1 + \gamma_n^{SD}) \right\}, \quad (4.33)$$

$$C_{SR-RD} = \mathbb{E}_{\{\mathbf{H}_{SR_l}, \mathbf{H}_{R_lD}\}_{l=1}^L} \left\{ \frac{1}{2} \sum_{n=1}^{N_A} \log_2 (1 + \gamma_n^{SR-RD}) \right\}, \quad (4.34)$$

where the factor $1/2$ in (4.34) accounts for the fact that the same data is transmitted over two time slots. Therefore, the ergodic capacity of the two independent channels SD and $SR_l - R_lD$, denoted as C , can be given as

$$C = C_{SD} + \zeta C_{SR-RD}, \quad (4.35)$$

where $\zeta = 1$ when there is a cooperation with relay nodes and $\zeta = 0$ otherwise.

4.3 Proposed modulation recognition algorithm

The destination receives two replicas of the data vector \mathbf{x} ; \mathbf{y}_{SD} (4.3) and \mathbf{y}_{RD} (4.8) via SD and $SR_l - R_lD$ links, respectively. To enhance the SNR at D , these two replicas are combined as follows

$$\begin{aligned} \mathbf{y}_D &= [y_{D1}, y_{D2}, \dots, y_{DN_A}]^T \\ &= \mathbf{y}_{SD} + \mathbf{y}_{RD}. \end{aligned} \quad (4.36)$$

Thereafter, an extraction of discriminating features is applied to each signal \mathbf{y}_D in order to implement the Bagging classifier.

4.3.1 Extraction of discriminating features

Features extraction is useful to extract features that will enable the proposed algorithm to correctly discriminate between different modulation schemes. In this work, we use the combination of HOM and HOC of the received signal up to order eight as features, which is proved to be efficient in discriminating between modulation schemes in cooperative MIMO system over uncorrelated channels with perfect CSI as shown in the above chapter. We recall that the o^{th} -order HOMs and HOCs of a sequence at the a^{th} antenna with size of N symbols (i.e., $\mathbf{y}_D^{(a)} = (y_{D1}^{(a)}, \dots, y_{DN}^{(a)})$, $a = 1, \dots, N_A$) are expressed in equations (3.8)

and (3.12), respectively. Given the fact that the magnitude of cumulants increases with their order, we raise each cumulant to the power of $2/o$ [102].

4.3.2 Bagging classifier

After extracting the key features, the modulation recognition problem can be viewed as a pattern recognition problem. Here, the considered set of modulation schemes is denoted by $\Theta_2 = \{\mathcal{M}_i, i = 1, \dots, \mu_2\}$, where μ_2 is the number of modulation schemes in Θ_2 . In this study, we use the Bagging classifier, which is a “bootstrap” ensemble method that makes decisions from multiple classifiers [116]. Knowing that Bagging classifier typically employs two phases of processing : training and testing. Before launching the training phase, we perform the PCA technique in order to reduce and equalize the original dimensionality of the features set [103]. In this work, only ten orthogonal components (i.e., $N_F = 10$) among twenty eight are selected for both training and testing. In the training phase, the Bagging classifier generates T new training subsets (i.e., $TS_t, t = 1, 2, \dots, T$). Each of the new subsets is built by randomly sampling training instances, with replacement, from the original training data (i.e., D). Hence, some examples may be selected repeatedly while others may be left out. In Bagging, all new training subsets have the same number of instances than D . Each of these subsets is used to construct one classifier employing the J48 [104] as a base classifier. Let $CM_t, t = 1, 2, \dots, T$ denote the constructed classifiers for modulation prediction. Thus, the final decision (i.e., CM_{final}) is obtained by combining the decisions of these T classifiers using un-weighted voting. Here, to classify an instance, denoted by $inst$, a vote for a modulation scheme (i.e., \mathcal{M}_i), is recorded by every classifier for which $CM_t(inst) = \mathcal{M}_i$. Then, the modulation scheme, which receives the largest number of votes, is selected as a final decision (i.e., $CM_{final}(inst)$). It is noteworthy that Bagging mainly enhances the recognition performance by minimizing the variance error [117]. The Bagging process is illustrated in Algorithm 1 and Figure 4.2, where the 5-th line of Algorithm 1 means that the final decision of an instance denoted, $inst$, is built from the constructed classifiers CM_1, CM_2, \dots, CM_T whose output is the class predicted most often by its sub-classifiers. It worth noting that the time complexity of Bagging using J48 as base classifier is $\mathcal{O}(T \cdot N_D \cdot N_F^2)$, where T is the number of the generated training subsets, N_D is the size of the training data and N_F is the number of selected features. After that, the training process is launched. It involves building a classifier from a trai-

J48 by using the AUC. Simulations were also run to assess the probability of modulation recognition of the proposed modulation recognition algorithm. In our simulations, we consider MIMO systems employing the V-BLAST technique under correlated and uncorrelated Rayleigh fading channels with and without perfect CSI. Without loss of generality, we assume that the correlation coefficients for sub-channels SD , SR_l , and R_lD are equal (i.e., $|\rho| = |\rho_{H_c, RX}| = |\rho_{H_c, TX}|$, $c = (SD, SR_l, R_lD)$). We also assume that the variances of estimation error for sub-channels SD and R_lD are equal (i.e., $e^2 = e_{SD}^2 = e_{R_lD}^2$). In all results, we set the number of antennas at all nodes to $N_A = 4$. Note that a spatially-white circularly complex Gaussian noise with variance σ_c^2 , $c = (SD, SR_l, RD)$ is added at each value of SNR_c such that $\text{SNR}_c = 10 \log_{10} \left(\frac{\sigma_s^2}{\sigma_c^2} \right)$, where σ_s^2 is the average transmitted power. Here, we consider that the SNRs for sub-channels SR_l are equal (i.e., $\text{SNR}_{SR} = \text{SNR}_{SR_l}$, $l = 1, 2, \dots, L$). SNR_{SR} must be higher in order to enhance the quality of transmission via the cooperative link $SR_l - R_lD$. In fact, for low SNR_{SR} , the non-cooperative system yields a better performance compared to cooperative one [118]. In addition, we suppose that the SNRs for sub-channels SD and RD are equal (i.e., $\text{SNR} = \text{SNR}_{SD} = \text{SNR}_{RD}$). It is worth noting that $L = 0$ represents the non-cooperative system (i.e., direct transmission).

4.4.1 Ergodic capacity as a function of relays number

In Figure 4.3, the ergodic capacity for cooperative MIMO systems with $N_A = 4$, $P_s = P_r = 12$ dB, $\text{SNR}_{SR} = 15$ dB and $\text{SNR} = 0$ dB is examined for different values of channel estimation error variances (i.e., $e^2 = \{0, 0.05 \text{ and } 0.1\}$) and compared to the non-cooperative case when considering uncorrelated MIMO channels (i.e., $|\rho| = 0$). Here, it is clear that the cooperative scheme offers a larger capacity gain than the non-cooperative case. In fact, the capacity improves significantly as the number of relays (i.e., L) increases. It can also be observed from Figure 4.3 that the ergodic capacity has a higher sensitivity to channel estimation errors. This latter drops remarkably as e^2 increases.

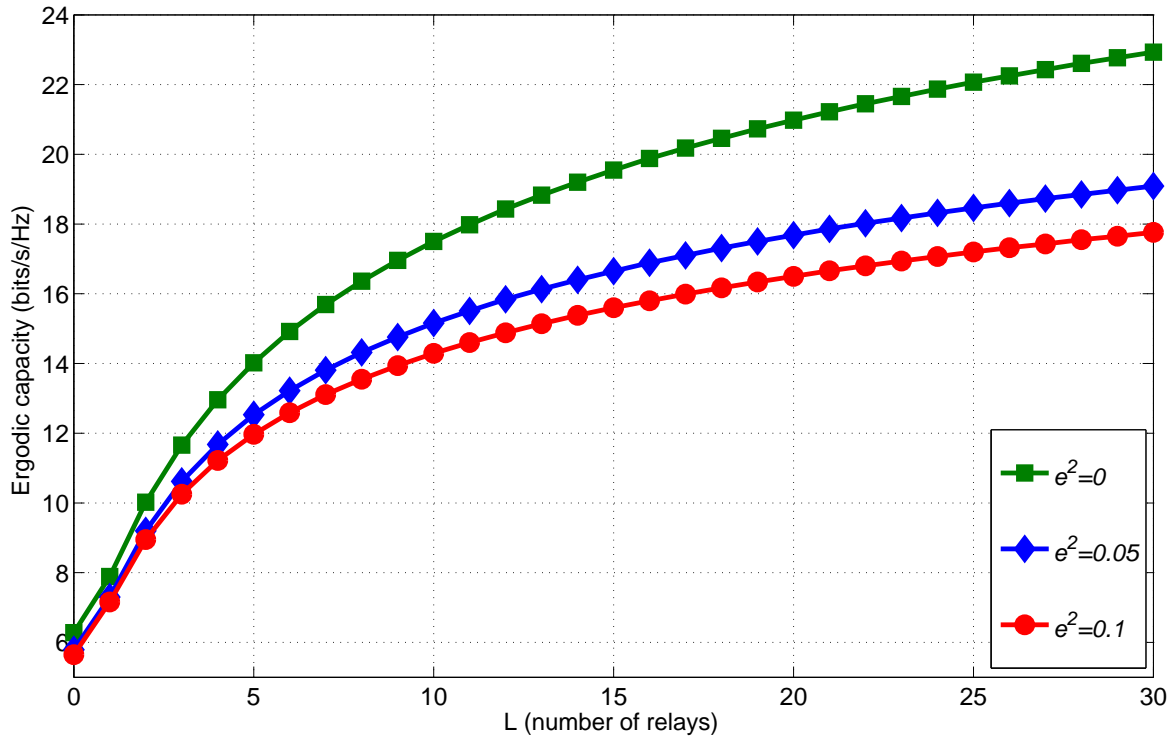


FIGURE 4.3 – Ergodic capacity as a function of L (number of relays) for different e^2 (variances of channel estimation error) with $N_A = 4$, $|\rho| = 0$, $P_s = P_r = 12$ dB, $\text{SNR}_{SR} = 15$ dB and $\text{SNR} = 0$ dB

The effects of different values of the Kronecker correlation coefficients (i.e., $|\rho| = \{0, 0.3, 0.5, 0.6, 0.7, 0.8\}$) on ergodic capacities for MIMO systems with $N_A = 4$, $P_s = P_r = 12$ dB, $\text{SNR}_{SR} = 15$ dB, $\text{SNR} = 0$ dB and $e^2 = 0.1$ are shown in Figure 4.4. It is observed that the ergodic capacity deteriorates significantly with increasing correlation coefficients. Here, we also show that the ergodic capacity improves considerably as the number of relay nodes L increases when all channels are slightly correlated (or uncorrelated). Furthermore, it can be seen that the capacity increases slightly with L when all channels are highly correlated (i.e., $|\rho| \rightarrow 1$). Consequently, the aid of multiple relay nodes is proved beneficial in all cases.

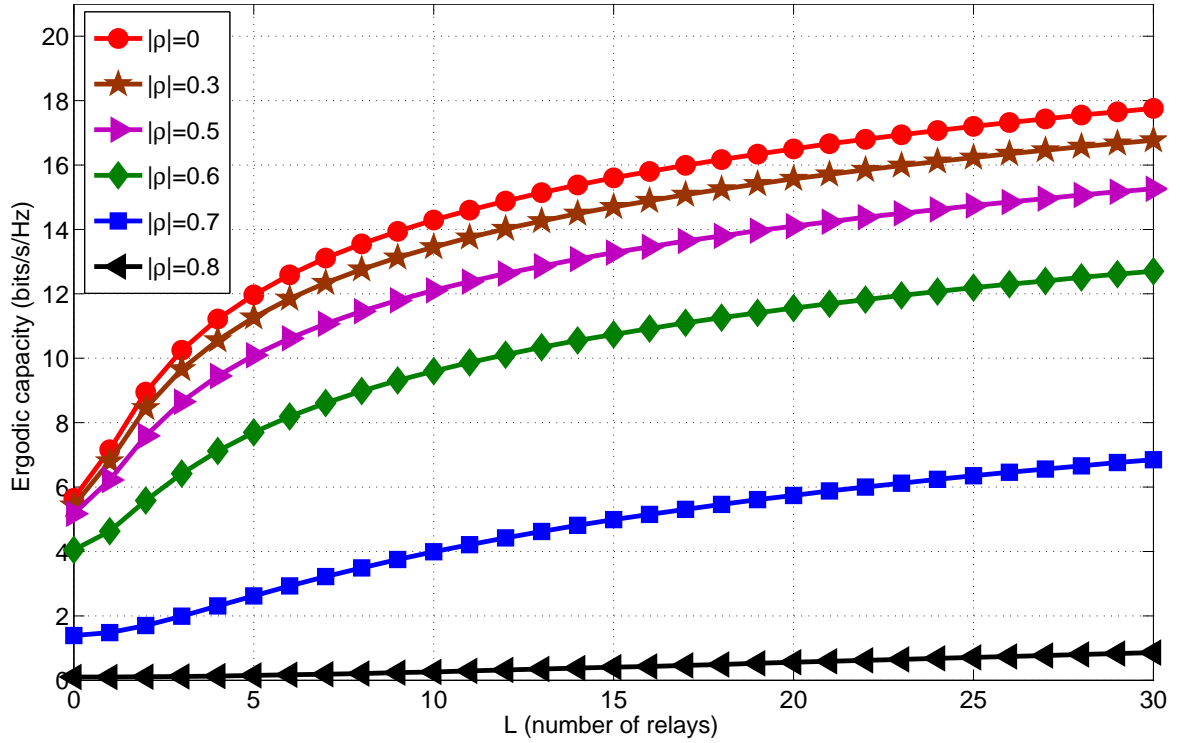


FIGURE 4.4 – Ergodic capacity as a function of L (number of relays) for different $|\rho|$ (Kronecker correlation coefficients) with $N_A = 4$, $e^2 = 0.1$, $P_s = P_r = 12$ dB, $\text{SNR}_{SR} = 15$ dB and $\text{SNR} = 0$ dB

In the following, the set of digital modulation types is $\Theta_2 = \{2\text{-PSK}, 4\text{-PSK}, 8\text{-PSK}, 16\text{-QAM}, 64\text{-QAM}\}$. For each modulation type, the training set consist of 50 realizations of test MIMO signals with $512 \times N_A$ symbols, where the source messages and the channels matrices are randomly generated for each realization. While the test set contains 5000 Monte Carlo trials in total (i.e., $N_{total} = 5000$), i.e., 1000 Monte Carlo trials for each modulation scheme. For each trial, N_A test signals are considered where each signal consists of 512 i.i.d. symbols. For both training and test phases, the features set is formed by calculating the combined HOM and HOC of the equalized signals at each antenna (i.e., $\mathbf{y}_D^{(a)} = (y_{D1}^{(a)}, \dots, y_{DN}^{(a)})$, $a = 1, \dots, N_A$). Then, features subset selection was performed as a preparation for the classifier. After training the classifier through selected training set, the N_A receiver antennas cooperate to make a better decision for each test trial i.e., each N_A test signals. In fact, the modulation that receives the majority of votes is considered the estimated modulation. In the case where no modulation has the majority number of votes, the trial is considered to be misrecognized. Here, the average probability of correct recog-

inition in percentage is given by

$$P_{ra} = \frac{\sum_{\mathcal{M}_i \in \Theta_2} N_{\mathcal{M}_i}}{N_{total}} \times 100, \quad (4.37)$$

where $N_{\mathcal{M}_i}$ is equal to the number of trials for which the modulation $\mathcal{M}_i \in \Theta_2$ is correctly recognized.

In the following, we carry out a comparative study of the Bagging with J48, TAN, NBD and MLP classifiers using the data mining tool Weka [113]. Recall that J48, TAN, NBD and MLP are described in subsection 3.3.2 of the above chapter. For Bagging, we find out through intensive simulations that the optimal number of iterations is 60 (i.e., $T = 60$). With this setting, Bagging gives a good tradeoff between accuracy of modulation recognition and speed of training.

4.4.2 Performance comparison of Bagging and J48 classifiers

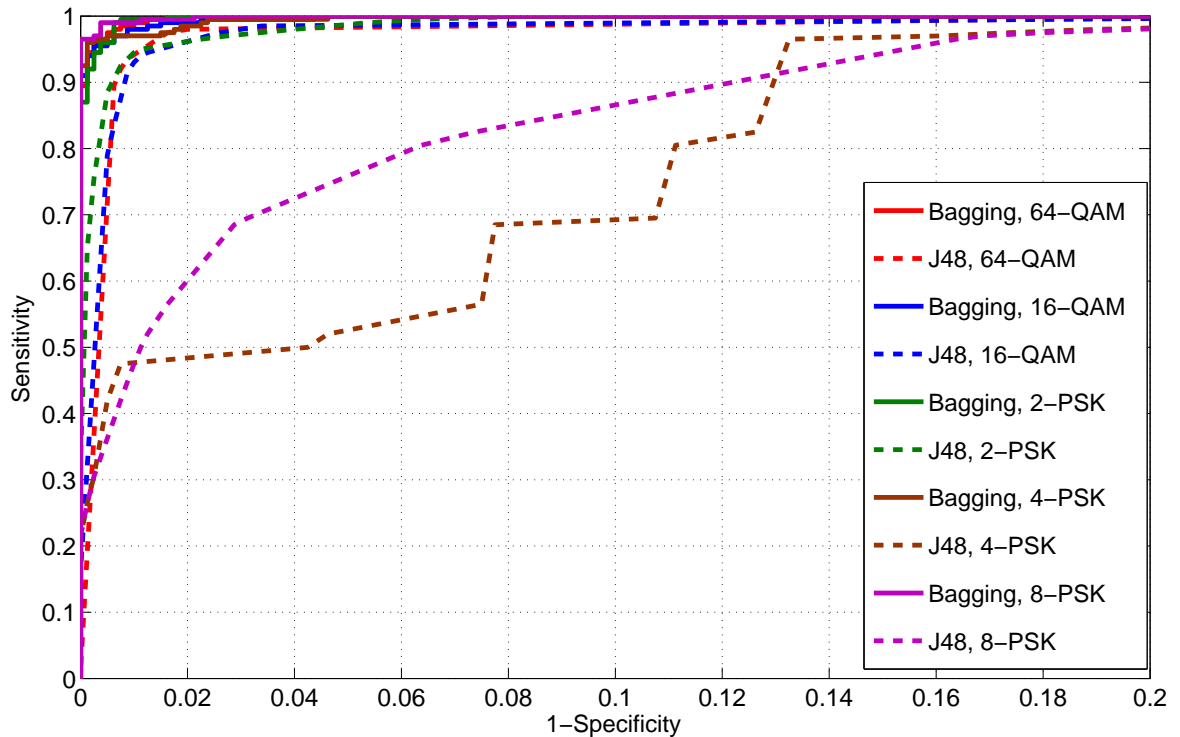


FIGURE 4.5 – ROC curves of Bagging and J48 methods for each type of modulation in the case of a MIMO scheme using the V-BLAST, $N_A = 4$, $L = 1$, $\text{SNR}_{SR} = 20$ dB, $\text{SNR} = -5$ dB, $e^2 = 0.1$ and $|\rho| = 0.5$

We provide a comparison between the Bagging and J48 classifiers through the ROC curves as depicted in Figure 4.5. For our comparison, we consider a cooperative MIMO

system using the V-BLAST technique with $N_A = 4$, $L = 1$, $\text{SNR}_{SR} = 20$ dB, $\text{SNR} = -5$ dB and $e^2 = 0.1$ when assuming moderately correlated MIMO channels (i.e., $|\rho| = 0.5$). The AUC of each recognition method given by the data mining tool Weka is summarized in Table 4.1. By comparing the weighted average of AUC, it is clearly seen that the Bagging classifier outperforms the J48 classifier in terms of modulation recognition.

TABLE 4.1 – AUC of each recognition method (in the case of V-BLAST MIMO scheme with $N_A = 4$, $L = 1$, $\text{SNR}_{SR} = 20$ dB, $\text{SNR} = -5$ dB, $e^2 = 0.1$ and $|\rho| = 0.5$)

Classifier	Bagging	J48
2-PSK	1	0.997
4-PSK	0.999	0.963
8-PSK	1	0.963
16-QAM	0.999	0.994
64-QAM	1	0.994
Weighted Avg. of AUC	0.999	0.982

As can be seen from Table 4.2, the duration of the training phase for the Bagging classifier is greater than that for the J48. Hence, the Bagging classifier provides a compromise between recognition performance and convergence speed in the proposed algorithm.

TABLE 4.2 – Time model building (in the case of MIMO scheme using V-BLAST with $N_A = 4$, $L = 1$, $\text{SNR}_{SR} = 20$ dB, $\text{SNR} = -5$ dB, $e^2 = 0.1$ and $|\rho| = 0.5$)

Classifier	Time taken to build model (seconds)
Bagging	1.53
J48	0.13

To confirm the efficiency of the Bagging, we plot in Figure 4.6 the probability of recognition for Bagging and J48 methods in the case of a cooperative MIMO system using the V-BLAST technique with $N_A = 4$ and $L = 1$. The performance of the non-cooperative system is further provided as a benchmark. We observe from these results that the Bagging classifier provides a performance improvement with respect to the J48 classifier in

both cooperative and non-cooperative cases for all SNRs. For instance, Bagging provides SNR gain of about 1.4 dB with respect to the J48 classifier in the non-cooperative case with $e^2 = 0.1$ and $|\rho| = 0.5$. Moreover, the probability of recognition attains about 97.5% for the Bagging classifier and 96.5% for the J48 classifier in the case where $L = 0$, $e^2 = 0.1$ and $|\rho| = 0.5$. On the same figure, it is also observed that the recognition performance has a higher sensitivity to channel estimation errors and correlation. Indeed, the probability of recognition is degraded and will not exceed an upper bound even for very large values of SNR contrary to the case of perfectly uncorrelated channels (i.e., $e^2 = 0$ and $|\rho| = 0$). Thus, this upper bound may pose a serious problem in practical applications. In order to solve this problem, we first propose to investigate the recognition performance with the aid of one relay node. From the same figure, it is clearly shown that this cooperation offers a large gain as compared with the non-cooperative case. In fact, the probability of recognition reaches about 99% for cooperative scheme with $L = 1$ and 97.5% for non-cooperative scheme in the case of imperfectly correlated channels (i.e., $e^2 = 0.1$ and $|\rho| = 0.5$) using Bagging classifier.

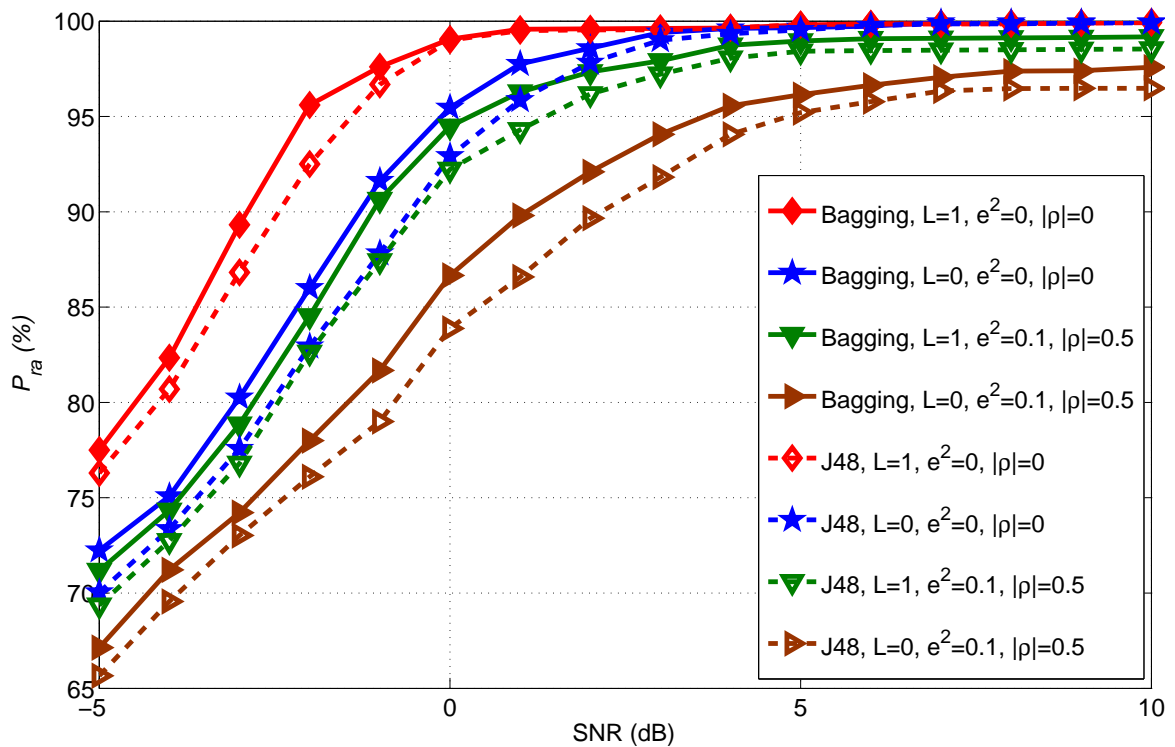


FIGURE 4.6 – Probability of recognition as a function of SNR for Θ_2 in a MIMO schemes using the V-BLAST with $N_A = 4$ and $\text{SNR}_{SR} = 20$ dB for Bagging and J48 classifiers

4.4.3 Performance comparison of Bagging, TAN, NBD and MLP classifiers

Figure 4.7 illustrates the probability of recognition for the Bagging, TAN, NBD and MLP methods in the case of a MIMO system using the V-BLAST technique with $N_A = 4$, $e^2 = 0.1$, $|\rho| = 0.5$ and $\text{SNR}_{SR} = 20$ dB. Here, we use the MLP with two hidden layers network (excluding the input and output layers), where the first layer consists of 10 nodes and the second of 15 nodes as in the above chapter. As shown from these results, the Bagging classifier also outperforms the TAN, the NBD and the MLP classifiers in terms of the probability of recognition in the cooperative ($L = 1$) and the non-cooperative cases ($L = 0$).

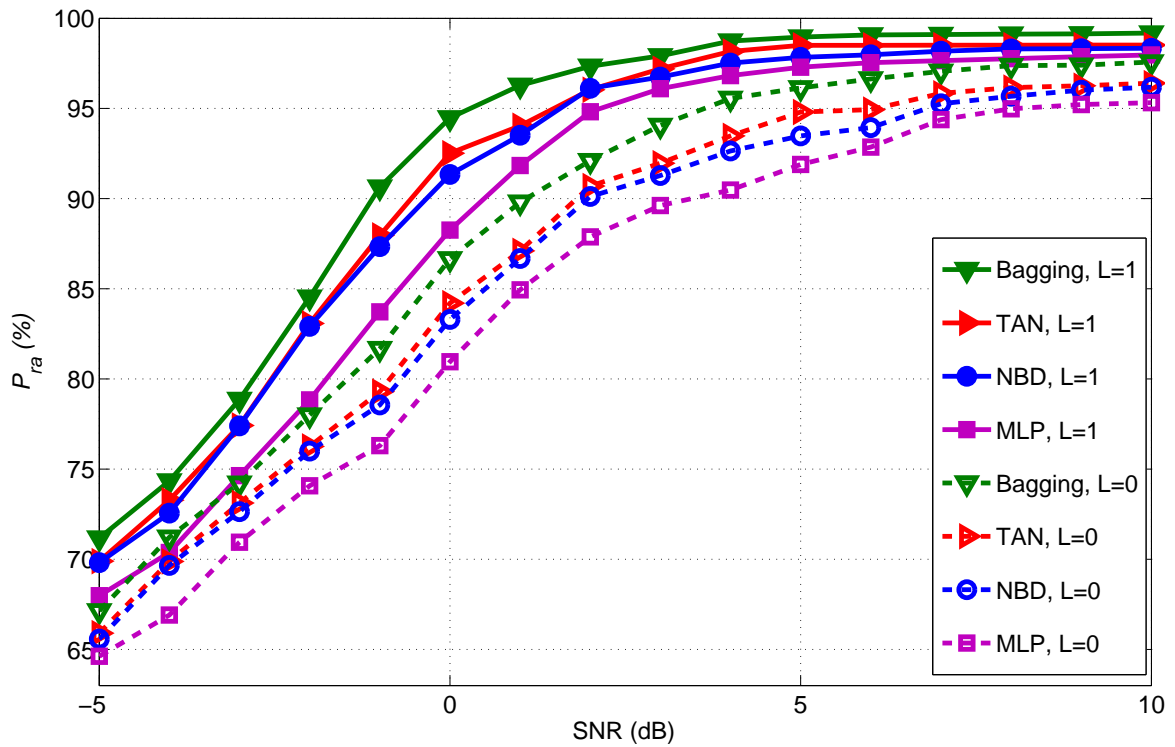


FIGURE 4.7 – Probability of recognition as a function of SNR for Θ_2 in MIMO schemes using V-BLAST with $N_A = 4$, $e^2 = 0.1$, $|\rho| = 0.5$ and $\text{SNR}_{SR} = 20$ dB for Bagging, TAN, NBD and MLP classifiers

Despite the improvement due to the use of one relay node, the performance of recognition will not reach 100% even at higher SNR. Dealing with this issue, we propose employing multiple relay nodes in MIMO systems in order to further assess the effect of increasing diversity gain.

4.4.4 Probability of modulation recognition as a function of relays number

Figure 4.8 examines the effect of increasing the number of relay nodes (i.e., L) on the recognition performance of the proposed algorithm compared to the ZF-DMI algorithm [26] under the same configuration i.e., V-BLAST MIMO systems with $N_A = 4$, $e^2 = 0.1$ and $|\rho| = 0.5$ employing the Bagging classifier. As observed, a remarkable improvement in the modulation recognition performance results from increasing L . These results exactly match those of ergodic capacities. It can also be shown from this figure that the cooperative schemes realized an important gain compared to both the non-cooperative one ($L = 0$) and the ZF-DMI algorithm. In fact, the probability of recognition for the cooperative scheme can reach about 100% from a certain relay number (i.e., $L = 3$) while the non-cooperative scheme and ZF-DMI algorithm not exceed 97.5% and 93% of recognition, respectively. Therefore, the cooperative MIMO system can remove the effect of the imperfect CSI and the correlation thanks to the cooperation of multi-relay nodes with the source node.

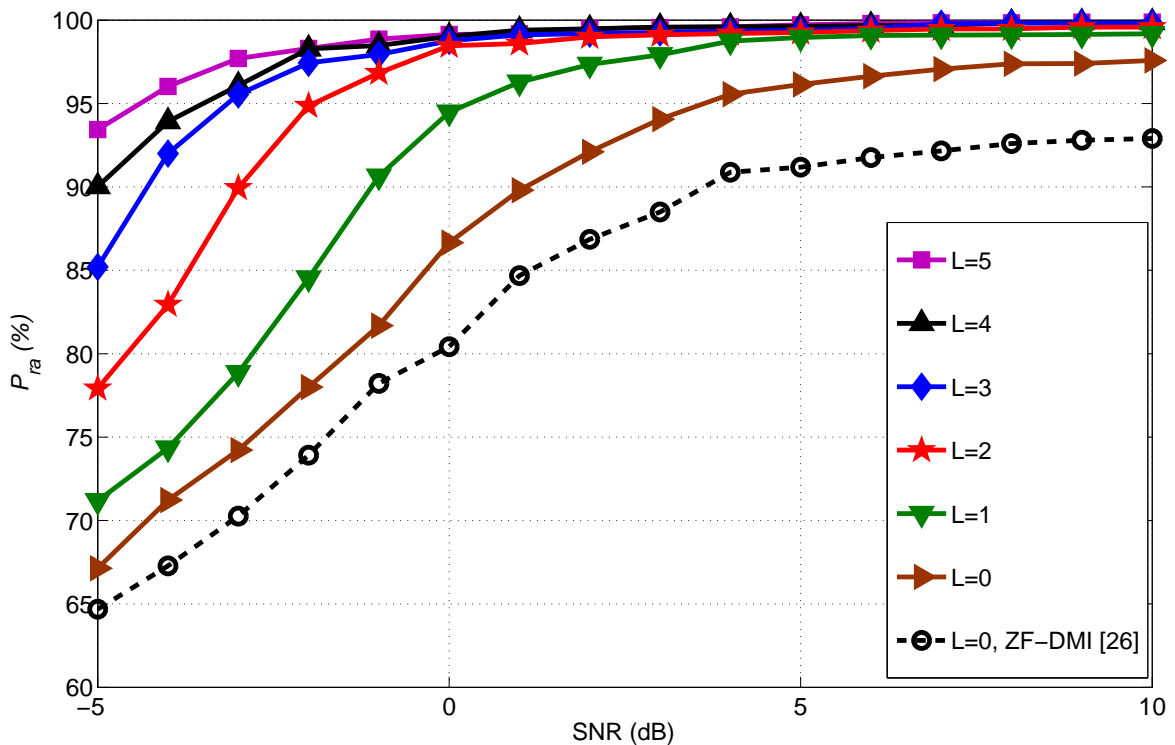


FIGURE 4.8 – Probability of recognition as a function of SNR for the proposed algorithm with different L (number of relay nodes) compared to the ZF-DMI algorithm [26] in MIMO schemes employing V-BLAST with $N_A = 4$, $\text{SNR}_{SR} = 20$ dB, $e^2 = 0.1$ and $|\rho| = 0.5$ using the Bagging classifier

4.5 Conclusion

In an effort to improve modulation recognition, we have proposed an algorithm designed for spatially-correlated MIMO relaying broadcast channels using multi-relay nodes with a direct link under imperfect CSI. This algorithm is based on combining HOM and HOC as features extraction subsystem and Bagging as a classifier subsystem. In order to quantify the effect of imperfect CSI and spatial correlation for the proposed transmission system, we have derived the ergodic capacity. For reasonable channel estimation error values and Kronecker correlation coefficients, the capacity increases with the number of relays. Through the probability of modulation recognition, we executed a comparative study of the Bagging classifier and the J48, TAN, NBD and MLP classifiers. We demonstrated that the Bagging classifier is more efficient than J48, TAN, NBD and MLP at discriminating between different linear modulation schemes. We have also shown that its effectiveness in discriminating between different linear modulation schemes, which is based on cooperative schemes, is significantly better than in the non-cooperative case. In the presence of spatially correlated channels and imperfect CSI, we have also shown that modulation recognition is improved by increasing the number of relay nodes. Consequently, the recognition performance degradation caused by both spatially correlated channels and channel estimation errors can be removed by means of a relaying scheme.

Recognition of superposed modulations for two way relay MIMO systems with PLNC

Contents

5.1 Introduction	71
5.2 Proposed modulation recognition algorithm	71
5.2.1 Motivation	71
5.2.2 Considered two-way MIMO relay channels	73
5.2.3 Extraction of discriminating features	75
5.2.4 Random forests classifier	76
5.3 Simulation results	77
5.3.1 Simulation setup	77
5.3.2 Effect of the relay position	78
5.3.3 Effect of the modulation types	79
5.3.4 Effect of the antennas number	81
5.3.5 Effect of the symbols number	81
5.3.6 Effect of the path loss exponent	82
5.4 Conclusion	83

5.1 Introduction

In TWRC, the two sources can diversify the modulation schemes for each transmission depending on the application requirements. Thus, each source requires the recognition of the modulation used by the other source to ensure correct data reception at the destinations. To solve the problem of the recognition of sources modulations for a two-way MIMO relay channel with PLNC, we propose in this chapter an algorithm for the recognition of superposed modulations.

The rest of this Chapter is organized as follows : Section 5.2 presents the proposed algorithm using HOMs and HOCs as a features extraction where the genetic algorithm and information theory (GA&IT) is employed as a features selection method and the Random Forests machine learning method as a classifier. Simulation results are discussed in Section 5.3. Section 5.4 concludes this chapter.

5.2 Proposed modulation recognition algorithm

5.2.1 Motivation

In the TWRC with PLNC, the two users' symbols are physically superposed by consuming only one time-slot in the multiple access phase. Let a_1 and a_2 denotes respectively the transmitting antennas in the sources S_1 and S_2 and let $x_{1a_1,t}$ and $x_{2a_2,t}$ be the two transmitted symbols at time instant t from the sources S_1 and S_2 using modulations of orders M_1 and M_2 , respectively. The superposition of the two modulations leads to a one of an order which is upper bounded by M_1M_2 . For instance, the superposition of a BPSK and a 16-QAM produces a constellation including 32 different points, as shown in Figure 5.2. We note that in the case of similar modulations of order M , the number of superposed symbols in the superposed constellation, can be lower than M^2 . This is due to the fact that several superposed symbols result from different scenarios of source symbols superposition. An example is illustrated in Table 5.1, where only 7 network-coded symbols denoted by x_{\oplus} emerge from two 4-ASK. It is seen that the symbol $x_{\oplus} = 3A$ is the superposition result of four distinct symbol pairs from S_1 and S_2 ($00 \oplus 11, 01 \oplus 10, 10 \oplus 01$ and $11 \oplus 00$), where A is

a constant with respect to the power normalization. It is worth noting that, in addition to the considerable increase in constellation size with an irregular spatial arrangement, the superposition of the useful symbols with the additional noise will disperse the constellation points from their original locations. Given the fact that there is no previous work, which addressed the problem of superposed modulations recognition, hence proposing an algorithm for recognition the sources modulations is a serious challenge.

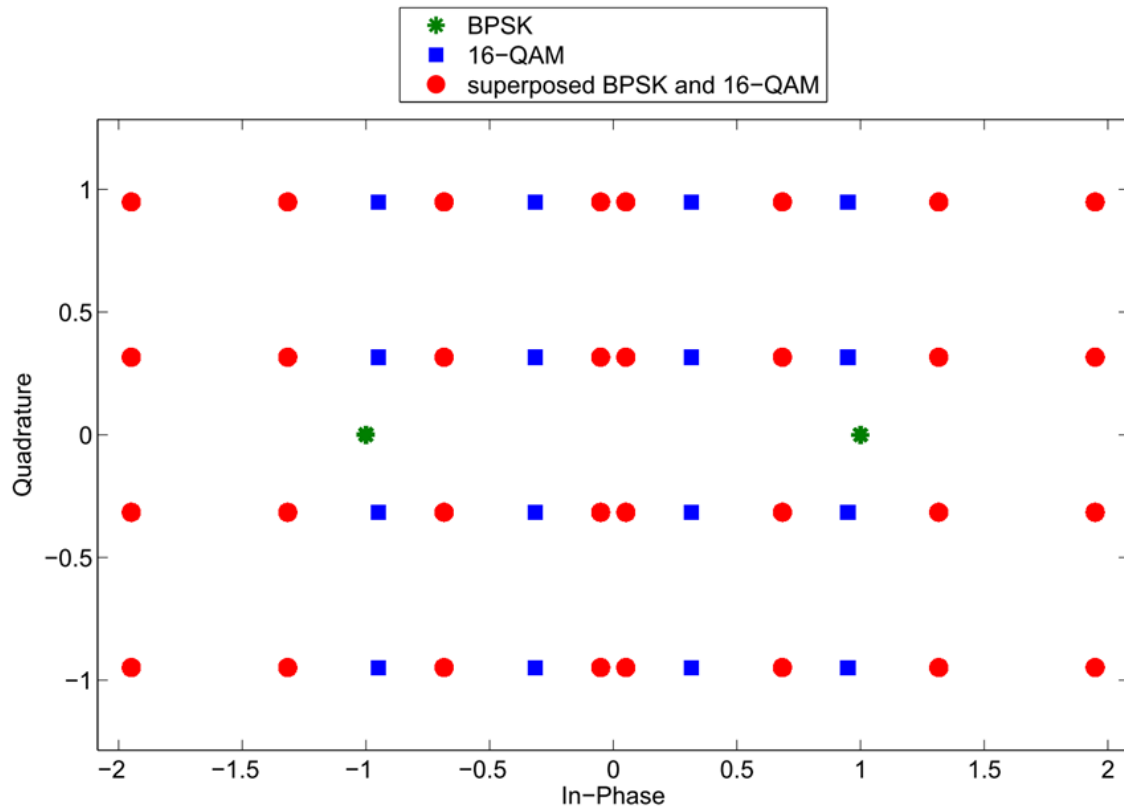


FIGURE 5.1 – Constellations : BPSK signal, 16-QAM signal and superposed BPSK and 16-QAM signal

TABLE 5.1 – Superposition of two 4-ASK signals at the relay node and the corresponding mapped bits using XOR operation

4-ASK	4-ASK	XOR	x_{\oplus}	4-ASK	4-ASK	XOR	x_{\oplus}
00	00	00	0	10	00	10	2A
00	01	01	A	10	01	11	3A
00	10	10	2A	10	10	00	4A
00	11	11	3A	10	11	01	5A
01	00	01	A	11	00	11	3A
01	01	00	2A	11	01	10	4A
01	10	11	3A	11	10	01	5A
01	11	10	4A	11	11	00	6A

5.2.2 Considered two-way MIMO relay channels

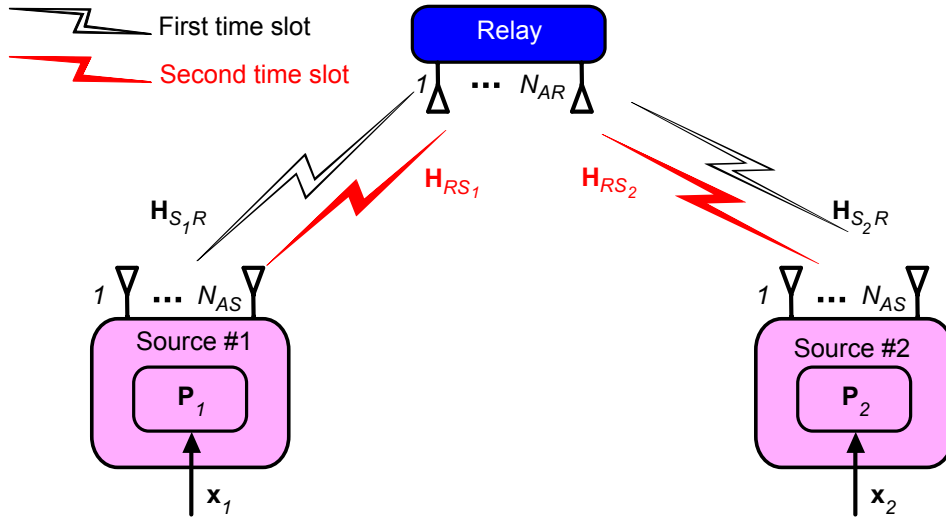


FIGURE 5.2 – Two-way MIMO relay channels

In the proposed transmission scheme, we consider a TWRC with MIMO wherein two transmitting source nodes S_1 and S_2 exchange information with the help of a relay node R , as depicted in Figure 5.2. In our transmission model, we assume that the direct link transmissions between the source nodes are not considered. Let N_{AS} and N_{AR} denote the number of antennas at each source node and the relay node, respectively.

In the first time slot, a ZF technique is applied at S_1 and S_2 to both data vectors $\mathbf{x}_1 = (x_{11}, \dots, x_{1N_{AS}})$ and $\mathbf{x}_2 = (x_{21}, \dots, x_{2N_{AS}})$ in form of a multiplication with a precoding matrix. Under the assumption of a frequency flat and time invariant MIMO channel, the precoding matrix of ZF at the source S_i , denoted by \mathbf{P}_i , is expressed as

$$\mathbf{P}_u = \mathbf{H}_{S_u R}^H \left(\mathbf{H}_{S_u R} \mathbf{H}_{S_u R}^H \right)^{-1}, \quad (5.1)$$

where $\mathbf{H}_{S_u R} \in \mathbb{C}^{N_{AR} \times N_{AS}}$ is the full rank gain matrices of the $S_u - R$ channel, $u = 1, 2$. The entries of $\mathbf{H}_{S_u R}$, $u = 1, 2$, follow a circularly symmetric complex Gaussian distribution with zero-mean and unit variance. Thereafter, both source nodes transmit the precoded data streams simultaneously to the relay node. The received superposed signal is denoted by $\mathbf{y}_R = (y_R^{(1)}, \dots, y_R^{(N_{AR})})^T$ and is given by

$$\mathbf{y}_R = \sqrt{P_{S_1 R}} \mathbf{H}_{S_1 R} \mathbf{P}_1 \mathbf{x}_1 + \sqrt{P_{S_2 R}} \mathbf{H}_{S_2 R} \mathbf{P}_2 \mathbf{x}_2 + \mathbf{n}_R, \quad (5.2)$$

where $P_{S_1 R}$ and $P_{S_2 R}$ are the received signal powers at the relay nodes from the sources S_1

and S_2 , respectively, and \mathbf{n}_R is the additive zero-mean spatially-white circularly complex Gaussian noise with variances σ_n^2 .

For the sake of realistic modeling, the distances between nodes have to be considered. Therefore, let $d_{T_X R_X}$ denote the geometrical distance between a transmitter node T_X and a receiver node R_X . The path loss between these two nodes can be modeled by [119]

$$g_{T_X R_X} = \frac{\kappa}{d_{T_X R_X}^\delta}, \quad (5.3)$$

where κ is a constant that depends on the carrier wavelength and the environment, and δ is the path-loss exponent with values typically in the range $2 \leq \delta \leq 6$. Assume that the two source nodes transmit with the same power $P_S = P_{S_1} = P_{S_2}$. For the sake of fair comparison with the one-hop communication, let $P_{SS'} = P_{S_1 S_2} = P_{S_2 S_1}$ be the received signal power at the end-node of the direct link as if the direct signal between the two source nodes were present. $P_{SS'}$ is considered as the reference signal power. Thus, the received signal power $P_{S_u R}$ at the relay node from the source node S_u can be expressed as follows :

$$P_{S_u R} = \frac{\kappa}{d_{S_u R}^\delta} P_S = \left(\frac{d_{S_1 S_2}}{d_{S_u R}} \right)^\delta P_{SS'}, \quad (5.4)$$

where $d_{S_1 S_2}$ is the distance between the sources S_1 and S_2 , and $d_{S_u R}$ is the distance between the source S_u , $u = 1, 2$ and R . The quotient $(d_{S_1 S_2} / d_{S_u R})^\delta$ is referred to as the power gain of the $S_u - R$ link with respect to the reference signal power $P_{SS'}$ and is denoted by $G_{S_u R}$, $u = 1, 2$. According to the normalized fading coefficients, the average SNRs of the $S_u - R$ link is given by

$$\begin{aligned} \bar{\gamma}_{S_u R} &= \frac{P_{S_u R}}{\sigma_n^2} \\ &= G_{S_u R} \frac{P_{SS'}}{\sigma_n^2}, u = 1, 2. \end{aligned} \quad (5.5)$$

Up to now, $P_{SS'}/\sigma_n^2$ is referred to as reference SNR and is denoted by $\bar{\gamma}$.

In the second transmission phase, the relay node broadcasts the superposed physical layer network-coded signal to both sources with an additional overhead referring to the estimated sources modulations pair. A necessary condition to provide correct data reception at the destinations is the perfect recognition of the sources modulations types and orders. Accordingly, the relay node R must recognize the sources modulations from the

received superposed signal $\mathbf{y}_{R,t}$. At this stage, an algorithm for recognition the sources modulations must take place.

In the following, we present the proposed algorithm as illustrated in Figure 5.5. The discriminating features from the received signal $\mathbf{y}_{R,t}$ are firstly extracted and then an appropriate features set is selected. Thereafter, the modulation recognition is carried out by employing the random forests classifier (RFC).

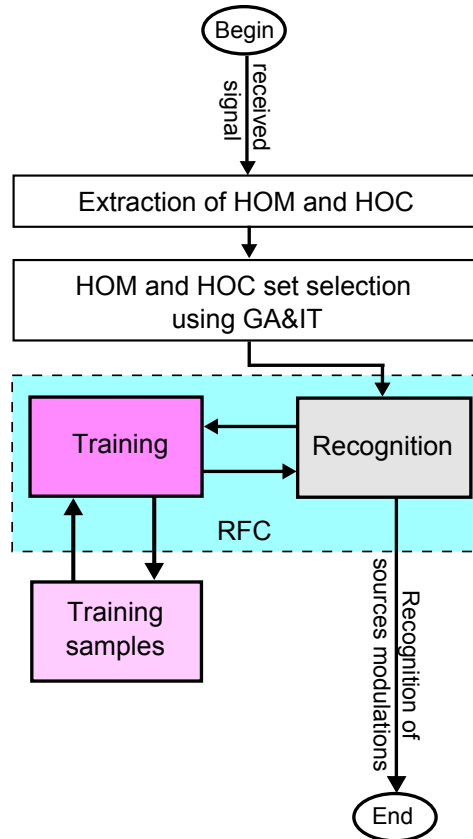


FIGURE 5.3 – Processes diagram of sources modulations recognition algorithm for an unknown received signal

5.2.3 Extraction of discriminating features

Features extraction is an essential step in modulation recognition algorithms. It is important to extract appropriate features that enable the algorithm to correctly recognize the sources modulations from the superposed constellation. The HOMs and the HOCs of a received signal have the capability to distinguish between linear modulation schemes as can be seen in the above chapters (3 and 4). Accordingly, we propose an algorithm suitable for superposed modulations recognition using HOMs and HOCs statistics. Here, we employ these statistics up to order eight. It is noteworthy that the o^{th} -order HOM and HOC

of a sequence at the a^{th} antenna with size of N symbols (i.e., $\mathbf{y}_R^{(a)} = (y_{R1}^{(a)}, \dots, y_{RN}^{(a)})$, $a = 1, \dots, N_{AR}$) can be computed using equations (3.8) and (3.12), respectively. Given the fact that the magnitude of cumulants increases with their order, we raise each cumulant to the power of $2/o$ [102].

In order to improve the accuracy of the proposed algorithm with low computational cost, features selection algorithm can be used as features filter. Here, we select an optimal features set based on a genetic algorithm and information theory (GA&IT) [120]. Through intensive simulations, we have observed that selecting more than five features ($N_F = 5$) among thirty-one features, which are involved in the implementation of the Random Forests classifier, does not improve the recognition performance.

5.2.4 Random forests classifier

It is well known, that the well functioning of the RFC on various recognition problems is provided thanks to the bootstrap nature and the random features selection [121]. In this study, we use RFC to recognize sources modulations from the superposed constellation based on the selected features. RFC is an ensemble learning technique that is based on the combination of a set of unpruned random decision trees. Typically, RFC includes two processing steps : a training step and a recognition step. In the training step, RFC builds multiple classification and regression tree (CART)-like classifiers [122], in which each tree is trained on a bootstrapped sample of the original training samples, where the algorithm only searches across a random subset of the features to find out a split at each node in each CART tree. In the recognition step, each tree in the RFC gives a unit vote for the most popular modulation pairs. Then, the modulation pairs receiving the biggest number of votes from the trees are the predicted sources modulations. RFC requires a complexity of $\mathcal{O}(N_{trees} \cdot N_{RFC} \cdot N_D \cdot \log_2(N_D))$, where N_{trees} is the number of trees to grow, $N_{RFC} = \lceil \log_2(N_F) + 1 \rceil$ represents the number of random features to be considered at each node, and N_D denotes the number of samples in the training data set.

5.3 Simulation results

5.3.1 Simulation setup

Computer simulations are carried out to highlight the benefits of the proposed modulation recognition algorithm. In this work, different combinations of modulation pairs from the ASK, QAM and PSK modulations are chosen to build the following three sets :

- ❖ $\Theta_3 = \{(2\text{-PSK}, 2\text{-PSK}), (2\text{-PSK}, 4\text{-PSK}), (2\text{-PSK}, 16\text{-QAM}), (2\text{-PSK}, 64\text{-QAM}), (4\text{-PSK}, 4\text{-PSK}), (4\text{-PSK}, 16\text{-QAM}), (4\text{-PSK}, 64\text{-QAM}), (16\text{-QAM}, 16\text{-QAM}), (16\text{-QAM}, 64\text{-QAM}), (64\text{-QAM}, 64\text{-QAM})\}$
- ❖ $\Theta_4 = \{(2\text{-PSK}, 2\text{-PSK}), (2\text{-PSK}, 4\text{-PSK}), (2\text{-PSK}, 4\text{-ASK}), (2\text{-PSK}, 8\text{-ASK}), (4\text{-PSK}, 4\text{-PSK}), (4\text{-PSK}, 4\text{-ASK}), (4\text{-PSK}, 8\text{-ASK}), (4\text{-ASK}, 4\text{-ASK}), (4\text{-ASK}, 8\text{-ASK}), (8\text{-ASK}, 8\text{-ASK})\}$
- ❖ $\Theta_5 = \{(4\text{-ASK}, 4\text{-ASK}), (4\text{-ASK}, 8\text{-ASK}), (4\text{-ASK}, 16\text{-QAM}), (4\text{-ASK}, 64\text{-QAM}), (8\text{-ASK}, 8\text{-ASK}), (8\text{-ASK}, 16\text{-QAM}), (8\text{-ASK}, 64\text{-QAM}), (16\text{-QAM}, 16\text{-QAM}), (16\text{-QAM}, 64\text{-QAM}), (64\text{-QAM}, 64\text{-QAM})\}$

We note that Θ_3 includes modulations pairs from PSK and QAM modulations, Θ_4 includes modulations pairs from PSK and ASK modulations, and Θ_5 includes modulations pairs from ASK and QAM modulations. For each superposed pair of modulations in Θ_d , $d = 3, 4, 5$, the training set consists of 200 test signals realizations, where the source messages \mathbf{x}_1 and \mathbf{x}_2 of S_1 and S_2 are randomly generated for each realization. In this work, the different channels are subject to flat fading, where perfect transmitter-side CSI is assumed. The test set contains 1000 Monte Carlo trials for each superposed pair of modulations, hence $N_{total} = 10 \times 1000 = 10000$ Monte Carlo trials results as each modulation set includes 10 modulation schemes. For each trial, N_{AS} test signals are considered. Unless otherwise mentioned, the number of symbols at each antenna consists of $N = 10000$ symbols, the number of antennas are $N_{AS} = N_{AR} = 4$ and the path loss model is a free-space with $\delta = 2$. For both training and classification steps, the features set is formed by calculating the HOMs and HOCs of the equalized signals at each antenna (i.e., $\mathbf{y}_R^{(a)} = \left(y_{R1}^{(a)}, \dots, y_{RN}^{(a)} \right)$ $a = 1, \dots, N_{AR}$). Then, the features subset selection based on GA&IT was performed and the five best features are selected as a preparation for the RFC. Here, we use RFC with the default configuration of the data mining tool Weka (i.e.,

$N_{trees} = 100$ and $N_{RFC} = 3$) [113]. With this setting, we find out that RFC gives a good tradeoff between accuracy of modulation recognition and speed of training. We note that the performance results presented in the following are given with respect to the above defined $\bar{\gamma}$.

The average probability of correct recognition in percentage can be computed as

$$P_{ra} = \frac{\sum_{\mathcal{M}_i \in \Theta_d} N_{\mathcal{M}_i}}{N_{total}} \times 100, \quad (5.6)$$

where $N_{\mathcal{M}_i}$ is equal to the number of trials for which the modulation $\mathcal{M}_i \in \Theta_d$, $d = 3, 4, 5$ is correctly recognized.

In this work, we use V-BLAST as a spatial multiplexing technique. It is worth noting that all the N_{AR} antennas cooperate to make a better decision for each test trial. In fact, the modulation pair that receives the majority of votes is considered to be the estimated modulation pair. In the case where no modulation has the majority number of votes, the trial is considered as misrecognized.

5.3.2 Effect of the relay position

The proposed transmission model incorporates the relay position as shown in equation (5.4). In the sequel, all distances involved in the calculation of the power gain in equation (5.4) are relative to the distance between the two sources S_1 and S_2 , i.e., $d_{S_1 S_2}$ is assumed to be unity and $d_{S_1 R} + d_{S_2 R} = 1$.

Figure 5.4 shows P_{ra} of the proposed algorithm as a function of $\bar{\gamma}$ at different relay positions for Θ_3 . It can be seen that the best performance in terms of probability of correct recognition is obtained when the relay is located at the middle point between the two sources. For instance, P_{ra} achieves an excellent performance ($P_{ra} \simeq 100\%$) at $d_{S_1 R} = 0.5$, while it reaches only 87% at $d_{S_1 R} = 0.1$ for $\bar{\gamma} = 3$ dB. The finding reveals that the proposed algorithm can achieve a good performance ($P_{ra} \simeq 100\%$) at all relay positions and for acceptable SNR ($\bar{\gamma} = 8$ dB).

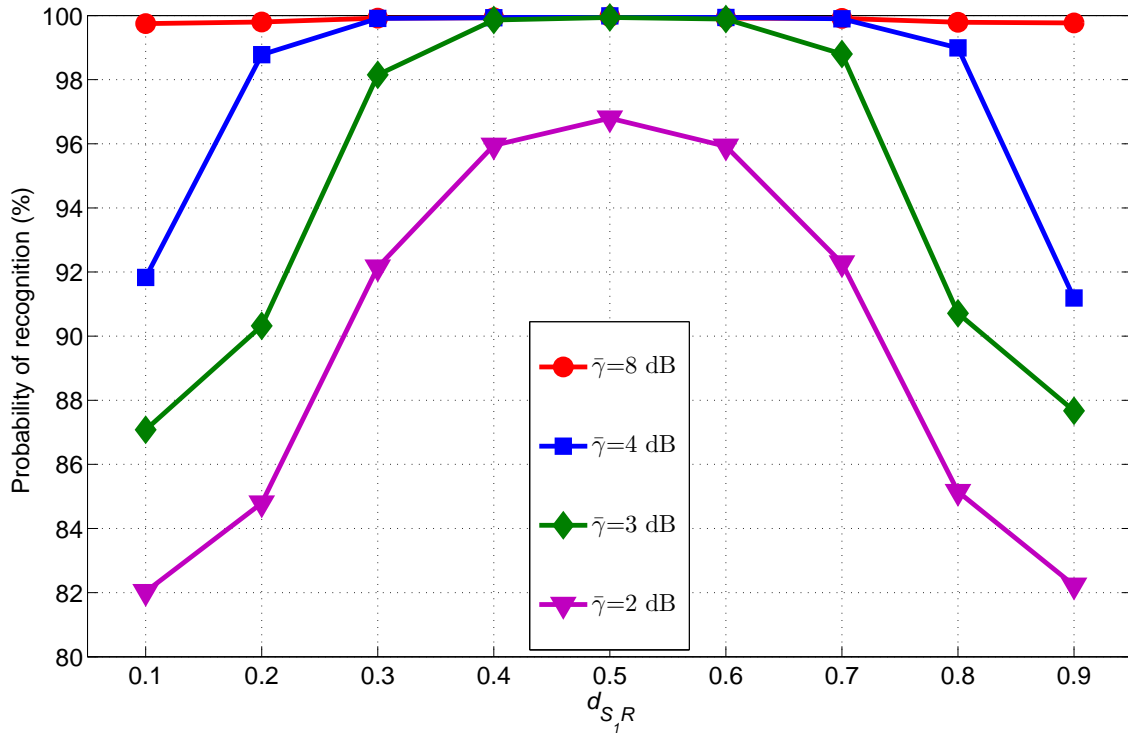


FIGURE 5.4 – The effect of the distance between S_1 and R , d_{S_1R} , on the average probability of correct recognition, P_{ra} , for Θ_3 , $N_{AS} = N_{AR} = 4$, $N = 10000$, $\delta = 2$ and $d_{S_1S_2} = d_{S_1R} + d_{S_2R} = 1$

5.3.3 Effect of the modulation types

Figure 5.5 illustrates the effect of modulation types, Θ_d , $d = 3, 4, 5$, on the average probability of correct recognition, P_{ra} , in the case when $d_{S_1R} = d_{S_2R} = 0.5$. As can be observed from these results, the proposed algorithm provides almost ideal modulation recognition for the different modulation sets at acceptable SNRs. Besides, we note that the modulation set Θ_4 is the best recognized one by the proposed algorithm. This can be explained by the fact that the modulation orders in Θ_4 are lower than those in Θ_3 and Θ_5 .

Additionally, and in order to prove the effectiveness of the RFC, we compare its performance to that of the Bagging classifier. In Chapter 4, we have shown that the Bagging classifier leads to better performance compared to several other classifiers, such as J48, NBD, TAN and MLP, for the price of training time. Simulation results employing the Bagging classifier are carried out. We note that the training subset number of Bagging using J48 as a base classifier is set to $T = 60$ as in Chapter 4. The findings in Figure 5.7 and Table 5.2 reveal that the RFC achieves nearly similar performance compared to the Bagging classifier. In addition, Table 5.3 shows that the time required for the RFC training phase is lower than that required for the Bagging classifier. This confirms the adequacy of the RFC in

terms of recognition performance and training time.

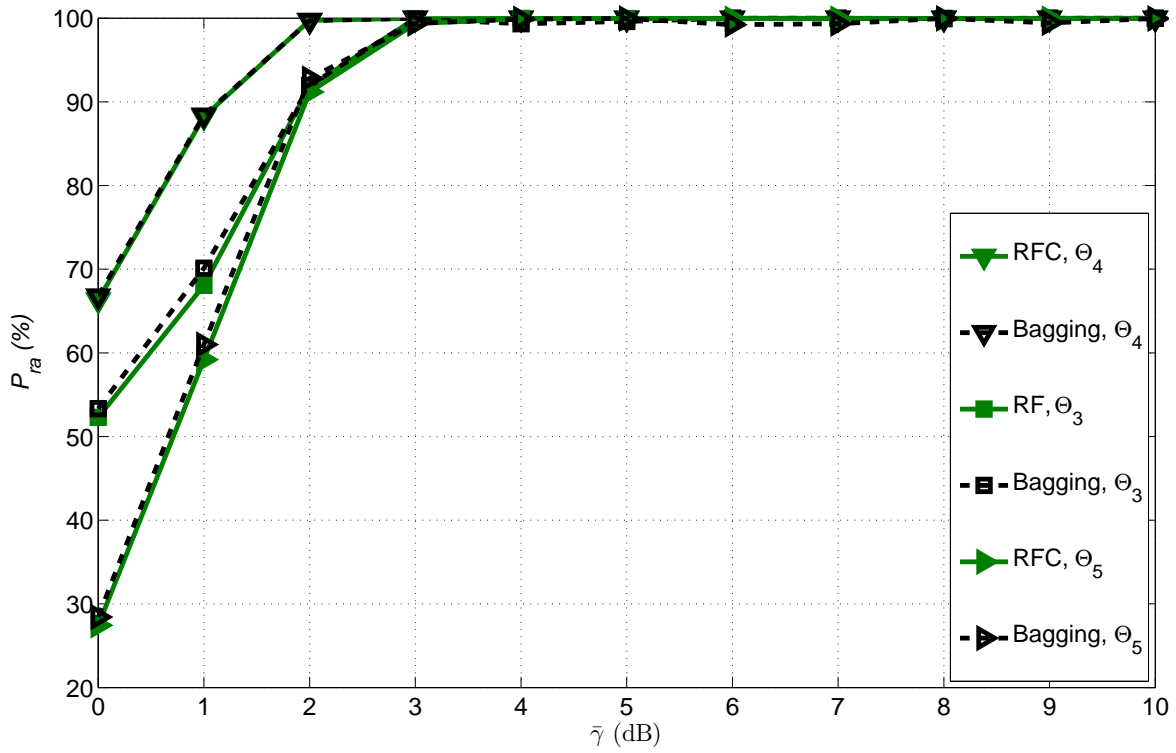


FIGURE 5.5 – The effect of the modulation schemes, $\Theta_d, d = 3, 4, 5$, on the average probability of correct recognition, P_{ra} , for RFC and Bagging classifiers using $N_{AS} = N_{AR} = 4, N = 10000, \delta = 2$ and $d_{S_1R} = d_{S_2R} = 0.5$

TABLE 5.2 – AUC of each classifier for Θ_4 with $N_{AS} = N_{AR} = 4, N = 10000, \delta = 2, d_{S_1R} = d_{S_2R} = 0.5$ and $\bar{\gamma} = 3$ dB

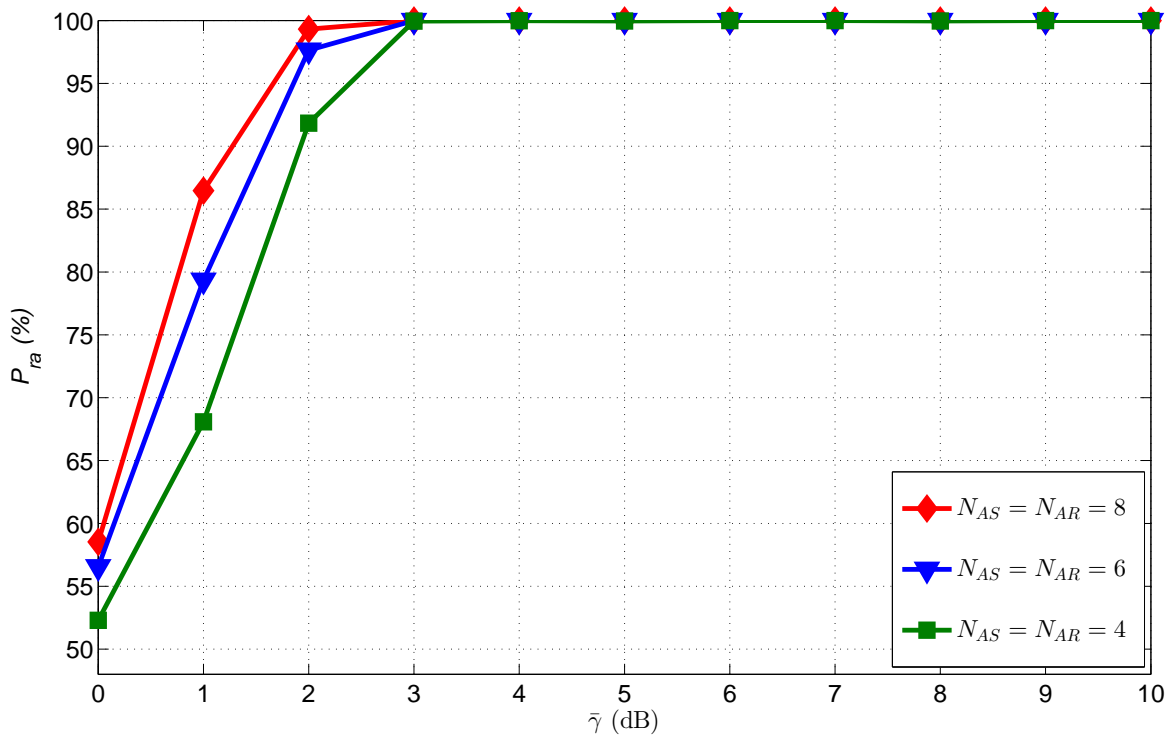
Modulation pair	Classifier		
	RFC	Bagging	
4-ASK, 4-ASK	0.959	0.958	
4-ASK, 8-ASK	0.962	0.957	
4-ASK, BPSK	0.958	0.958	
4-ASK, QPSK	0.959	0.958	
8-ASK, 8-ASK	0.96	0.957	
8-ASK, BPSK	0.958	0.958	
8-ASK, QPSK	0.958	0.958	
BPSK, BPSK	0.958	0.958	
BPSK, QPSK	0.958	0.958	
QPSK, QPSK	0.958	0.958	
Weighted Average of AUC		0.959	0.958

TABLE 5.3 – Time model building for Θ_4 with $N_{AS} = N_{AR} = 4$, $N = 10000$, $\delta = 2$, $d_{S_{1R}} = d_{S_{2R}} = 0.5$ and $\bar{\gamma} = 3$ dB

Classifier	Time taken to build model (seconds)
RFC	5.08
Bagging	7.09

5.3.4 Effect of the antennas number

Figure 5.6 presents P_{ra} of the proposed algorithm as a function of $\bar{\gamma}$, for Θ_3 and $d_{S_{1R}} = d_{S_{2R}} = 0.5$. It is clearly seen that increasing the number of antennas leads to an improvement in the recognition performance. For instance, a good performance ($P_{ra} \approx 100\%$) is obtained at $\bar{\gamma} = 2$ dB for $N_{AS} = N_{AR} = 8$, whereas a similar performance is obtained at $\bar{\gamma} = 3$ dB for $N_{AS} = N_{AR} = 4$.

FIGURE 5.6 – The effect of the number of antennas, N_{AS} and N_{AR} , on the average probability of correct recognition, P_{ra} , for Θ_3 , $N = 10000$, $\delta = 2$ and $d_{S_{1R}} = d_{S_{2R}} = 0.5$

5.3.5 Effect of the symbols number

Figure 5.7 shows P_{ra} of the proposed algorithm as a function of $\bar{\gamma}$, at various values of symbols number N , for Θ_3 and $d_{S_{1R}} = d_{S_{2R}} = 0.5$. It is apparent that an important gain can

be achieved when increasing N . This result reflects the improvement in the HOMs estimation accuracy when increasing N in equation (3.8). Even though, we observe a certain saturation up to a number of 20000 symbols.

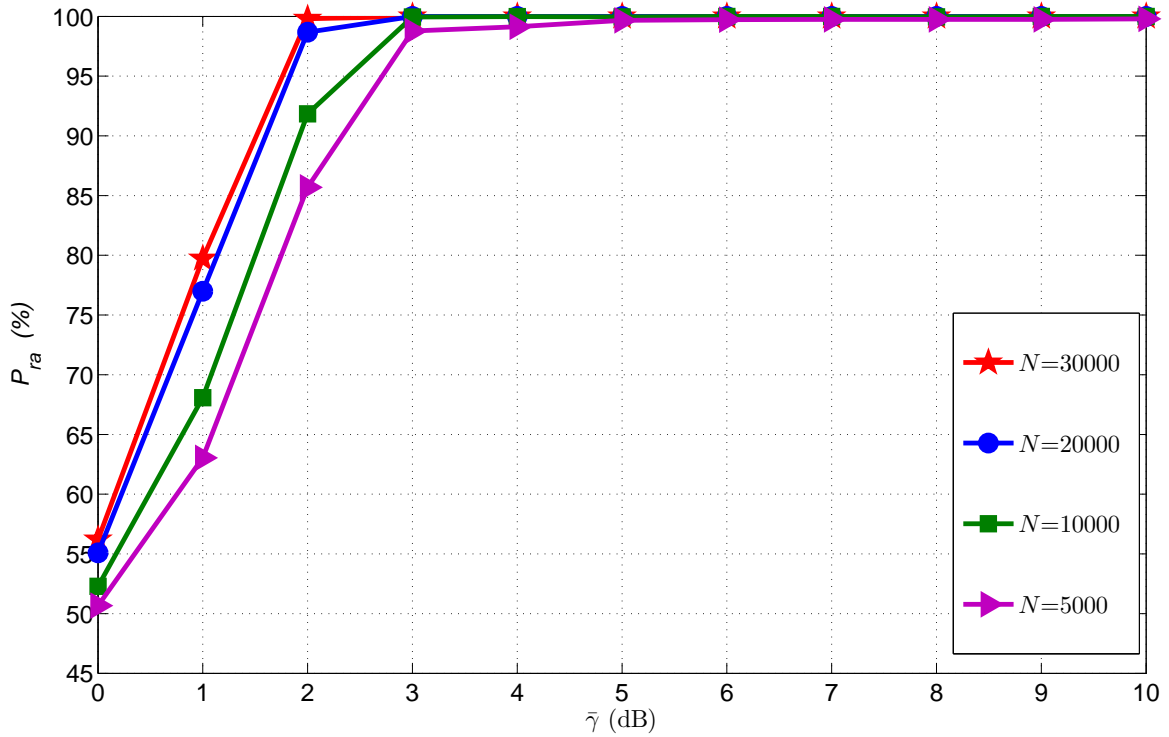


FIGURE 5.7 – The effect of the number of symbols, N , on the average probability of correct recognition, P_{ra} , for Θ_3 , $N_{AS} = N_{AR} = 4$, $\delta = 2$ and $d_{S_1R} = d_{S_2R} = 0.5$

5.3.6 Effect of the path loss exponent

Figure 5.8 illustrates P_{ra} of the proposed algorithm plotted as a function of $\bar{\gamma}$, for several values of δ , using Θ_3 and $d_{S_1R} = d_{S_2R} = 0.5$. A significant improvement in P_{ra} is noticed when increasing δ . This behavior is due to the fact that the SNR at the relay increases when increasing the path loss exponent for the same reference $\bar{\gamma}$ as given in equation (5.4).

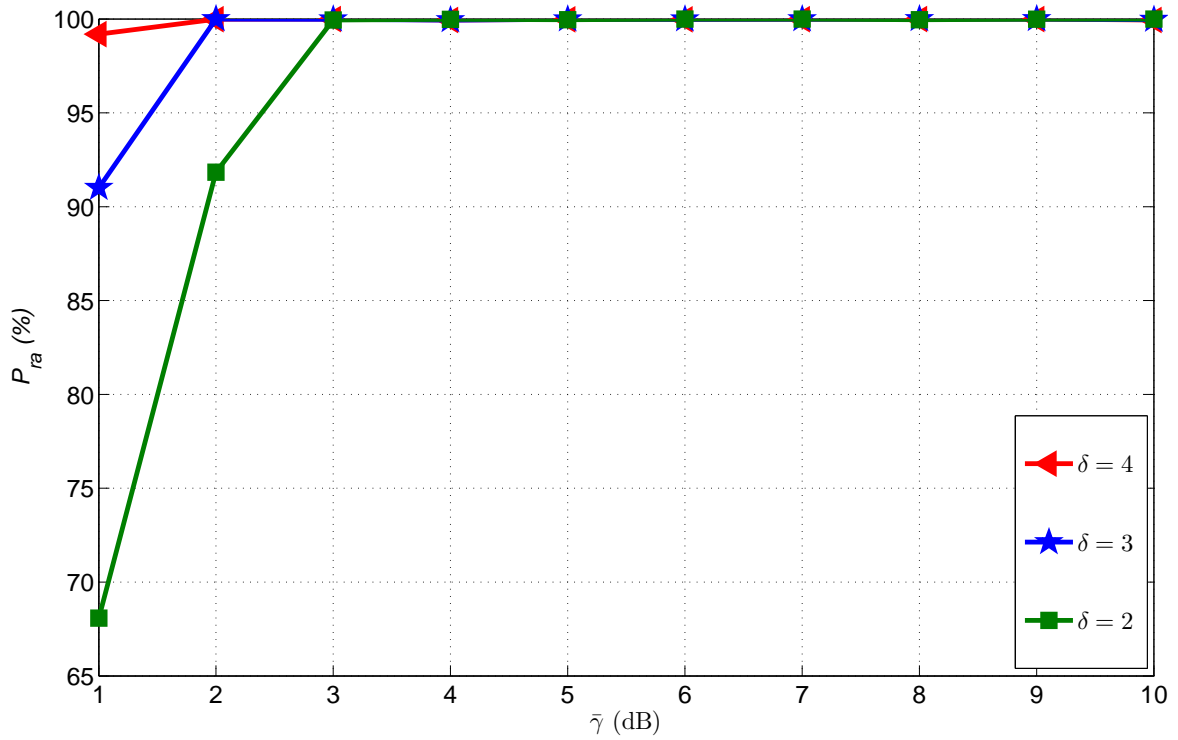


FIGURE 5.8 – The effect of the path loss exponent, δ , on the average probability of correct recognition, P_{ra} , for Θ_3 , $N_{AS} = N_{AR} = 4$, $N = 10000$, and $d_{S_1R} = d_{S_2R} = 0.5$

5.4 Conclusion

In this chapter, we have proposed an algorithm for recognizing superposed modulations designed for two-way relaying MIMO systems with PLNC. This algorithm extracts the HOMs and the HOCs as features from the superposed received signals at the relay node. The features selection is done to select the best ones using GA&IT. For the purpose of recognition, the Random Forests machine learning method was used. Different simulations were carried out to assess the efficiency of the proposed algorithm in an acceptable SNR range.

General conclusion and Future Works

Contents

6.1 Summary of results	84
6.2 Future works	86

Cooperative MIMO communications are considered among the most promising technologies in wireless telecommunication systems. The research work presented in this thesis has covered many important issues in modulation recognition for cooperative MIMO communications. The contributions of this thesis present a good starting point for further research. In this concluding chapter, all the key findings discussed in each Chapter are summarized and possible near-future work and perspectives are suggested.

6.1 Summary of results

In Chapter 3, we have presented a modulation recognition algorithm suitable for cooperative MIMO networks over uncorrelated channels with perfect CSI. It is based on a pattern recognition approach. For this purpose, the proposed modulation recognition algorithm is composed of two subsystems. The first subsystem concerns the features extraction whose role is to select the best subset of HOS using the PCA technique. The second subsystem is called the classifier, and its function is to recognize the modulation scheme. From the ROC curves, the probability of recognition and the learning period time, we have executed a comparative study of the J48 classifier, MLP classifier and the Bayesian network classifiers. We demonstrated that the J48 classifier and the Bayesian network classifiers have acceptable performance to discriminate among different linear modulation

types with a reasonable training time. Therefore, the J48 classifier and the Bayesian network classifiers can be applied for recognition modulation and hence achieve better monitoring of intercepted signals in broadband technologies with low complexity. We have also shown that the cooperative schemes can offer an important gain in modulation recognition compared to the non-cooperative case.

Assuming uncorrelated channels with perfect CSI in cooperative MIMO systems is not always a practical assumption. In fact, diversity, multiplexing and capacity gains can be directly influenced by spatial correlation effects due to insufficient spacing between antenna elements and/or poor scattering. In addition, an imperfect CSI may arise because of errors introduced by channel estimation, reciprocity mismatch, quantization, and delay. For these reasons, in Chapter 4 we addressed the problem of modulation recognition for cooperative MIMO systems over spatially-correlated channels with imperfect CSI. The spatial correlation channels are modeled according to the well-known Kronecker model and the imperfect CSI is modeled by a complex Gaussian distribution. We first derived the expression for the ergodic capacity to assess the performance of the proposed transmission system with imperfect CSI in the presence of spatial correlation. Thereafter, we investigate the performance of modulation recognition based on a pattern recognition approach using HOS as a features extraction and the Bagging as a classifier. The robustness of the Bagging classifier is demonstrated through a comparative study with the J48, TAN, NBD and MLP classifiers. We also evaluate the modulation recognition gain for the cooperative MIMO scheme relative to the non-cooperative one under spatially correlated channels and in the presence of imperfect CSI. In order to compensate for the performance degradation induced by both the spatial correlation and the imperfect CSI, we evaluated the effect of increasing the number of relay nodes for the modulation recognition. Simulation results showed that the recognition performance degradation caused by both spatially correlated channels and channel estimation errors can be removed by means of a relaying scheme.

In TWRC, the two source nodes (S_1 and S_2) can vary the modulation scheme and the modulation order for each transmission depending on applications according to its requirement. Consequently, S_1 (S_2) requires the recognition of the type and the order of the modulation used by S_2 (S_1) in order to demodulate the received signal. A necessary requirement for guaranteeing correct data reception at the destinations is the perfect re-

cognition of the sources modulations schemes and orders. To this end, in Chapter 5, we solved the problem of recognizing sources modulations for a two-way MIMO relay channel with PLNC. In the proposed algorithm, we use HOS-based features where the GA&IT is employed as a method of features selection and the Random Forests machine learning method as a classifier. For the sake of realistic modeling, we incorporated different relay positions. Simulation results showed that the proposed algorithm achieves a high recognition performance in an acceptable SNR range at different relay positions.

6.2 Future works

Beyond the contributions presented in this thesis, several possible research paths can be explored in future work. We shall list some of them below :

- ❖ The proposed algorithms in this thesis speculate that the radio-frequency (RF) operations are previously performed at the reception. Their performance degrades in the presence of estimation error in the RF parameters (carrier frequency, symbol time and sampling time). One improvement would be to design robust algorithms to handle these estimation errors.
- ❖ Our study considers the case of communications without frequency multiplexing. The modulation recognition for cooperative MIMO systems using frequency multiplexing in a multi-user environment is a challenge to be faced in future work.
- ❖ We addressed in our work the case of frequency non-selective channels degraded by additive Gaussian noise. We think it would be of great interest to develop algorithms of modulation recognition in the most difficult context of frequency-selective channels in conjunction with the orthogonal frequency division multiplexing (OFDM) system.
- ❖ Finally, it would be really interesting to propose robust algorithms for the recognition of other communication parameters dedicated to cooperative MIMO systems, such as the type of coding and the number of the transmitter antennas.

References

- [1] G. J. Foschini, "Layered space-time architecture for wireless communication in a fading environment when using multi-element antennas," *Bell labs technical journal*, vol. 1, no. 2, pp. 41–59, 1996.
- [2] S. M. Alamouti, "A simple transmit diversity technique for wireless communications," *IEEE Journal on Selected Areas in Communications*, vol. 16, no. 8, pp. 1451–1458, October 1998.
- [3] V. Tarokh, N. Seshadri, and A. R. Calderbank, "Space-time codes for high data rate wireless communication : Performance criterion and code construction," *IEEE Transactions on Information Theory*, vol. 44, no. 2, pp. 744–765, March 1998.
- [4] L. Korowajczuk, *LTE, WiMAX and WLAN network design, optimization and performance analysis*. John Wiley & Sons, 2011.
- [5] G. J. Foschini and M. J. Gans, "On limits of wireless communications in a fading environment when using multiple antennas," *Wireless personal communications*, vol. 6, no. 3, pp. 311–335, March 1998.
- [6] S. Hussain, A. Azim, and J. H. Park, "Energy efficient virtual MIMO communication for wireless sensor networks," *Telecommunication Systems*, vol. 42, no. 1-2, pp. 139–149, October 2009.
- [7] S. Cui, A. J. Goldsmith, and A. Bahai, "Energy-efficiency of MIMO and cooperative MIMO techniques in sensor networks," *IEEE Journal on Selected Areas in Communications*, vol. 22, no. 6, pp. 1089–1098, August 2004.
- [8] F.-S. Tseng and W.-R. Wu, "Nonlinear transceiver designs in MIMO amplify-and-forward relay systems," *IEEE Transactions on Vehicular Technology*, vol. 60, no. 2, pp. 528–538, February 2011.

- [9] F.-S. Tseng and W.-R. Wu, "Linear MMSE transceiver design in amplify-and-forward MIMO relay systems," *IEEE transactions on Vehicular Technology*, vol. 59, no. 2, pp. 754–765, February 2010.
- [10] Q. Zhang, S. Kota, V. Lau, W. Su, and A. Kwasinski, "Introduction to the issue on cooperative communication and signal processing in cognitive radio systems," *IEEE Journal of Selected Topics in Signal Processing*, vol. 5, no. 1, pp. 1–4, February 2011.
- [11] H. Wan, W. Chen, and J. Ji, "Efficient linear transmission strategy for MIMO relaying broadcast channels with direct links," *IEEE Wireless Communications Letters*, vol. 1, no. 1, pp. 14–17, February 2012.
- [12] M. Arti, R. K. Mallik, and R. Schober, "Beamforming and combining in two-way AF MIMO relay networks," *IEEE Communications Letters*, vol. 17, no. 7, pp. 1400–1403, 2013.
- [13] M. Arti and M. R. Bhatnagar, "Maximal ratio transmission in AF MIMO relay systems over Nakagami-fading channels," *IEEE Transactions on Vehicular Technology*, vol. 64, no. 5, pp. 1895–1903, 2015.
- [14] Y. Yang, H. Hu, J. Xu, and G. Mao, "Relay technologies for WiMAX and LTE-advanced mobile systems," *IEEE Communications Magazine*, vol. 47, no. 10, pp. 100–105, October 2009.
- [15] D.-S. Shiu, G. J. Foschini, M. J. Gans, and J. M. Kahn, "Fading correlation and its effect on the capacity of multielement antenna systems," *IEEE Transactions on Communications*, vol. 48, no. 3, pp. 502–513, March 2000.
- [16] A. D. Dabbagh and D. J. Love, "Multiple antenna MMSE based downlink precoding with quantized feedback or channel mismatch," *IEEE transactions on Communications*, vol. 56, no. 11, pp. 1859–1868, November 2008.
- [17] O. A. Dobre, "Signal identification for emerging intelligent radios : classical problems and new challenges," *IEEE Instrumentation & Measurement Magazine*, vol. 18, no. 2, pp. 11–18, April 2015.
- [18] O. A. Dobre, A. Abdi, Y. Bar-Ness, and W. Su, "Survey of automatic modulation classification techniques : classical approaches and new trends," *IET Communications*, vol. 1, no. 2, pp. 137–156, April 2007.

- [19] J. L. Xu, W. Su, and M. Zhou, "Software-defined radio equipped with rapid modulation recognition," *IEEE Transactions on Vehicular Technology*, vol. 59, no. 4, pp. 1659–1667, 2010.
- [20] J. L. Xu, W. Su, and M. Zhou, "Likelihood-ratio approaches to automatic modulation classification," *IEEE Transactions on Systems, Man, and Cybernetics, Part C (Applications and Reviews)*, vol. 41, no. 4, pp. 455–469, July 2011.
- [21] M. D. Wong and A. K. Nandi, "Automatic digital modulation recognition using artificial neural network and genetic algorithm," *Signal Processing*, vol. 84, no. 2, pp. 351–365, February 2004.
- [22] H.-C. Wu, M. Saquib, and Z. Yun, "Novel automatic modulation classification using cumulant features for communications via multipath channels," *IEEE Transactions on Wireless Communications*, vol. 7, no. 8, pp. 3098–3105, August 2008.
- [23] O. A. Dobre, A. Abdi, Y. Bar-Ness, and W. Su, "Cyclostationarity-based modulation classification of linear digital modulations in flat fading channels," *Wireless Personal Communications*, vol. 54, no. 4, pp. 699–717, September 2010.
- [24] M. Marey and O. A. Dobre, "Blind modulation classification for Alamouti STBC system with transmission impairments," *IEEE Wireless Communications Letters*, vol. 4, no. 5, pp. 521–524, October 2015.
- [25] M. S. Muhlhaus, M. Oner, O. A. Dobre, and F. K. Jondral, "A low complexity modulation classification algorithm for MIMO systems," *IEEE Communications Letters*, vol. 17, no. 10, pp. 1881–1884, October 2013.
- [26] K. Hassan, I. Dayoub, W. Hamouda, C. N. Nzeza, and M. Berbineau, "Blind digital modulation identification for spatially-correlated MIMO systems," *IEEE Transactions on Wireless Communications*, vol. 11, no. 2, pp. 683–693, February 2012.
- [27] J. Liu, D. Goeckel, and D. Towsley, "The throughput order of ad hoc networks employing network coding and broadcasting," in *IEEE Military Communications conference (MILCOM)*. IEEE, 2006, pp. 1–7.
- [28] C. Fragouli, J. Widmer, and J.-Y. Le Boudec, "A network coding approach to energy efficient broadcasting : from theory to practice," Tech. Rep., 2005.

- [29] T. Ho, B. Leong, R. Koetter, M. Médard, M. Effros, and D. R. Karger, "Byzantine modification detection in multicast networks with random network coding," *IEEE Transactions on Information Theory*, vol. 54, no. 6, pp. 2798–2803, 2008.
- [30] S. C. Liew, S. Zhang, and L. Lu, "Physical-layer network coding : Tutorial, survey, and beyond," *Physical Communication*, vol. 6, pp. 4–42, March 2013.
- [31] G. P. John, "Digital communications," *Columbus : McGraw-Hill Companies*, 2001.
- [32] E. G. Larsson and P. Stoica, *Space-time block coding for wireless communications*. Cambridge university press, 2008.
- [33] R. S. Blum, "Some analytical tools for the design of space-time convolutional codes," *IEEE Transactions on Communications*, vol. 50, no. 10, pp. 1593–1599, October 2002.
- [34] M. Luo, L. Li, G. Qian, and H. Liao, "Multidimensional blind separation using higher-order statistics : Application to non-cooperative stbc systems," *Circuits, Systems, and Signal Processing*, vol. 33, no. 7, pp. 2173–2192, 2014.
- [35] V. Tarokh, H. Jafarkhani, and A. R. Calderbank, "Space-time block codes from orthogonal designs," *IEEE Transactions on Information Theory*, vol. 45, no. 5, pp. 1456–1467, July 1999.
- [36] H. Jafarkhani, "A quasi-orthogonal space-time block code," *IEEE Transactions on Communications*, vol. 49, no. 1, pp. 1–4, January 2001.
- [37] O. Tirkkonen, A. Boariu, and A. Hottinen, "Minimal non-orthogonality rate 1 space-time block code for 3+ Tx antennas," in *IEEE Sixth International Symposium on Spread Spectrum Techniques and Applications*, vol. 2. IEEE, 2000, pp. 429–432.
- [38] C. B. Papadias and G. J. Foschini, "Capacity-approaching space-time codes for systems employing four transmitter antennas," *IEEE Transactions on Information Theory*, vol. 49, no. 3, pp. 726–732, March 2003.
- [39] S. K. Jayaweera and H. V. Poor, "Capacity of multiple-antenna systems with both receiver and transmitter channel state information," *IEEE Transactions on Information Theory*, vol. 49, no. 10, pp. 2697–2709, October 2003.
- [40] A. Scaglione, P. Stoica, S. Barbarossa, G. B. Giannakis, and H. Sampath, "Optimal designs for space-time linear precoders and decoders," *IEEE Transactions on Signal Processing*, vol. 50, no. 5, pp. 1051–1064, May 2002.

- [41] M. Joham, W. Utschick, and J. A. Nossek, "Linear transmit processing in MIMO communications systems," *IEEE Transactions on Signal Processing*, vol. 53, no. 8, pp. 2700–2712, August 2005.
- [42] A. Wiesel, Y. C. Eldar, and S. Shamai, "Zero-forcing precoding and generalized inverses," *IEEE Transactions on Signal Processing*, vol. 56, no. 9, pp. 4409–4418, September 2008.
- [43] G. Caire and S. Shamai, "On the achievable throughput of a multiantenna Gaussian broadcast channel," *IEEE Transactions on Information Theory*, vol. 49, no. 7, pp. 1691–1706, July 2003.
- [44] A. H. Roger and R. J. Charles, *Matrix analysis*. Cambridge University Press, New York, 1985.
- [45] C. B. Peel, B. M. Hochwald, and A. L. Swindlehurst, "A vector-perturbation technique for near-capacity multiantenna multiuser communication-part I : channel inversion and regularization," *IEEE Transactions on Communications*, vol. 53, no. 1, pp. 195–202, January 2005.
- [46] P. Guguen and G. El Zein, *Les techniques multi-antennes pour les réseaux sans fil*. Edition Hermes-Science : Lavoisier, Paris, 2004.
- [47] T. Aulin, "Characteristics of a digital mobile radio channel," *IEEE Transactions on Vehicular Technology*, vol. 30, no. 2, pp. 45–53, May 1981.
- [48] E. Al-Hussaini and A. Al-Bassiouni, "Performance of MRC diversity systems for the detection of signals with Nakagami fading," *IEEE Transactions on Communications*, vol. 33, no. 12, pp. 1315–1319, December 1985.
- [49] W. R. Braun and U. Dersch, "A physical mobile radio channel model," *IEEE Transactions on Vehicular Technology*, vol. 40, no. 2, pp. 472–482, May 1991.
- [50] A. U. Sheikh, M. Abdi, and M. Handforth, "Indoor mobile radio channel at 946 MHz : Measurements and modeling," in *43rd IEEE Vehicular Technology Conference (VTC)*. IEEE, 1993, pp. 73–76.
- [51] H. E. Whitney, J. Aarons, R. Allen, and D. Seemann, "Estimation of the cumulative amplitude probability distribution function of ionospheric scintillations," *Radio Science*, vol. 7, no. 12, pp. 1095–1104, December 1972.

- [52] M. K. Simon and M.-S. Alouini, *Digital communication over fading channels*. John Wiley & Sons, 2005, vol. 95.
- [53] D. Gore, R. Heath, and A. Paulraj, "Statistical antenna selection for spatial multiplexing systems," in *IEEE International Conference on Communications (ICC)*, vol. 1. IEEE, 2002, pp. 450–454.
- [54] S. L. Loyka, "Channel capacity of MIMO architecture using the exponential correlation matrix," *IEEE Communications Letters*, vol. 5, no. 9, pp. 369–371, September 2001.
- [55] D. J. Love, R. W. Heath, V. K. Lau, D. Gesbert, B. D. Rao, and M. Andrews, "An overview of limited feedback in wireless communication systems," *IEEE Journal on Selected Areas in Communications*, vol. 26, no. 8, pp. 1341–1365, October 2008.
- [56] H. B. Chikha, I. Dayoub, and M. Berbineau, "Distributed turbo coded cooperative networks under imperfect channel state information in Rayleigh fading channels," *IET Communications*, vol. 7, no. 10, pp. 973–979, July 2013.
- [57] B. Vucetic and J. Yuan, *Space-time coding*. John Wiley & Sons, 2003.
- [58] M. Turan, M. Öner, and H. A. Çırpan, "Joint modulation classification and antenna number detection for MIMO systems," *IEEE Communications Letters*, vol. 20, no. 1, pp. 193–196, January 2016.
- [59] M. Mohammadkarimi, E. Karami, and O. A. Dobre, "A novel algorithm for blind detection of the number of transmit antenna," in *International Conference on Cognitive Radio Oriented Wireless Networks*. Springer, 2015, pp. 441–450.
- [60] M.-R. Oularbi, S. Gazor, A. Aissa-El-Bey, and S. Houcke, "Enumeration of base station antennas in a cognitive receiver by exploiting pilot patterns," *IEEE Communications Letters*, vol. 17, no. 1, pp. 8–11, January 2013.
- [61] S. Aouada, A. M. Zoubir, and C. M. S. See, "A comparative study on source number detection," in *Seventh International Symposium on Signal Processing and Its Applications*, vol. 1. IEEE, 2003, pp. 173–176.
- [62] M. Shi, Y. Bar-Ness, and W. Su, "Adaptive estimation of the number of transmit antennas," in *IEEE Military Communications Conference (MILCOM)*. IEEE, 2007, pp. 1–5.

- [63] O. Somekh, O. Simeone, Y. Bar-Ness, and W. Su, "Detecting the number of transmit antennas with unauthorized or cognitive receivers in MIMO systems," in *IEEE Military Communications Conference (MILCOM)*. IEEE, 2007, pp. 1–5.
- [64] M. Marey, O. A. Dobre, and B. Liao, "Classification of STBC systems over frequency-selective channels," *IEEE Transactions on Vehicular Technology*, vol. 64, no. 5, pp. 2159–2164, May 2015.
- [65] E. Karami and O. A. Dobre, "Identification of SM-OFDM and AL-OFDM signals based on their second-order cyclostationarity," *IEEE Transactions on Vehicular Technology*, vol. 64, no. 3, pp. 942–953, May 2015.
- [66] V. Choqueuse, K. Yao, L. Collin, and G. Burel, "Hierarchical space-time block code recognition using correlation matrices," *IEEE Transactions on Wireless Communications*, vol. 7, no. 9, pp. 3526–3534, September 2008.
- [67] K. Liu, J. P. C. da Costa, H. So, and A. L. de Almeida, "Semi-blind receivers for joint symbol and channel estimation in space-time-frequency MIMO-OFDM systems," *IEEE Transactions on Signal Processing*, vol. 61, no. 21, pp. 5444–5457, November 2013.
- [68] S. Cai, T. Matsumoto, and K. Yang, "SIMO channel estimation using space-time signal subspace projection and soft information," *IEEE Transactions on Signal Processing*, vol. 60, no. 8, pp. 4219–4235, August 2012.
- [69] S. Shahbazpanahi, A. B. Gershman, and J. H. Manton, "Closed-form blind MIMO channel estimation for orthogonal space-time block codes," *IEEE Transactions on Signal Processing*, vol. 53, no. 12, pp. 4506–4517, December 2005.
- [70] O. A. Dobre, A. Abdi, Y. Bar-Ness, and W. Su, "Blind modulation classification : a concept whose time has come," in *IEEE/Sarnoff Symposium on Advances in Wired and Wireless Communication*. IEEE, 2005, pp. 223–228.
- [71] E. Azzouz and A. Nandi, *Automatic modulation recognition of communication signals*. Springer Science & Business Media, 2013.
- [72] P. Prakasam and M. Madheswaran, "Modulation identification algorithm for adaptive demodulator in software defined radios using wavelet transform," *International Journal of Signal Processing*, vol. 5, no. 1, pp. 74–81, 2009.

- [73] K. Hassan, I. Dayoub, W. Hamouda, and M. Berbineau, "Automatic modulation recognition using wavelet transform and neural networks in wireless systems," *EUR-ASIP Journal on Advances in Signal Processing*, vol. 2010, no. 1, p. 1, July 2010.
- [74] A. K. Nandi and E. E. Azzouz, "Algorithms for automatic modulation recognition of communication signals," *IEEE Transactions on communications*, vol. 46, no. 4, pp. 431–436, April 1998.
- [75] L. Hong and K. Ho, "Identification of digital modulation types using the wavelet transform," in *IEEE Military Communications Conference Proceedings (MILCOM)*, vol. 1. IEEE, 1999, pp. 427–431.
- [76] A. Swami and B. M. Sadler, "Hierarchical digital modulation classification using cumulants," *IEEE Transactions on Communications*, vol. 48, no. 3, pp. 416–429, March 2000.
- [77] M. R. Bahloul, M. Z. Yusoff, A.-H. Abdel-Aty, M. N. M. Saad, and M. Al-Jemeli, "Modulation classification for MIMO systems : State of the art and research directions," *Chaos, Solitons & Fractals*, vol. 89, pp. 497–505, 2016.
- [78] V. Choqueuse, S. Azou, K. Yao, L. Collin, and G. Burel, "Blind modulation recognition for MIMO systems," *Military Technical Academy Review*, vol. 19, no. 2, pp. 183–196, 2009.
- [79] J. N. Laneman, D. N. Tse, and G. W. Wornell, "Cooperative diversity in wireless networks : Efficient protocols and outage behavior," *IEEE Transactions on Information theory*, vol. 50, no. 12, pp. 3062–3080, December 2004.
- [80] A. Nosratinia, T. E. Hunter, and A. Hedayat, "Cooperative communication in wireless networks," *IEEE Communications Magazine*, vol. 42, no. 10, pp. 74–80, October 2004.
- [81] M. Peng, H. Liu, W. Wang, and H.-H. Chen, "Cooperative network coding with MIMO transmission in wireless decode-and-forward relay networks," *IEEE Transactions on Vehicular Technology*, vol. 59, no. 7, pp. 3577–3588, September 2010.
- [82] A. K. Sadek, W. Su, and K. R. Liu, "Multinode cooperative communications in wireless networks," *IEEE Transactions on Signal Processing*, vol. 55, no. 1, pp. 341–355, January 2007.

- [83] A. Sendonaris, E. Erkip, and B. Aazhang, "User cooperation diversity. part II. Implementation aspects and performance analysis," *IEEE Transactions on Communications*, vol. 51, no. 11, pp. 1939–1948, November 2003.
- [84] Y. Kim and H. Liu, "Infrastructure relay transmission with cooperative MIMO," *IEEE Transactions on Vehicular Technology*, vol. 57, no. 4, pp. 2180–2188, July 2008.
- [85] S. Yang and J.-C. Belfiore, "Optimal space–time codes for the MIMO amplify-and-forward cooperative channel," *IEEE Transactions on Information Theory*, vol. 53, no. 2, pp. 647–663, February 2007.
- [86] J. N. Laneman and G. W. Wornell, "Distributed space-time-coded protocols for exploiting cooperative diversity in wireless networks," *IEEE Transactions on Information Theory*, vol. 49, no. 10, pp. 2415–2425, October 2003.
- [87] W.-J. Huang, Y.-W. Hong, and C.-C. J. Kuo, "Decode-and-forward cooperative relay with multi-user detection in uplink CDMA networks," in *IEEE Global Telecommunications Conference (GLOBECOM)*. IEEE, 2007, pp. 4397–4401.
- [88] J. Luo, R. S. Blum, L. Cimini, L. J. Greenstein, and A. M. Haimovich, "Decode-and-forward cooperative diversity with power allocation in wireless networks," *IEEE Transactions on Wireless Communications*, vol. 6, no. 3, pp. 793–799, March 2007.
- [89] Y. Jing and H. Jafarkhani, "Distributed differential space-time coding for wireless relay networks," *IEEE Transactions on Communications*, vol. 56, no. 7, pp. 1092–1100, July 2008.
- [90] V. Havary-Nassab, S. Shahbazpanahi, A. Grami, and Z.-Q. Luo, "Distributed beamforming for relay networks based on second-order statistics of the channel state information," *IEEE Transactions on Signal Processing*, vol. 56, no. 9, pp. 4306–4316, September 2008.
- [91] H. B. Chikha, S. Chaoui, I. Dayoub, J.-M. Rouvaen, and R. Attia, "A parallel concatenated convolutional-based distributed coded cooperation scheme for relay channels," *Wireless Personal Communications*, vol. 67, no. 4, pp. 951–969, December 2012.
- [92] W. Xu, X. Dong, and W.-S. Lu, "MIMO relaying broadcast channels with linear precoding and quantized channel state information feedback," *IEEE Transactions on Signal Processing*, vol. 58, no. 10, pp. 5233–5245, October 2010.

- [93] B. Zhang, Z. He, K. Niu, and L. Zhang, "Robust linear beamforming for MIMO relay broadcast channel with limited feedback," *IEEE Signal Processing Letters*, vol. 17, no. 2, pp. 209–212, February 2010.
- [94] R. Zhang, C. C. Chai, and Y.-C. Liang, "Joint beamforming and power control for multiantenna relay broadcast channel with QoS constraints," *IEEE Transactions on Signal Processing*, vol. 57, no. 2, pp. 726–737, February 2009.
- [95] X. Tang and Y. Hua, "Optimal design of non-regenerative MIMO wireless relays," *IEEE Transactions on Wireless Communications*, vol. 6, no. 4, pp. 1398–1407, 2007.
- [96] T. Koike-Akino, P. Popovski, and V. Tarokh, "Optimized constellations for two-way wireless relaying with physical network coding," *IEEE Journal on Selected Areas in Communications*, vol. 27, no. 5, pp. 773–787, June 2009.
- [97] Z. Li, X.-G. Xia, and B. Li, "Achieving full diversity and fast ML decoding via simple analog network coding for asynchronous two-way relay networks," *IEEE Transactions on Communications*, vol. 57, no. 12, pp. 3672–3681, December 2009.
- [98] S. Wang, Q. Song, X. Wang, and A. Jamalipour, "Rate and power adaptation for analog network coding," *IEEE Transactions on Vehicular Technology*, vol. 60, no. 5, pp. 2302–2313, June 2011.
- [99] K. Lee and L. Hanzo, "Resource-efficient wireless relaying protocols," *IEEE Wireless Communications*, vol. 17, no. 2, pp. 66–72, April 2010.
- [100] A. Ebrahimzadeh and A. Ranjbar, "Intelligent digital signal-type identification," *Engineering Applications of Artificial Intelligence*, vol. 21, no. 4, pp. 569–577, June 2008.
- [101] P. McCullagh, *Tensor methods in statistics*. Chapman and Hall London, 1987, vol. 161.
- [102] C. M. Spooner, "On the utility of sixth-order cyclic cumulants for RF signal classification," in *Conference Record of the Thirty-Fifth Asilomar Conference on Signals, Systems and Computers*, vol. 1. IEEE, 2001, pp. 890–897.
- [103] N. Kwak, "Principal component analysis based on L1-norm maximization," *IEEE transactions on pattern analysis and machine intelligence*, vol. 30, no. 9, pp. 1672–1680, September 2008.

- [104] R. Kohavi and J. R. Quinlan, "Data mining tasks and methods : Classification : decision-tree discovery," in *Handbook of data mining and knowledge discovery*. Oxford University Press, Inc., 2002, pp. 267–276.
- [105] M. Riedmiller and H. Braun, "A direct adaptive method for faster backpropagation learning : The RPROP algorithm," in *IEEE International Conference On Neural Networks*. IEEE, 1993, pp. 586–591.
- [106] R. R. Bouckaert, *Bayesian network classifiers in weka*. Department of Computer Science, University of Waikato Hamilton, 2004.
- [107] G. H. John and P. Langley, "Estimating continuous distributions in Bayesian classifiers," in *Proceedings of the Eleventh conference on Uncertainty in artificial intelligence*. Morgan Kaufmann Publishers Inc., 1995, pp. 338–345.
- [108] U. Fayyad and K. Irani, "Multi-interval discretization of continuous attributes as preprocessing or classification learning," in *Proceedings of the Thirteenth International Joint Conference on Artificial Intelligence, Morgan Kaufmann*, pp. 1022–1027.
- [109] N. Friedman, D. Geiger, and M. Goldszmidt, "Bayesian network classifiers," *Machine learning*, vol. 29, no. 2-3, pp. 131–163, November 1997.
- [110] C. Chow and C. Liu, "Approximating discrete probability distributions with dependence trees," *IEEE transactions on Information Theory*, vol. 14, no. 3, pp. 462–467, May 1968.
- [111] T. Fawcett, "An introduction to ROC analysis," *Pattern recognition letters*, vol. 27, no. 8, pp. 861–874, June 2006.
- [112] A. P. Bradley, "The use of the area under the ROC curve in the evaluation of machine learning algorithms," *Pattern recognition*, vol. 30, no. 7, pp. 1145–1159, July 1997.
- [113] "Weka data mining software," <http://www.cs.waikato.ac.nz/ml/weka/>, 2013, Version 3.6.5.
- [114] A. Van Zelst and J. Hammerschmidt, "A single coefficient spatial correlation model for multiple-input multiple-output (MIMO) radio channels," in *Proc. of URSI General Assembly*, 2002, pp. 17–24.
- [115] Z. Wang, W. Chen, F. Gao, and J. Li, "Capacity performance of relay beamformings for MIMO multirelay networks with imperfect-CSI at relays," *IEEE Transactions on Vehicular Technology*, vol. 60, no. 6, pp. 2608–2619, July 2011.

- [116] L. Breiman, "Bagging predictors," *Machine learning*, vol. 24, no. 2, pp. 123–140, August 1996.
- [117] L. Breiman *et al.*, "Arcing classifier," *The annals of statistics*, vol. 26, no. 3, pp. 801–849, 1998.
- [118] F.-S. Tseng, W.-R. Wu, and J.-Y. Wu, "Joint source/relay precoder design in nonregenerative cooperative systems using an MMSE criterion," *IEEE Transactions on Wireless Communications*, vol. 8, no. 10, pp. 4928–4933, October 2009.
- [119] H. Ochiai, P. Mitran, and V. Tarokh, "Design and analysis of collaborative diversity protocols for wireless sensor networks," in *60th IEEE Vehicular technology conference (VTC)*, vol. 7. IEEE, 2004, pp. 4645–4649.
- [120] O. Ludwig and U. Nunes, "Novel maximum-margin training algorithms for supervised neural networks," *IEEE Transactions on Neural Networks*, vol. 21, no. 6, pp. 972–984, June 2010.
- [121] L. Breiman, "Random forests," *Machine learning*, vol. 45, no. 1, pp. 5–32, October 2001.
- [122] L. Breiman, J. Friedman, C. J. Stone, and R. A. Olshen, *Classification and regression trees*. CRC press, 1984.